BOSCH

From	Our Reference	Telephone	Anderson
GS-SI/ENG-NA	Claus Schnabel	(248) 876-2533	March 30, 2016

Project DE- EE0005975 REGIS
Subject Final Technical Report For Project End Date 12/31/15

Cover Page

Report Title	Principle Findings from Development of a Recirculated Exhaust Gas Intake Sensor (REGIS) Enabling Cost-Effective Fuel Efficiency Improvement
Type of Report	Final Technical Report
Reporting Period	10/01/12 to 12/31/15
Principle Author	Claus Schnabel Director of Engineering for Exhaust Gas Sensors Diesel and Gasoline Systems North America Robert Bosch LLC
Report Issue Date	03/30/16
DoE Award Number	DE-EE0005975
Submitting Organization	Robert Bosch LLC 38000 Hills Tech Drive Farmington Hills, MI 48331 USA
Disclaimer	The author submits this report knowing the contents will be published and become part of the public knowledge and record.

BOSCH

From	Our Reference	Telephone	Anderson
GS-SI/ENG-NA	Claus Schnabel	(248) 876-2533	March 30, 2016

Project DE- EE0005975 REGIS
Subject Final Technical Report For Project End Date 12/31/15

Contents

From
GS-SI/ENG-NA

Our Reference
Claus Schnabel

Telephone
(248) 876-2533

Anderson
March 30, 2016

Project DE- EE0005975 REGIS
Subject Final Technical Report For Project End Date 12/31/15

1 Executive Summary

1.1 Distribution

Department of Energy	Roland Gravel, Ralph Nine
GS-SI/NA	Schnabel, Etherington, Carwile, Magera, Knipple, Pilgrim, Runge, Roder, Ritz
GS/ENS-NA	Jiang, Schwanke, Jade
CR/RTC2-NA	Oudart
RBNA/GOV	Caruso, Smith, Shannahan
Oakridge	Sluder
Clemson	Prucka

1.2 Subject

REGIS – Recirculated Exhaust Gas Intake Sensor - Final Technical Report for Project Ending Date 12/31/2015.

1.3 Executive Summary Narratives

Kick-off of the Bosch scope of work for the REGIS project started in October 2012. The primary work-packages included in the Bosch scope of work were the following: overall project management, development of the EGR sensor (design of sensor element, design of protection tube, and design of mounting orientation), development of EGR system control strategy, build-up of prototype sensors, evaluation of system performance with the new sensor and the new control strategy, long-term durability testing, and development of a 2nd generation sensor concept for continued technology development after the REGIS project. The University of Clemson was a partner with Bosch in the REGIS project. The Clemson scope of work for the REGIS project started in June 2013. The primary work-packages included in the Clemson scope of work were the following: development of EGR system control strategy, and evaluation of system performance with the new sensor and new control strategy. This project was split into phase I, phase II and phase III. Phase I work was completed by the end of June 2014 and included the following primary work packages: development of sensor technical requirements, assembly of engine test-bench at Clemson, design concept for sensor housing, connector, and mounting orientation, build-up of EGR flow test benches at Bosch, and build-up of first sensor prototypes. Phase II work was completed by the end of June 2015 and included the following primary work pack-

ages: development of an optimizing function and demonstration of robustness of sensor, system control strategy implementation and initial validation, completion of engine in the loop testing of developed control algorithm, completion of sensor testing including characteristic line, synthetic gas test stand, and pressure dependency characterization, demonstration of benefits of control w/o sensing via simulation, development of 2nd generation sensor concept. Notable technical achievements from phase II were the following: publication of two new technical papers by Clemson detailing the control strategies used for the EGR system control. The two papers was published in the 2016 SAE World Congress in April 2016. The titles of each paper are, "Physics-Based Exhaust Pressure and Temperature Estimation for Low Pressure EGR Control in Turbocharged Gasoline Engines," by K. Siokos, and "A Control Algorithm for Low Pressure – EGR Systems using a Smith Predictor with Intake Oxygen Sensor Feedback", by R. Koli. All phase III work packages have been completed. The primary work packages in phase III were the following: completion of long-term sensor durability testing, final demonstration of benefits of EGR control w/o sensing, final decision of the second generation sensor development path.

Phase I work-packages – development of sensor technical requirements, assembly of engine test-bench at Clemson, design concept for sensor housing and connector, build-up of EGR flow test benches at Bosch, build-up of first sensor prototypes – were completed on time and on budget by June 2014. Phase II work-packages – development of an optimizing function and demonstration of robustness of sensor, system control strategy implementation and initial validation, completion of engine in the loop testing of developed control algorithm, completion of sensor testing including characteristic line, synthetic gas test stand, and pressure dependency characterization, demonstration of benefits of control without sensing via simulation on sensor design, development of 2nd generation work plan – were completed on-time and on budget with the exception of demonstration of robustness of sensor. This work-package ran past the planned phase II duration, but was completed during the early part of phase III of REGIS and it was still completed on budget. The reason for the extended duration of this work-package was because of an unexpected EGR gas leak through the sensor housing seal which required detailed study to find mitigating measures. A liquid plastic mold flow analysis was conducted by the supplier of the connector assembly as requested by Bosch. The objective of the analysis was to evaluate and optimize the filling and packing of the assembly. Adequate conclusions and recommendations from the study by the supplier were acquired and were documented in the Q3 2015 report. Phase III work-packages – completion of long-term sensor durability testing, final demonstration of benefits of EGR control w/o sensing, final decision of the second generation sensor development path – were been completed on time and on budget. There were,

however, several findings made during the long-term durability testing work package. The findings are recommended follow-up analyses Bosch believes should be executed if a phase two sensor is kicked-off. The specific findings are documented in section 2.10 below.

1.4 Administrative Status

Completion of this project, including all phase 1-3 work-packages finished on schedule by December 31, 2015 and on budget.

1.5 Budget Status

The total federal budget for the REGIS project is $2,750,000 ($1,311,325 in phase 1, $809,859 in phase 2, and $628,816 in phase 3) and, as of December 31, 2013, $2,750,000 has been obligated by the Department of Energy to the project. As of March 30, 2016, $2,750,000.00 has been booked to the project and, of that; $2,750,000.00 has been invoiced and received.

	Non-Federal	Federal
Actual to date	$ 1,696,686.00	$ 2,750,000.00
Budget	$ 1,696,686.00	$ 2,750,000.00
Remaining	$ 0.00	$ 0.00

Table 1: Project financial summary.

1.6 Project Objectives

The primary objective of this project is to develop an Intake Air Oxygen (IAO2) sensor which directly and accurately measures the oxygen concentration in the intake manifold.

1.7 Scope of Work

This project addressed the technical barriers in fundamental research, technology application, and system implementation to accelerate the development of an IAO2 sensor to directly and accurately measure the oxygen concentration in the intake manifold for gasoline engines using external EGR. Figure 1 below illustrates the tasks allocated to phase I, phase II, and phase III of the project as well as the breakdown of sensor development related tasks and system level related tasks.

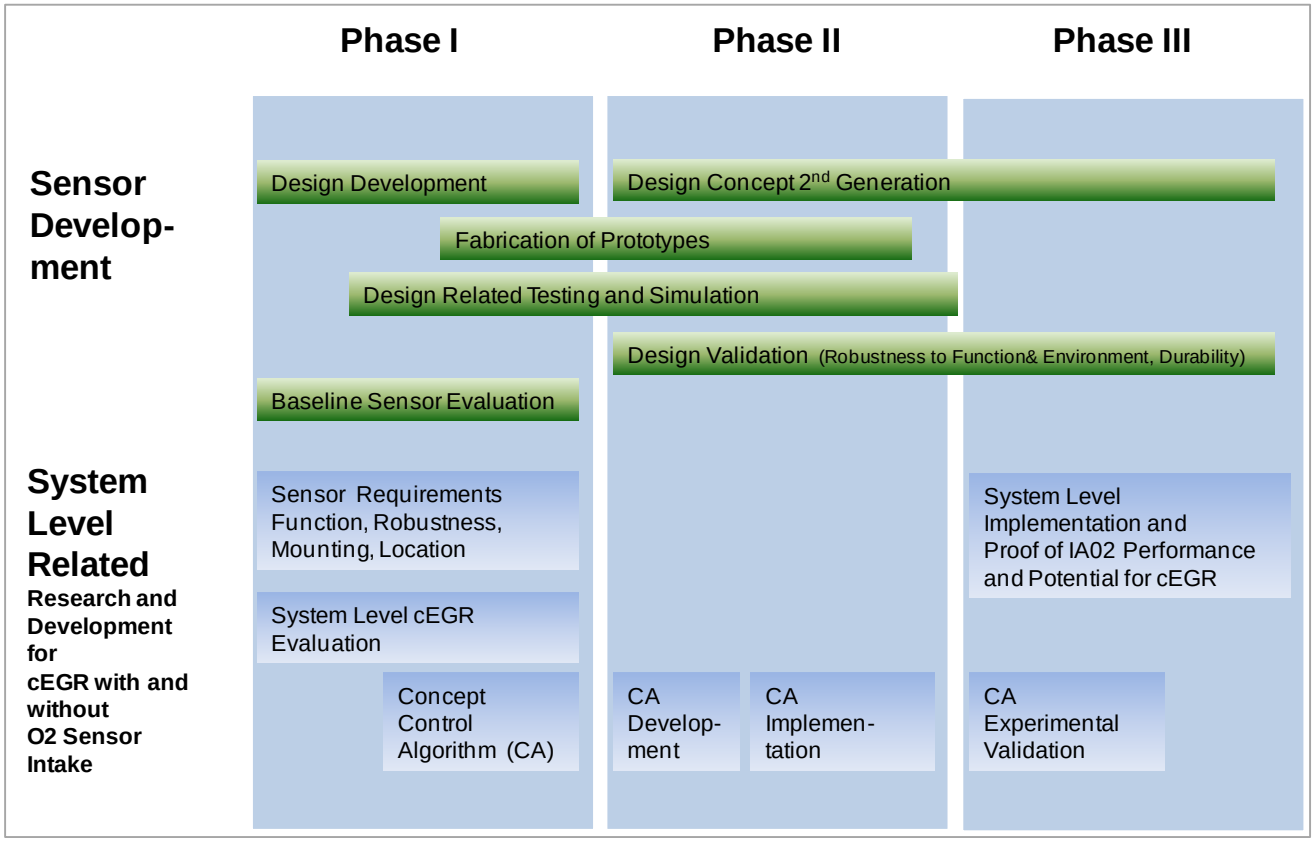

Figure 1: Project Timeline.

1.8 Project Work Package and Milestone List

Tables 2, 3 and 4 below show the complete list of project work packages (tasks) and milestones broken down into phase 1, 2 and 3 including work package (task) and milestone ID number, work package name, description, and status at project close. In tables 2, 3 and 4 T indicates a work-package (task) and MS indicates a milestone.

				Phase 1			
	T 1.0			**Project Man-agement**		green	done.

	T 1.1			**Baseline Sensor Evaluation and Development of Testing Procedure**		green	done.
	T 1.2			**cEGR System Level Evaluation**		green	done.
	T 1.3			**Controls**		green	done.
	T 1.4			**Sensor Housing and Mounting System Design**		green	done.
	T 1.5			**Requirements for Sensor Location**	For HP and LP EGR following tasks have to be followed through 1. Define sensor positions (in inlet runner, in manifold, before throttle, before intercooler) 2. What needs to be assessed: pressures, temperatures, velocities, homogeneity and exposure to contaminates and their influence on functional (response time, accuracy) and mechanical (thermal management, thermal shock) with CFD and experiment as best seemed fit 3. Define needed requirements 4. make recommendation on sensor position	green	done.

Table 2: Work package description and status (phase 1).

			Phase 2			
	T 2.0		**Project Management and Reporting**		green	done.
	T 2.1		**Robustness of Function**			
			Accuracy	Study impact of fuel including E15-E85 and their impact on signal accuracy	green	done.
		MS 2.1	Assessment of Sensor Accuracy	Quantifying the impact of multiple HCs found in intake on signal accuracy. Composition was derived from exhaust and purge gases seen for gasoline and gasoline ethanol. mixtures	green	done.
	T 2.2		**Optimizing Function and Robustness of Sensor**			
			Design Optimization for Function	Transient response of the new sensor designs was evaluated with gasoline engine testing at Clemson, and verified at ORNL, to enable improvements to the sensor and the control strategy. This will improve the overall real-time control capability.	green	done.
			Design Optimization for Robustness	Identification of Designs ensuring robustness against thermal shock and intake contaminates (soot water oil emulsions)	green	done.
			Thermal Shock Robustness	Two high volume test benches was used to enable thermal shock testing under intake conditions with and without simulation of pressure oscillations. A test profile describing the sensors exposure to water in the intake was developed on basis of the results of WP 1.2.8 and refined throughout the project. A method to quantify	green	done.

				protection from thermal shock was developed. The thermal shock resistance of the baseline sensor was evaluated with these tests and the test procedure used to evaluate progress in design work.		
		MS 2.2	Demonstration of improved functionality and robustness of the optimized sensor.		green	done.
	T 2.3		**EGR System Evaluation and Control Development**			
			Control Strategy Development - Air Path EGR Control	Characterization of pressure pulsation effects as well as static pressure differential on EGR flow. Used to create comparison to delta pressure sensor (Bosch) and to allow for better pre-setting of the valve. Determine necessary changes to classical throttle equation (KLAF)	green	done.
			Control Strategy Development - Sensor fusion and transient control	Fuse sensor signal with improved modeled EGR flow based on analysis of classical throttle equation and system pulsations. Develop transient control strategy for spark and cam position based on the modeled air path delays for cylinder-to-cylinder transient prediction (WP 2.3.2)	green	done.
			Control Strategy Development - Ethanol and water detection	Study ORNL data showing the effects of water and ethanol on the sensor and develop an on-line algorithm to use the sensor to identify the water content in ambient air and EGR based on water cracking phenomena.	green	done.
			Cylinder-by-Cylinder Transient Prediction	Modeling of transport delays in EGR system. GTPower modeling done to predict the distri-	green	done.

				bution in the engine based on physical phenomon. Creation of control logic to realize this on a RP system.		
			Control Validation and Optimization	Engine-in-loop testing of the algorithms using rapid prototyping	green	done.
			Engine Combustion Characterization	Clemson will perform a sensitivity analysis of the sensor EGR estimation accuracy and analyze the impact of the baseline series sensor on fuel economy. ORNL will investigate several steady-state operating modes on a modified Ecotec engine, similar to the Clemson engine, to examine the potential efficiency improvements high EGR levels provide. ORNL will also monitor changes in the engine emissions and in-cylinder pressure as a combustion process metric as the EGR rate is varied. EGR efficiency curves was developed to further estimate the benefit of closed loop EGR control and determine maximum EGR rates for inclusion in control algorithm development. Clemson will lead the efforts in the part-load driving cycle conditions, and ORNL will lead the efforts in high-load conditions for knock mitigation strategies.		
		MS 2.3	EGR Estimation Model and EGR control algorithm	Experimental validation results of the EGR estimation model Demonstration of proposed control functionalities using rapid prototyping	green	done.
	T 2.4		**Build IA02 Sensors**			
			IA02 Sensor Assembly	Assemble IAO2 sensors for testing	green	done.
			IA02 Sensor Validation	Perform standard sensor testing including characteristic line, synthetic gas test stand, pressure dependency measurements to verify performance	green	done.

		MS 2.4	IA02 Prototypes	Complete IAO2 sensors for performance and robustness testing	green	done.
	T 2.5		**Sensor Element Concept (improved cost and functionality)**	**Research 2nd generation sensor element concept for improved cost and functionality, this will also be part of phase II and phase III work**		
			2nd Generation Sensor Element Concept	Based on understanding the intake manifold requirements gained from intake manifold environment analysis and control strategy development, the objective is to develop concept for 2nd generation sensor element to meet these requirements	green	done.
		MS 2.5	Concept for 2nd generation sensor element	Overview of possible design options for improved sensor design, Overview of chosen design	green	done.
		MS 2	Review Phase 2		green	done.

Table 3: Work package description and status (phase 2).

			Phase 3			
	T 3.0		**Project Management and Reporting**			
		MS 3.0	Quarterly progress reports and phase review presentation		green	done.
	T 3.1		**EGR System Evaluation and Control Development**			
			Control Algorithm Integration	Based on the algorithm validation results at Clemson, the target control algorithms to be integrated was determined. The real-time control algorithms was	green	done.

				integrated into the Bosch MED software if beneficial for the progress of the project.		
			Experimental Validation of Control Algorithm - Transient Fuel Control	Conduct engine tests to determine performance, fuel economy, and emissions comparing the baseline hardware and software condition to the IAO2-equipped condition.	green	done.
			Experimental Evaluation of EGR and IAO2 Sensor Benefits	Conduct engine experiments under drive-cycle conditions to evaluate the benefits of EGR system and the additional sensor on fuel economy, emissions, and performance	green	done.
		MS 3.1	Finalized control strategies validated on engine dynamometer		green	done.
		MS 3.2	Demonstration of potential fuel economy improvement and emissions performance achieved with IAO2 compared to a model-based EGR control strategy		green	done.
	T 3.2		**Long-Term Durability Testing (Bosch)**			
			Test Preparation	Design Validation (DV) test specification to be prepared to demonstrate robustness of IAO2 sensor to soot contamination and water thermal shock, as well as thermal and vibration stresses found in the intake under continual lean conditions.	green	done.
				*Different bench scenarios was used instead of engine dyno to achieve more comprehensive results over lifetime. Approach		

				had been confirmed during Q1/2015 project review.		
			Durability Testing	Perform DV test to confirm life-time robustness of the developed sensor.	green	done.
				*Different bench scenarios was used instead of engine dyno to achieve more comprehensive results over lifetime. Approach had been confirmed during Q1/2015 project review.	green	
		MS 3.3	Present durability testing results		yellow	done.
	T 3.3		**Concept 2nd generation IAO2 sensor**			
		MS 3.4	Concept for 2nd generation sensor	Overview of possible design options for improved sensor design, Overview of chosen design	green	done.

Table 4: Work package description and status (phase 3).

1.9 Summary of Primary Project Accomplishments

The following list summarizes the primary accomplishments achieved during phase 1, 2, and 3 in this project.

COMPLETED WORK PHASE I

- Design concept for IAO2 sensor connector and housing complete.
- Developed requirements and references for developing bench and endurance tests.
- Flow test benches build and / or adjusted for sensor evaluation.
- Engine assembled at Clemson.
- Procured components to build IAO2 prototypes.
- Built IAO2 prototypes.
- Engine and simulation work for system evaluation and control development.
- Testing and Validation IA02 sensor on engine and test bench.
- Development of technical requirements sensor.

COMPLETED WORK PHASE II

- Robustness in Function.
- Build and Design of Engine Durability Run for fouling.
- Procured components to build IAO2 prototypes.
- Development of fouling investigation process across a wide range of parameters.
- Recursion of the design to improve sealing.
- Completed ignition risk studies on Natural Gas applications.
- Control strategy refinement.
- Demonstration of benefits of control w/o sensing via simulation.
- IAO2 2nd Generation work plan.
- Completion of fouling testing.
- Control strategy implementation and initial validation.
- Built of IAO2 for Phase III work.
- Completion of engine in the loop testing of developed control algorithm.
- Completion of sensor testing including characteristic line, synthetic gas test stand and pressure dependency.

COMPLETED WORK PHASE III

- Specification of test plan for long-term durability validation.
- Execution of long-term durability validation of IAO2 sensor.
- Implementation of cEGR control strategy in Bosch ECU.

- Demonstration of benefits of control w/o sensing.
- Study of possible second generation designs.

2 IA02 Component Package Development

2.1 Sensor Housing and Mounting

The IAO2 sensor is based on an existing Bosch oxygen sensor design. The baseline sensor is a traditional threaded sensor with a wire harness. The goal of the IAO2 sensor is to have a non-threaded mounting and a direct connection to the vehicle wire harness, thereby eliminating the pigtail attached to the sensor.

The traditional exhaust gas oxygen sensor has a well-defined set of requirements based on the exhaust environment. The exhaust gas can be very hot – over 1000°C. These temperatures lead to design and material choices for robustness in that environment. In the intake environment, the working gas is at much lower temperatures – about 200°C. At these temperatures different materials and design configurations can be made. The largest thermal issue for the intake sensor actually comes from the self-heating of the sensing element. This heat must be dissipated to the environment.

The four main subsystems of the sensor was modified to take advantage of the application environment for the IAO2. The short sensor holds the sensing element in place and is the anchor for the other systems. The protection tube protects the sensing element from water, oil and the EGR particles in the intake air. The mounting components attach the sensor to the engine. The electrical connection provides power to the sensing element as well as conducting the signal to the vehicles ECU. The electrical connection also provides environmental sealing to the sensor from the under-hood environment.

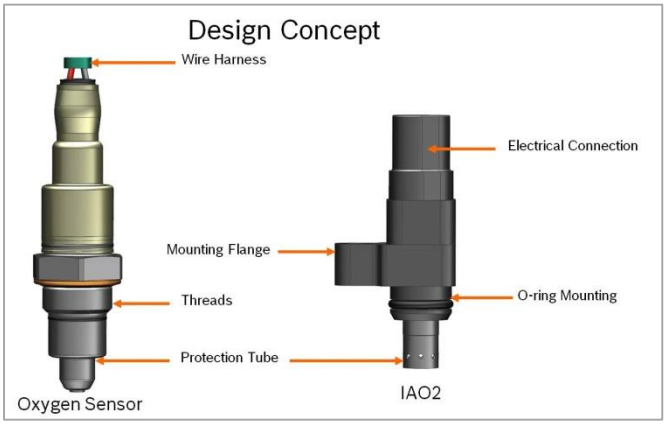

Figure 2: Comparison of traditional Oxygen Sensor to IAO2.

2.2 Initial Design Concepts

During the design process the concept evolved to accommodate for the intake environment. Due to space constraints of the under-hood environment and lower environmental temperatures, there is an opportunity to change from the traditional wire harness concept for oxygen sensors towards more of an integrated connector concept that is employed on many sensors in the engine compartment. This type of design is usually accomplished with a plastic housing and connector, however due to the high operating temperatures of the sensing element there was heat concerns with using plastics and its use will have to be carefully considered in new designs. Other design considerations include the mounting method, element protection and electrical connection.

The first design concepts included a short sensor that holds the sensing element and serves as the basis to mount other components. The first concept seen in figure 3 joins the short sensor to a connector and flange mount over-molded with a lead-frame.

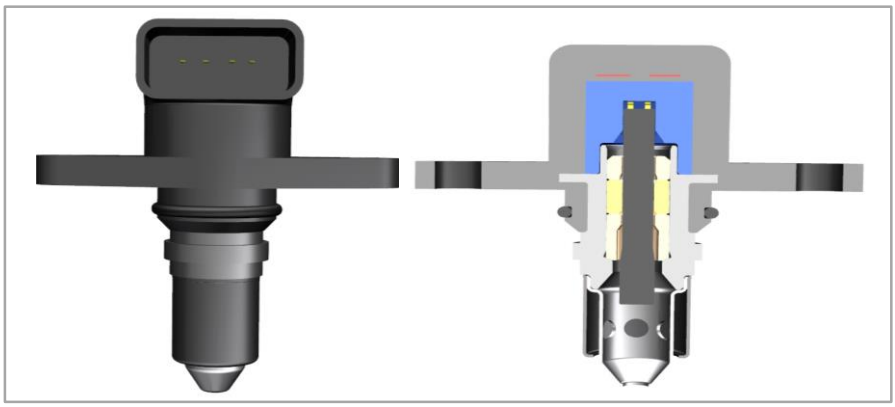

Figure 3: Flange and Connector Over-mold Concept.

Prototypes for this design were created for the purpose of temperature testing. The prototypes were made with a machined housing, rapid prototype connector pieces, and existing oxygen sensor components. Results from temperature testing indicate that plastic materials are not suitable to handle the temperatures generated by the sensing element at the flange location as well as the contact end of the element.

The next design concept, seen in figure 4, utilizes a turned housing for the short sensor and incorporates a stamped or machined metal flange which would be assembled to the short sensor. This flange concept has the advantage of improving the heat robustness and because the flange is assembled to the short sensor separately it allows for other mounting concepts to be easily interchanged without much redesign of the base sensor. The plastic housing for this sensor was created to mate with the short sensor and the sensor element in one step, which would simplify the assembly process. The plastic material in this design had been moved further from the heat source to prevent melting.

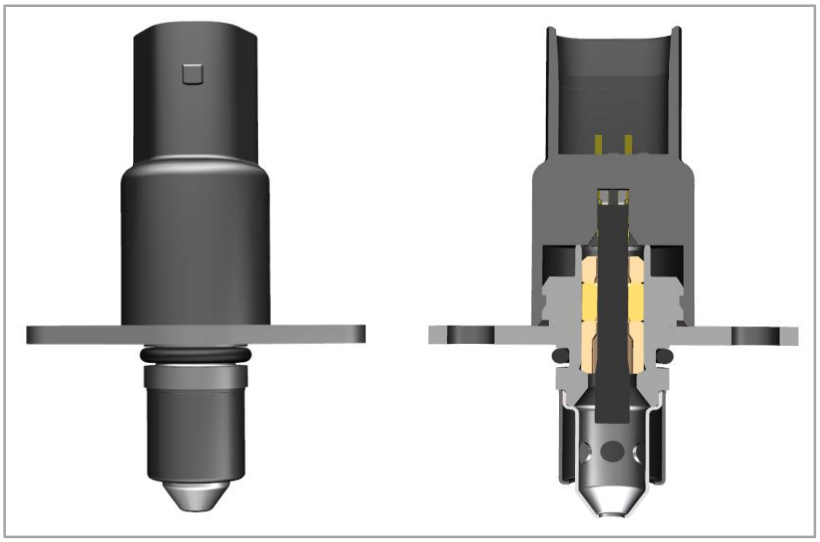

Figure 4: Snap Fit Plastic Connector Housing with Integrated Contacts.

Prototypes for this design were created for the purpose of temperature testing. The prototypes were made with a machined housing, rapid prototype connector pieces, and existing oxygen sensor components. Results from temperature testing indicate that plastic materials are not suitable to handle the temperatures generated by the sensing element at the contact end of the element.

The next design concept, seen in figure 5, utilizes a turned housing for the short sensor and incorporates a stamped or machined metal flange which would be assembled to the short sensor. This concept is similar to the concept seen in figure 4, however the design of the connector housing had been changed to incorporate a ceramic contact assembly that is used in existing oxygen sensors which are designed for high temperatures. The plastic housing for this sensor was created to mate with the short sensor and the sensor element in one step, which would simplify the assembly process. The plastic material in this design had been moved further from the heat source to prevent melting.

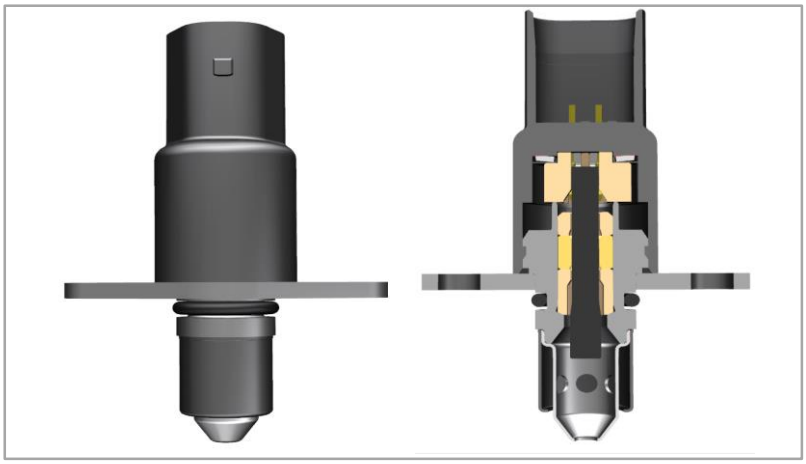

Figure 5: Snap Fit Plastic Connector Housing Contact Holder Assembly.

Prototypes for this design were created for the purpose of temperature testing. The prototypes were made with a machined housing, rapid prototype connector pieces, and existing oxygen sensor components. Results from temperature testing indicate that plastic material mated to the short sensor is a marginal solution and may not be suitable long term.

The next design concept, seen in figure 6, utilizes a turned housing for the short sensor and incorporates a stamped or machined metal flange which would be assembled to the short sensor. This concept is similar to previous designs, however the design of the connector housing had been changed to incorporate a ceramic contact assembly and metal sleeve that is used in existing oxygen sensors which are designed for high temperatures. The plastic connector housing for this sensor would be over-molded with the protective metal sleeve and lead frame assembly. The plastic material in this design had been moved further from the heat source to prevent melting.

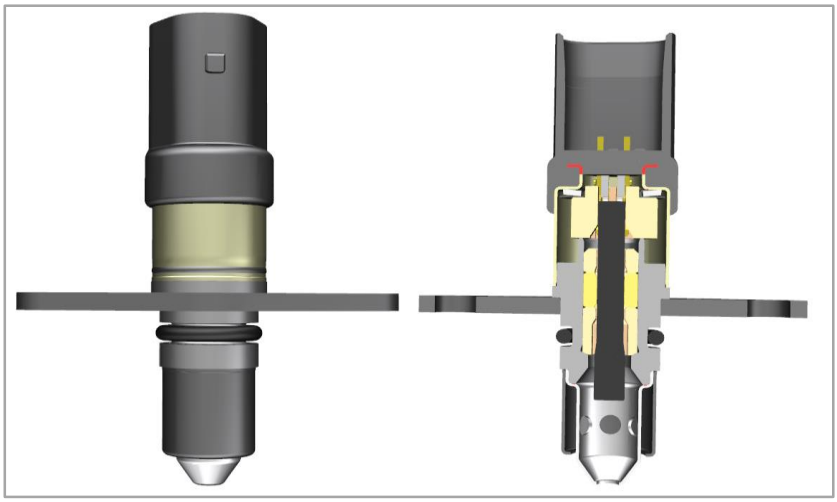

Figure 6: Welded Metal Sleeve with integrated plastic over-mold connector.

Prototypes for this design were created for the purpose of temperature testing. The prototypes were made with a machined housing, rapid prototype connector pieces, and existing oxygen sensor components. Results from temperature testing indicate that plastic material mated to the protective sleeve allows for better heat dissipation and brings temperatures within a range that would allow for the use of some high temperature thermoplastic materials.

The next design concept, seen in figure 7, utilizes a turned housing for the short sensor and incorporates a stamped or machined metal flange which would be assembled to the short sensor. This concept is similar to the previous design seen in figure 6, however the design of the connector housing had been changed to a right angle design to allow for more space in the engine compartment. The plastic connector housing has been designed to be over-molded with a lead-frame terminal set and the protective metal sleeve.

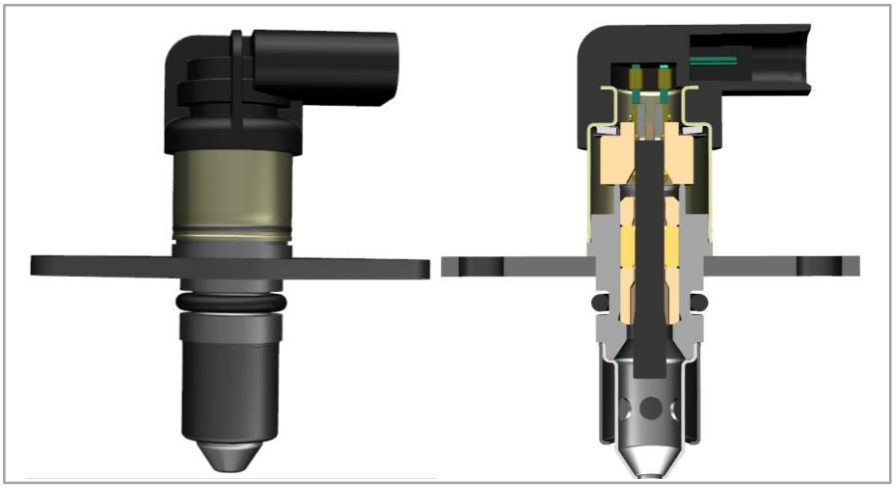

Figure 7: Design Concept.

Prototypes for this design were created for the purpose of temperature testing. The prototypes were made with a machined housing, rapid prototype connector pieces, and existing oxygen sensor components. Results from temperature testing indicate that plastic material mated to the protective sleeve allows for better heat dissipation and brings temperatures within a range that would allow for the use of some high temperature thermoplastic materials. New prototypes are being made with molded connector halves in different materials and further ongoing testing was done with these prototypes. One area of concern with this design is the seal created between the over-molded plastic connector housing and metal sleeve. Due to differing thermal expansion rates and poor adhesion strength a leak path may be created due to thermal cycling. This will have to be considered in future designs.

2.3 Protection Tube Optimization

Sensor function and durability are direct results of the sensor protection tube and its ability to not only protect the sensing element from contaminants but also pass the sampling gas across the sensing element. The IAO2, as designed, provides the opportunity to utilize a directionally fixed protection tube. All other protection tubes give up a level of function in the sense the tubes must be operable at any installed angle. The flange mount for the IAO2 fixes the installation orientation and thus permits directional installation.

The IAO2 utilizes a cyclone separator style tube for protection and operation. This protection tube was designed and further optimized utilizing Design for Six Sigma strategy and can be seen below in figure 8.

Figure 8: Protection tube.

This concept was tested for function and deemed sufficient to continue development. The further development of this tube centers around providing positive results as related to: Sensor switch time, heater power demand, water thermal shock protection for the element and robustness to soot development. Taking these requirements into consideration, control factors were established and a test and designing matrix was established to measure and analyze the individual impact of each of the control factors on the overall sensor performance. Figure 9 shows the variants that were tested.

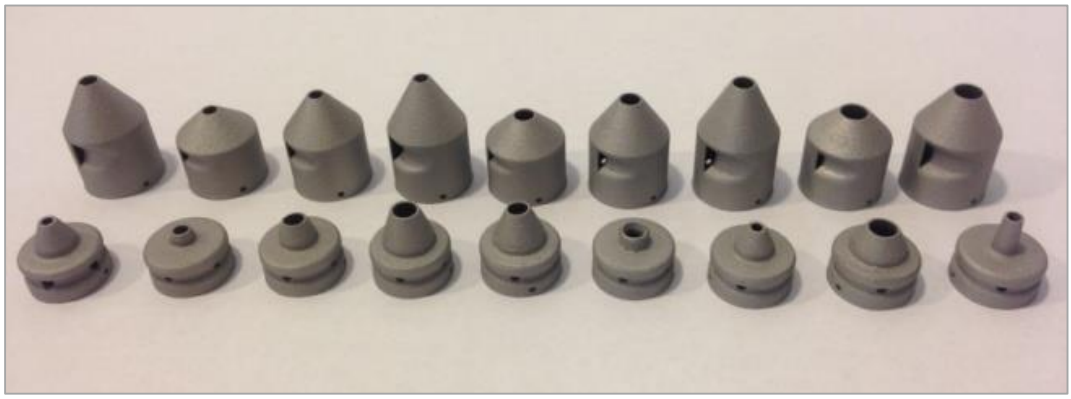

Figure 9: Protection tube variants

The combinations of inner and outer protection tubes were assembled and tested and the results were used to select the ideal combination of control factors that provide the most benefit to

the performance of the protection tube. Figures 10-12 show graphical representations of some of the data generated during the functional testing.

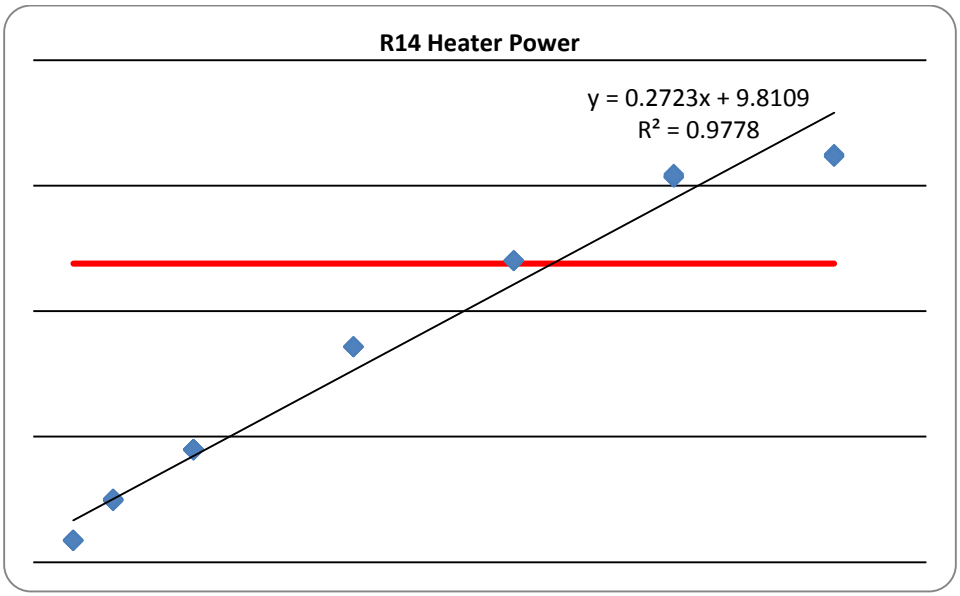

Figure 10: Heater Power Consumption.

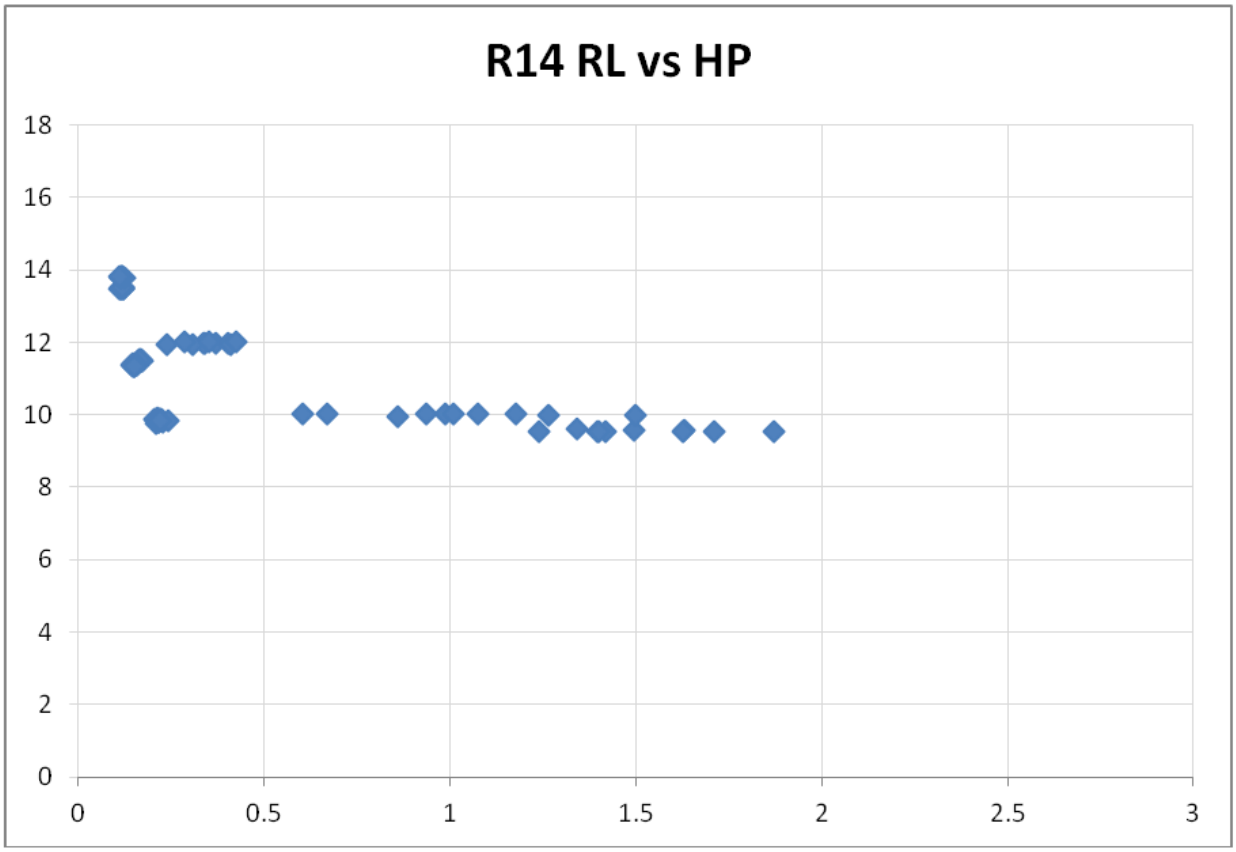

Figure 11: Response Time.

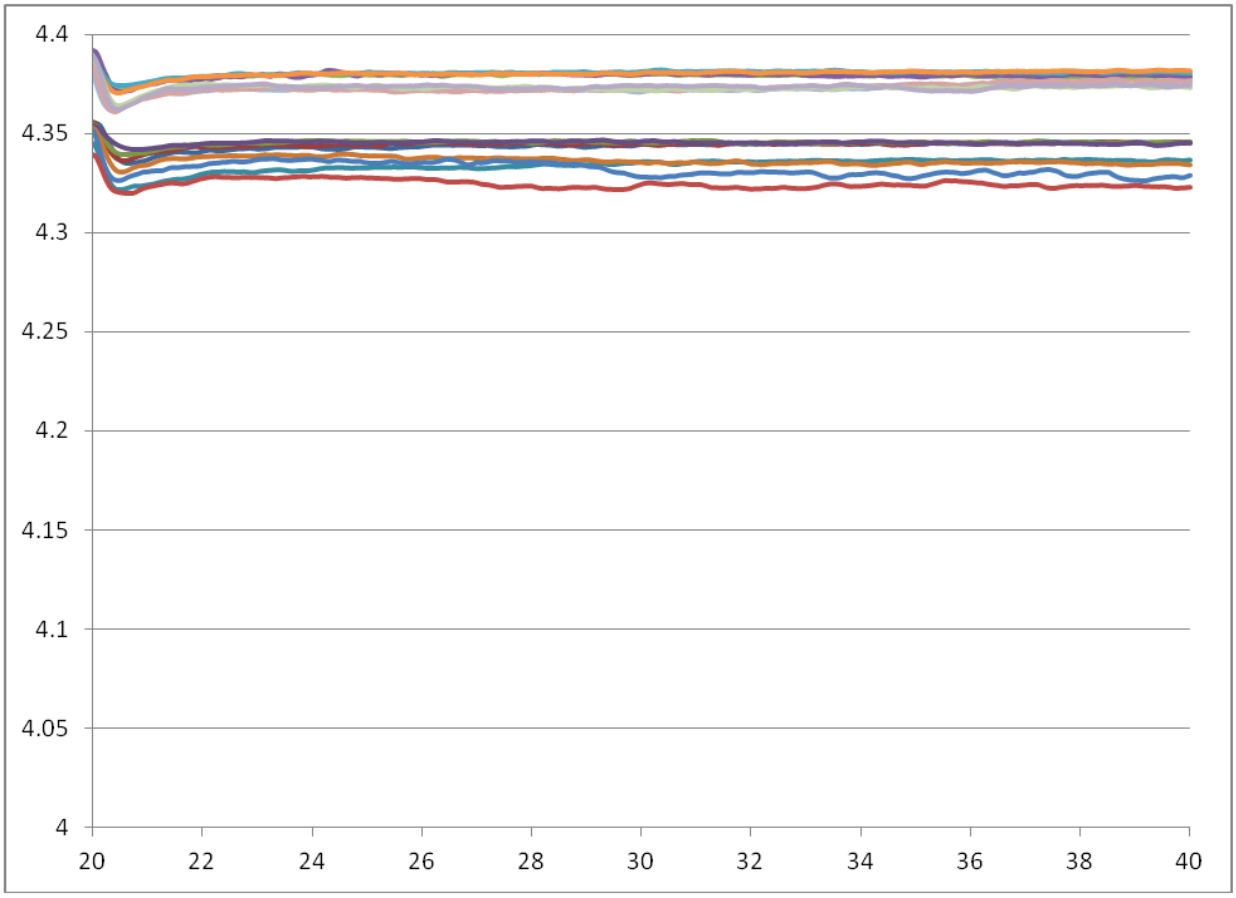

Figure 12: Thermal Shock Resistance.

The influence of each of the control factors was analyzed for the effects on sensor function and performance. From this analysis the control factors was combined into one design and this was the optimized protection tube.

2.4 Sensor Location

While evaluating the impacts of sensor location on cEGR control, it is important to understand the dynamic response time of the LSU-IM1 sensor. Unlike normal lambda sensor applications, the concentration of inert material and the temperature of the gas within the intake environment are very low. Response time is a paramount concern for sensing the presence of externally introduced exhaust gases since a large error can result in engine misfire or flameout. A flow

bench, as shown in **Error! Reference source not found.**2, was established to allow the introduction of inert gas (nitrogen) in precise quantities.

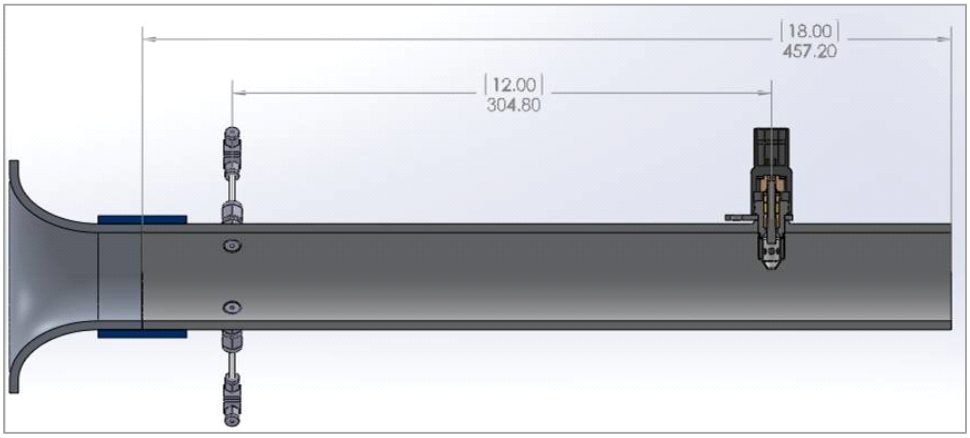

Figure 13: Layout for transient testing. LSU is located downstream of a CNG PFI injector connected to a nitrogen source. Dimensions shown in [inches] and mm.

Testing has been conducted for LSU-IM1 sensor with a standard protection tube designed for the exhaust gas sensing application and compared to a sensor without a protection tube. The testing results have indicated that the sensor with the standard protection tube leads to a first-order response time of 2.5 times longer than that of a sensor without protection tube. Design efforts are currently on-going to optimize the design of protection tube for the application of sensing in the intake manifold. In the mean-time, engine simulation efforts was conducted to understand the impacts of such dynamic response time on cEGR control. The task of sensor location determination has started. Location data is also being collected from potential users of the IAO2 sensor.

2.5 Prototype Sensor Fabrication

A critical element for the assembly process is the pressing and welding operation. There are three operations that will require fixing and welding of components: Protective sleeve to housing, flange to housing and the protection tube to housing. Test parts were machined to represent the actual parts. These test parts were used to validate that the laser welding process works for fixing and sealing the necessary components. The next steps are to design and build the requisite tooling for the protection tube press operation. Since this is a known process for the currently produced sensor, there is no concern related to our ability to execute this step. As purchased components are received,

quantities of 6 are pulled along with the drawing and a full dimensional evaluation is conducted to ensure the parts meet the design. Any deviation was fed back to the design team such that replacement parts can be ordered or the deviations may be incorporated into the design. No deviations have been found thus far.

Purchased components for the IAO2 were received dimensionally verified prior to the build. All purchased parts met the print and no unplanned modifications were required in order to obtain proper fitment.

During the evaluation phase of the on line and off line assembly process, it was determined the existing production line could not be used for prototype assembly due to tooling space restrictions that are created by the features unique to the IAO2 such as the flange and the over-molded housing. This necessitated the focus to be directed to off-line assembly methods. Various fixtures and part holding mechanisms were built and validated for effective operation. Of these, the most suitable were selected and refined.

Short sensor assembly and protection tube welding is an established process and further development was not required.

Maintaining the desired press force during welding was accomplished by using specially designed tooling that fixes the orientation of the components and also holds a load cell for dialing in the specified loading.

2.6 Thermal Shock Resistance Testing

To assess the robustness of the sensor to liquid water, the distribution of water in the intake needs to be understood. Water can come from several sources – liquid water passing through the air filter, condensed water from the exhaust collected and discharged by the charge air cooler and water condensed from the air flowing past the throttle into a low pressure region.

For the thermal shock resistance testing of the baseline exhaust sensor protection tubes (PT1 and PT2) and the design optimization of the new protection tube, a prototype test stand was designed and built by the oxygen sensor engineering group in Anderson, SC. Once the test stand was assembled, air speed measurements were recorded at the sensor test position for the available power settings on the blower and the flow rates of both water injection nozzles were determined at multiple pressure settings to ensure that testing could be completed according to

customer and Bosch internal specifications. Then experiments were run to determine the optimum set-up parameters for air and water flow rates, pulsation speed, water nozzle position, test duration and water cycle in order to evaluate the performance of the different protection tubes. With the test procedure established, the test bench was validated for repeatability by completing ten test runs on a new protection tube design with the same input parameters for each run.

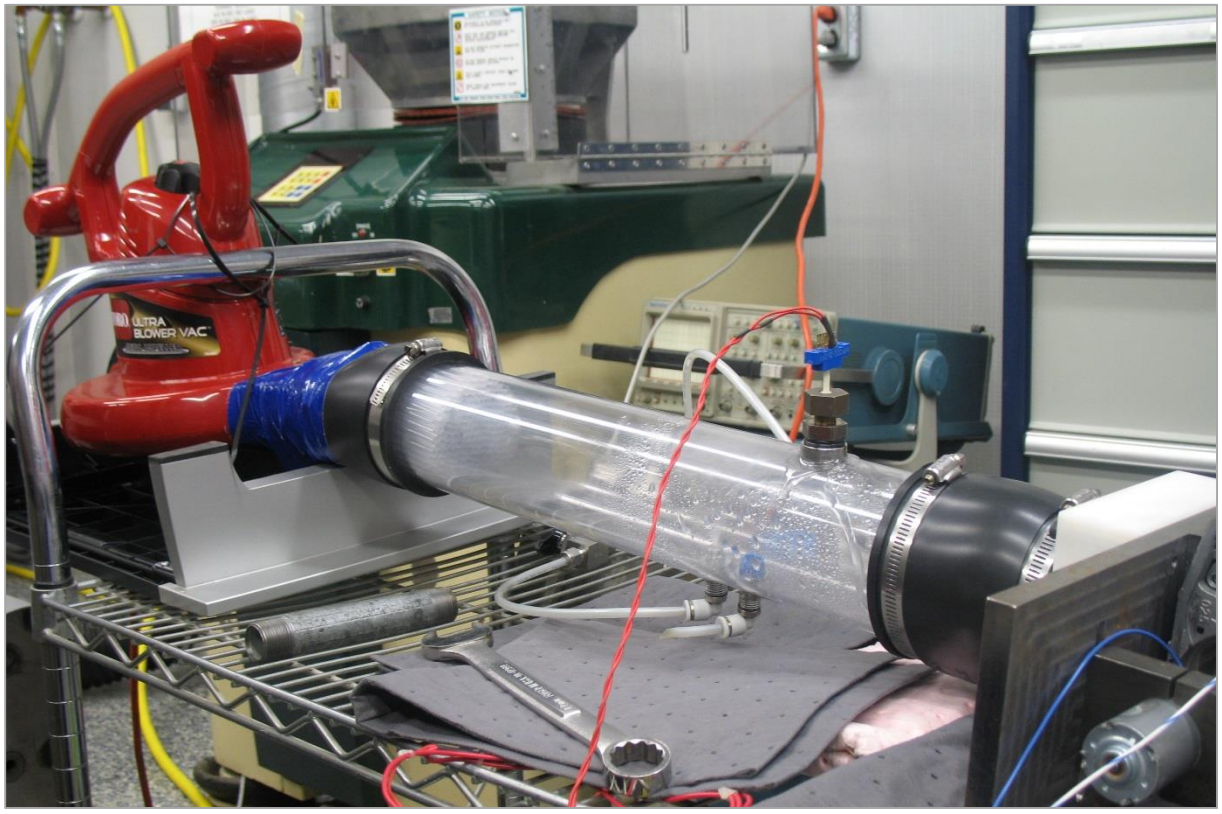

Figure 14: Prototype Thermal Shock Test Bench (initial set-up).

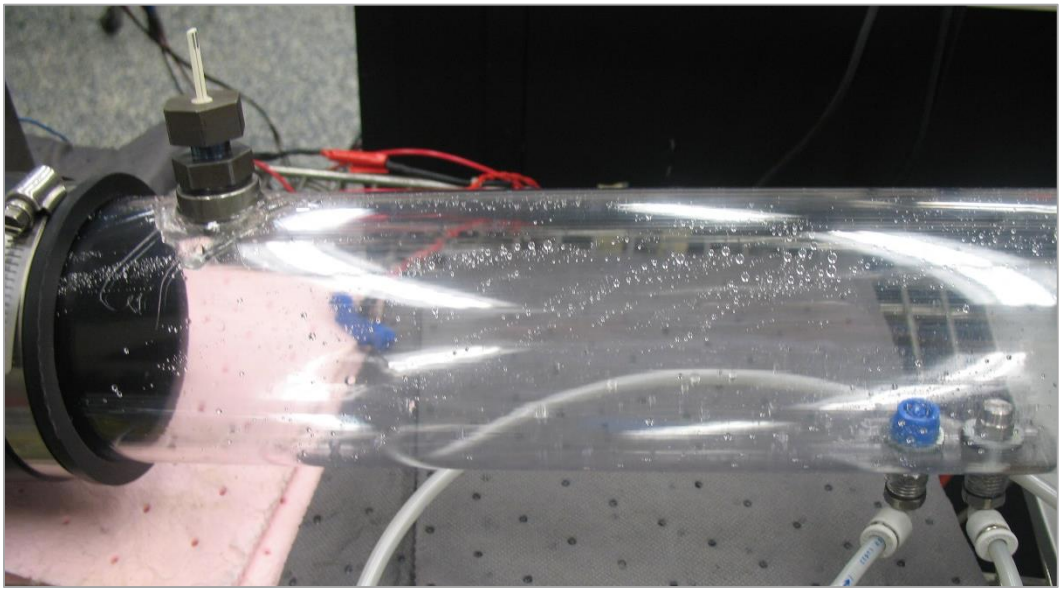

Figure 15: Prototype Thermal Shock Test Bench (final position of water nozzles).

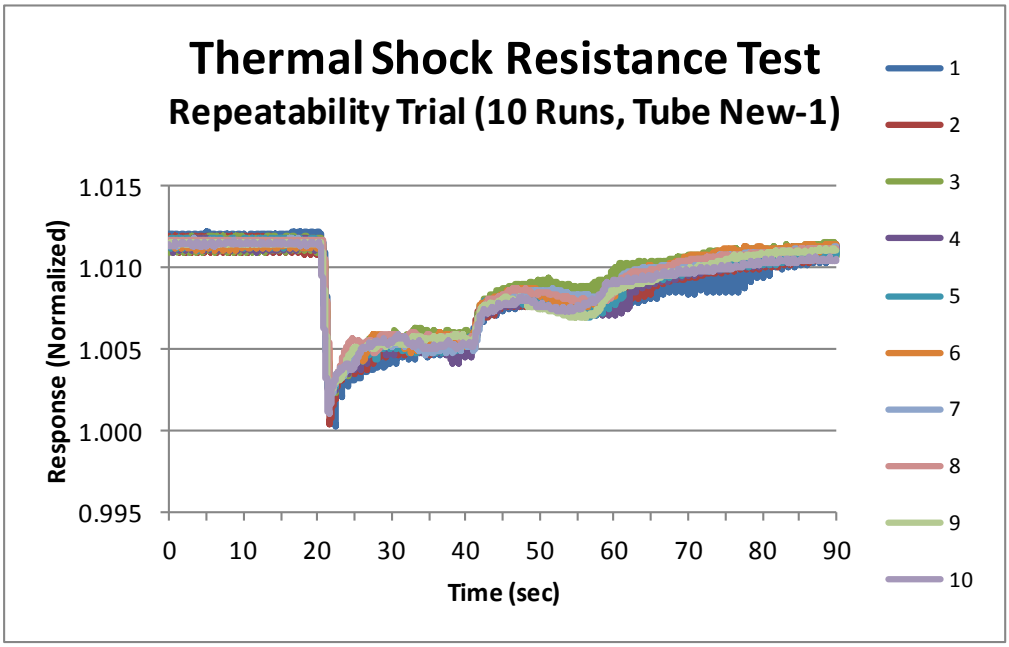

Figure 16: Thermal Shock Test Bench Repeatability Trial Results.

Then two test runs were completed using the same input parameters with two different protection tubes (New-1 and New-2) to determine if there was separation between the designs.

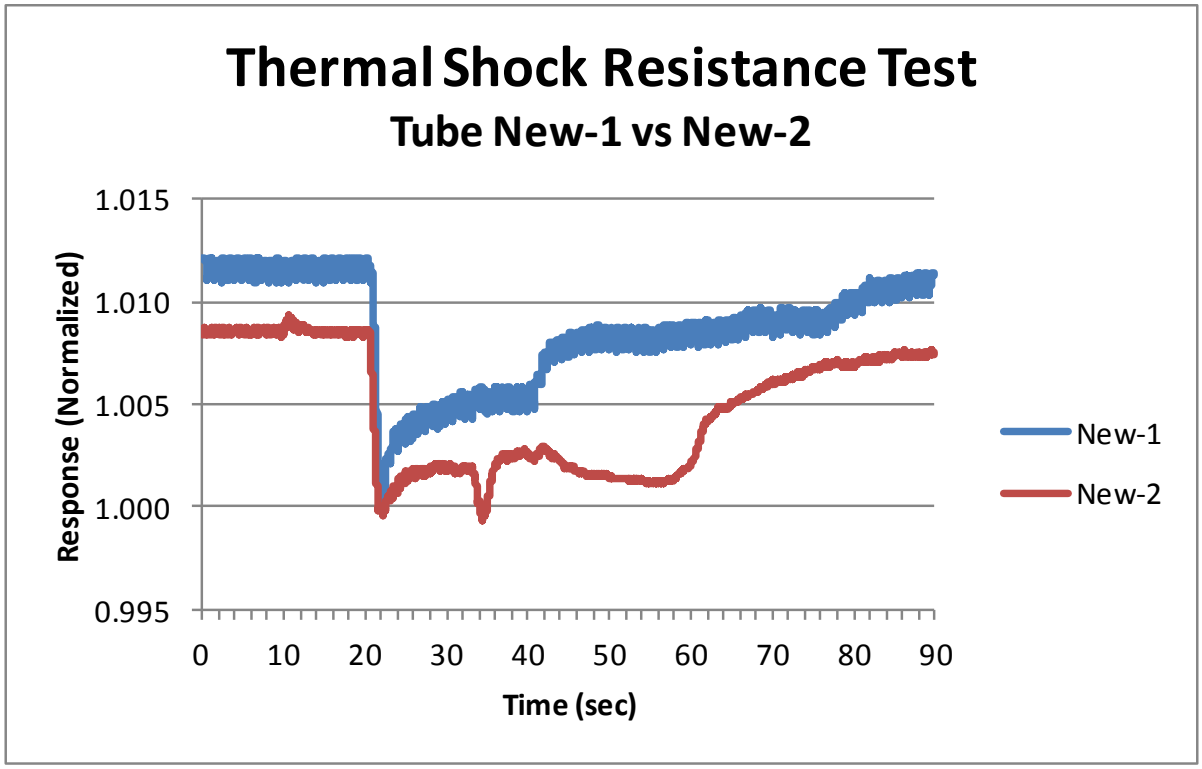

Figure 17: Thermal Shock Test Bench Trial with New Design Protection Tubes.

For B-sample protection tube evaluation, the flow bench test stand in Bosch Anderson, SC mentioned in the section above was modified to add thermal shock testing capability. This test stand will allow parts to be tested at lower air velocities (simulating car idle condition), give a more constant air flow rate and have real time monitoring of air speed and pressure. The initial design concept for the piping and sensor mounting has been agreed to by the team. The water injection system and final design was completed at the beginning of the 1st quarter 2014 so that test bench was ready by the beginning of the next quarter. In addition, thermal shock testing was validated on an engine at Oak Ridge National Laboratory (ORNL) using a water injection system.

The customer requirements gathered for the intake manifold environment related to water amount and flow rate for thermal shock vary to a large degree and should be verified by the Bosch application engineering group with the different customers before test parameters are established to validate the IAO2 sensor. Confirmation of intake manifold conditions was performed at ORNL on an engine. Thermal shock as well as contamination testing on engine will assess the robustness of the IAO2 to this environment.

2.7 Contamination Testing

A flow bench was used to conduct contamination tests on the IAO2 sensor at ORNL. The intake manifold that will hold the test sensors is currently being constructed. The first study will determine the effect of water in the intake gas on the sensor. The first part of the experiment will measure the sensor response as the percentage of water is increased as the percentage of N2 is decreased in steady increments. The second group of tests measure the sensor output as the EGR amount is steady increased. The second study will measure the cross-sensitivity of the sensor to various concentrations of CO, NO_x, C_3H_6 and NH_3.

2.8 Water Condensation Management

Due to the substantial cooling of the EGR in some extreme operating conditions, there is the possibility of water saturation/condensation downstream the EGR cooler. Water condensates could be harmful to the intake oxygen sensor and affect the oxygen measurement accuracy. For that reason, a first study on water saturation has been conducted using the GT-Power model. Using a DoE approach to sweep through different ambient temperatures, EGR fractions and exhaust gas temperatures downstream the EGR cooler, the water saturation effect was identified. Figure 1818 demonstrates the water partial pressure of the working fluid as a function of temperature as it passes through the various components of the EGR configuration. It is evident that several operating conditions can be found where the working fluid is below the saturation line and condensation occurs.

Figure 1919 shows the actual simulation results on water condensation. Three different locations in the LP EGR path are being shown. Downstream the EGR cooler and before mixing with air, the most important parameter for water condensation is the EGRcooler_Out temperature. Below 60°C, condensation will probably occur for every EGR dilution. After mixing with air and upstream of the compressor, the main parameter that dictates condensation is the ambient temperature since air is the main component of the mixture. For EGR dilution above 10%, ambient air temperature less than 3°C will cause condensation (EGRcooler_Out temperature=85°C is assumed). Finally, downstream the compressor, the working fluid's elevated pressure drives the

mixture above the saturation line and thus much colder ambient temperatures are required for the water to condensate.

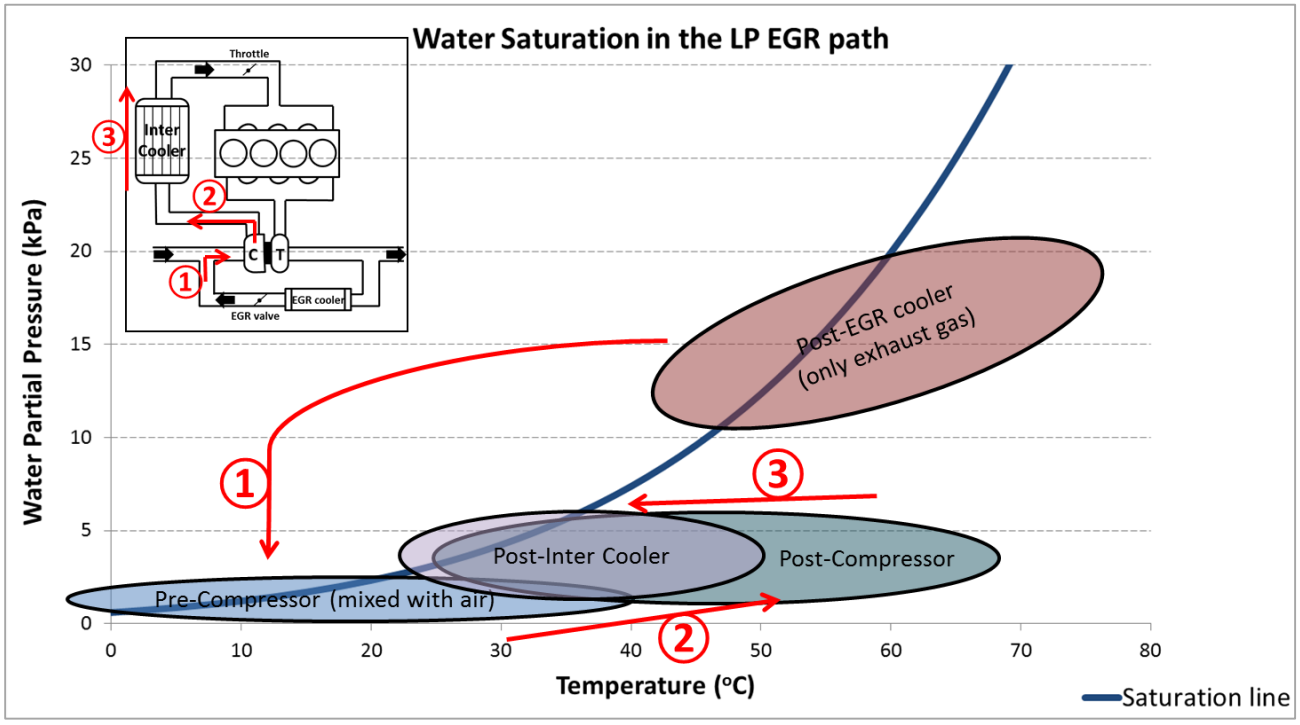

Figure 18: Water saturation in the Low Pressure EGR path

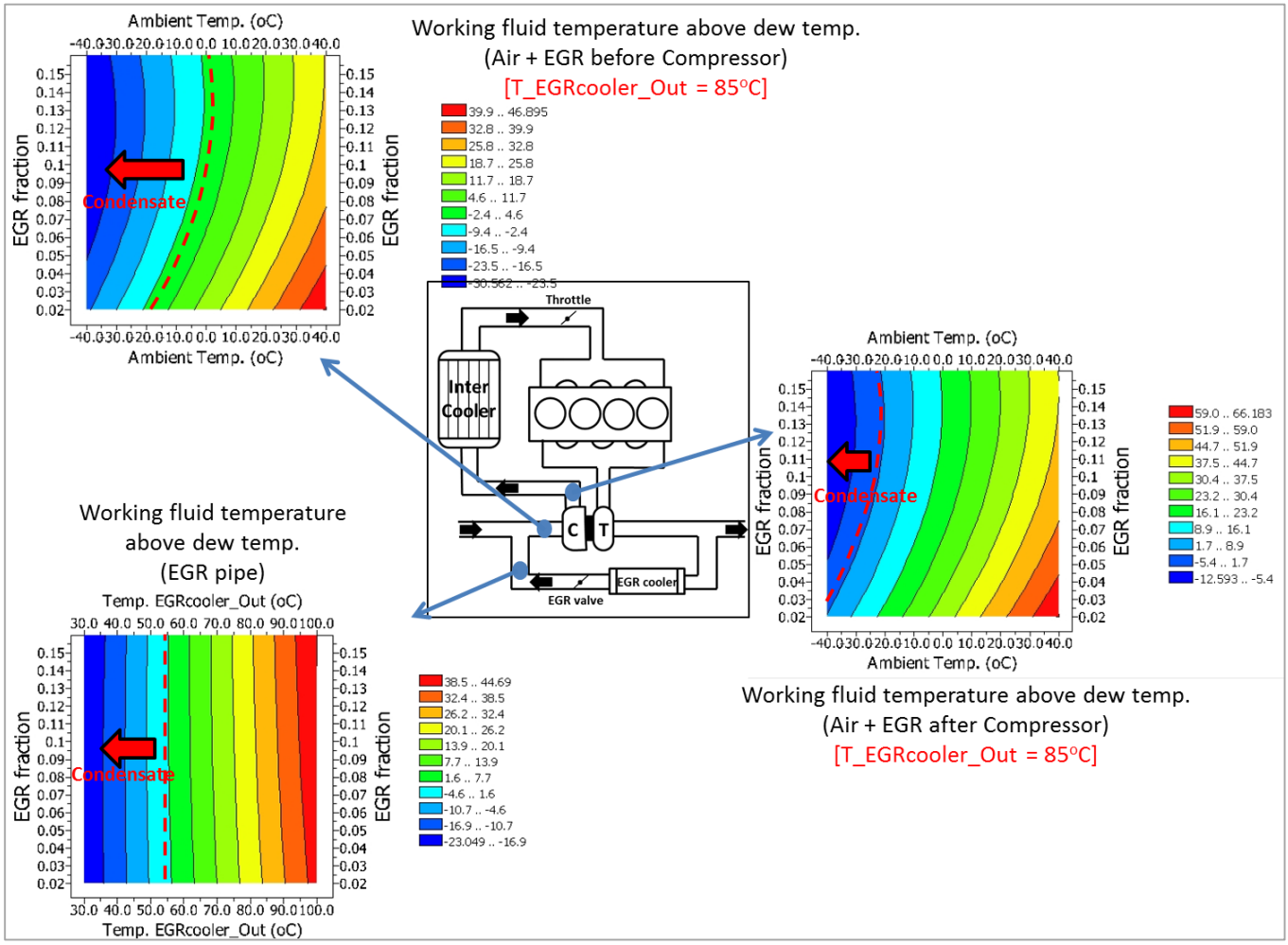

Figure 19: Working fluid temperature above dew temperature in three different locations of the LP EGR path. Negative values in the graphs depict water condensation is likely

2.9 Thermal Management

The thermal interaction of the sensor and the engine is of concern for the materials at the interface. The use of non-metallic manifolds and piping limits the amount of heat that can be transmitted from the sensor to the mounting location. The sensor itself generates heat which must be conducted into the mounting. To evaluate the temperature limits engine tests were made at high and low load conditions as well as normal and elevated ambient conditions. The data from an instrumented sensor was recorded and used to create temperature maps for the mounting

flange and the sealing O-ring. Figure 20 shows that for high load conditions the flange temperature can exceed 180C and the O-ring temperature can exceed 200C.

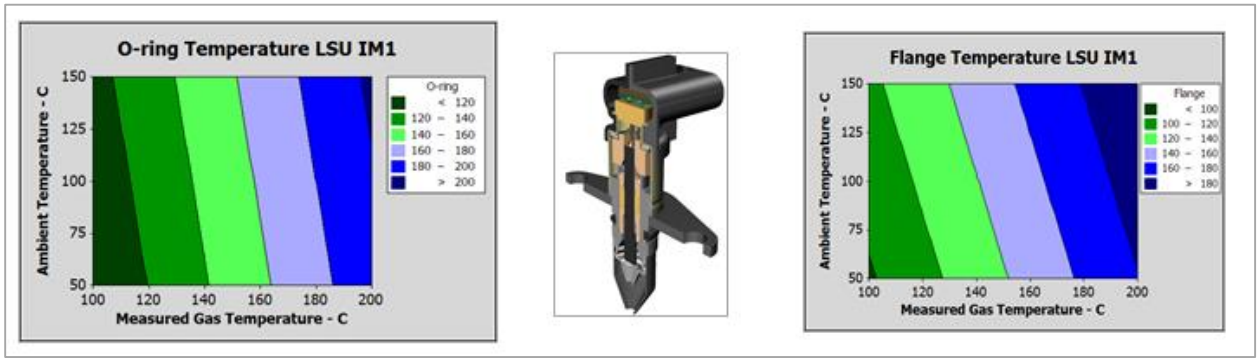

Figure 20: Thermal mapping at rated power conditions.

2.10 Long-Term Durability Testing

The long term durability test plan was established to validate the sensor to a service life of 250,000km (155,000 miles) / 15 years with a combination of environmental, mechanical, functional, and endurance tests. The samples were produced in three mounting configurations (Figure 21) due to varying customer assembly method requirements and for ease of testing. The testing was completed in two groups (see Figures x and x) due to the availability of components.

Figure 21: Sensor build configurations.

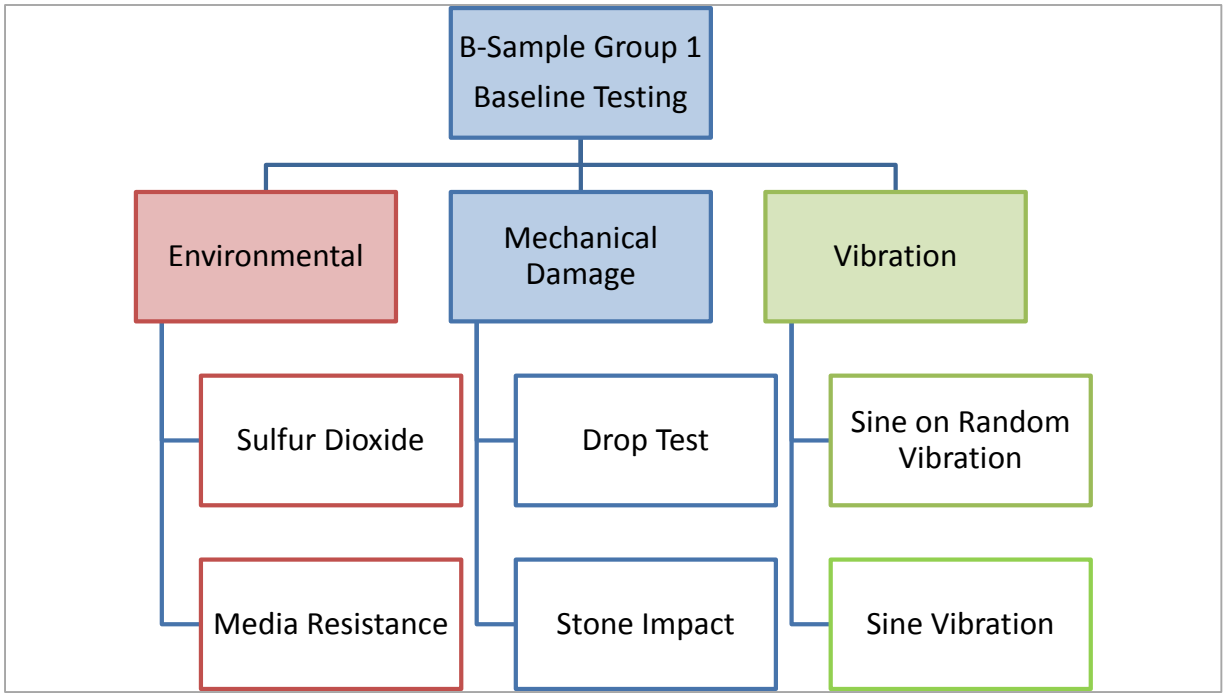

Figure 22: Group 1 test plan and status update.

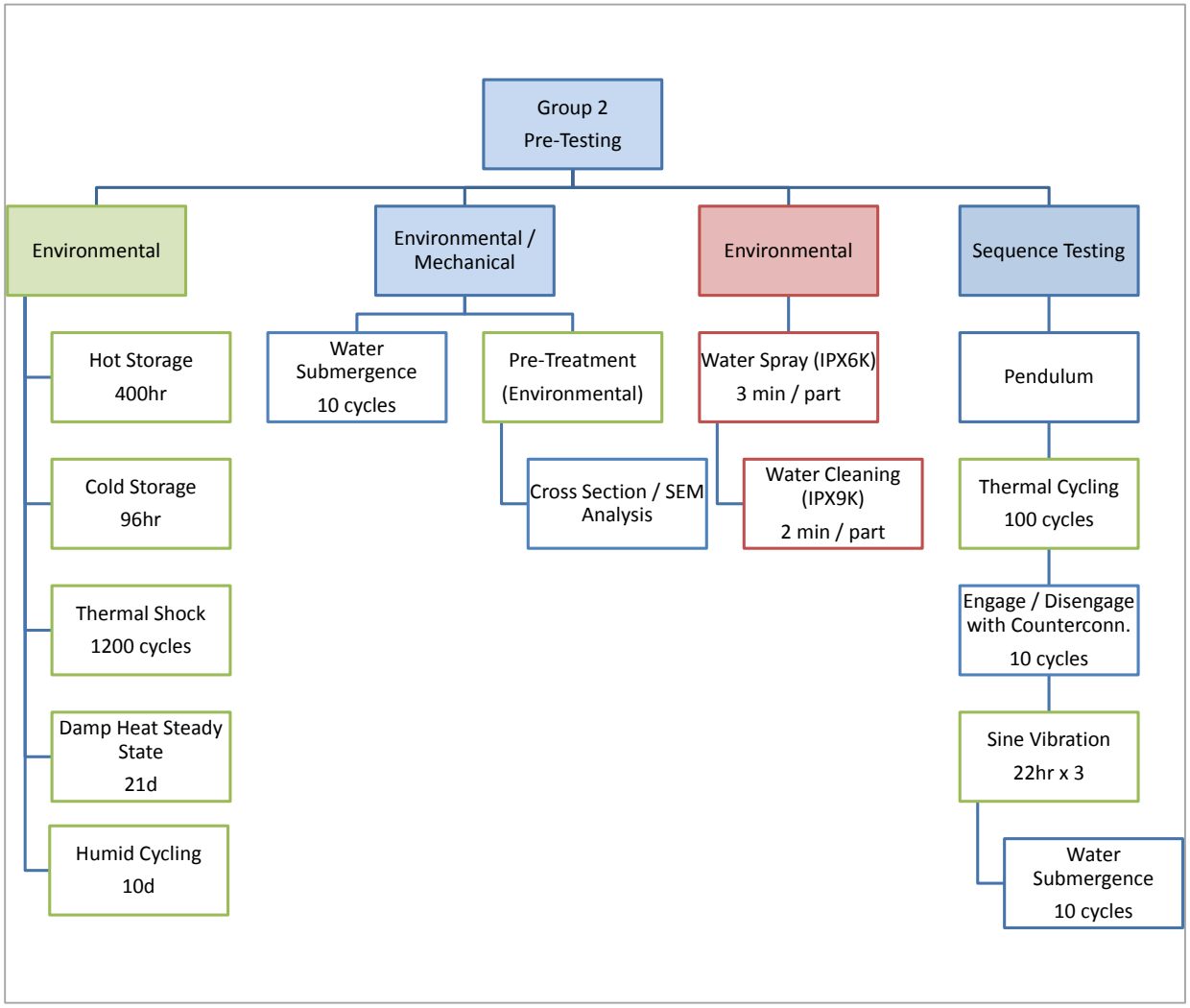

Figure 23: Group 2 test plan and status update.

After completion of the validation testing at the end of December, it became apparent several items additionally needed to be addressed before moving forward to the next sample phase. These items are the following:

- Voids were found in the sealant that is used to ensure a leak tight seal between the connector assembly and the metal sleeve. Despite the voids, all parts passed bubble leak

testing with the exception of one part that produced bubbles between the connector assembly and the mating counter-connector assembly. The root cause analysis is still underway.

- Two sensors failed functional testing before any durability testing was initiated. The sample shop assembly process was investigated to determine the root cause.

- One sensor failed functional testing as a result of the stone impact testing. This type of mechanical damage testing is a standard design validation test for oxygen sensors, however the impact positions on the sensor had to be modified due to the flange and integrated connector assembly. The test procedure is under investigation to ensure that the test is representative of application conditions.

- One sensor failed high pressure water spray testing. The sensor is being evaluated to determine if water entry from the spray testing was cause of the failure or if the sensor malfunction occurred due to improper handling of the sensor during or after the testing.

3 IA02 Sensor Control System Development

3.1 Overview

The Clemson University team focused on two primary objectives during this research project; (1) determining the fuel economy benefits of using low-pressure and cooled EGR (LP-cEGR) on a spark-ignition gasoline engine, and (2) developing EGR control and adaptation algorithms that utilized feedback from an intake oxygen sensor. A modified GM LTG turbocharged engine was also installed in a dynamometer cell at CU-ICAR, and a corresponding GT-Power engine model was built and calibrated. The test engine was utilized for data collection as was equipped with a rapid-prototype control system for testing intake oxygen sensor-based feedback algorithms. Significant conclusions from the Clemson University research are:

- Simulation and optimization techniques using calibrated GT-Power engine models are proven to be capable of predicting EGR fuel efficiency benefits with high accuracy, thus helping to guide and support research while at the same time reducing dynamometer testing during the design phase of this new concept.

- Low Pressure cooled EGR system provides efficiency benefits from 2% up to more than 3% over a base vehicle without EGR, for the FUDS and FHDS driving cycles.

- Accurate prediction and control of EGR (using the intake oxygen sensor) provides about 0.5% efficiency benefit over the current state-of-the-art EGR control, for the FUDS and FHDS driving cycles.

- A simulation study of Artificial Neural Networks shows the possibility of effectively actuating on the VVT system to minimize burned gas dilution in order to avoid misfires during aggressive throttle tip-outs; such approach accommodates transient control challenges to allow for higher EGR rates, thus maximizing fuel efficiency benefits.

- Compressor outlet proves to be the most effective location for intake oxygen sensor installation, considering EGR valve feedback quality, sensor response time and sensor operation (affected by pressure pulsations, water condensates, etc.).

- Open-loop modeling of EGR mass flow is challenging due to low pressure differential and significant influence of pressure pulsations across the EGR system
- Transport delay from the air-EGR mixing location to the intake oxygen sensor restricts controller performance due to reduced stability margins.

- Transport delay modeling of the entire EGR flow path shows good correspondence with experimental testing of the actual delay, with less than one engine cycle error for each of the three individual sections of the flow path (from the exhaust to the intake manifold).

- Lower level EGR valve position controller performance is critical for EGR dilution control.

- A dynamic orifice mass flow model is investigated and calibrated for the EGR system and shows improvement in feed-forward prediction compared to the conventional orifice mass flow model.

- A physics-based coupled exhaust temperature and pressure model was developed to provide EGR valve inlet (turbine outlet) pressure estimation to the orifice flow model, without the need of a physical sensor in the exhaust; real-time transient experimental testing of the model shows average absolute error of the exhaust pressure estimation to be less than 0.2 kPa with standard deviation less than 0.15 kPa.

- A Smith Predictor-based feedback control and dead-time delay compensator was designed and tested experimentally; average step response overshoot is reduced by up to 22% over pure feedback control.

- A Sliding Mode controller was designed to improve EGR valve position control over conventional PID.

- An Extended Kalman Filter-based adaptation algorithm was developed in order to correct the calibrated orifice flow estimation (using intake oxygen sensor measurement) and to create an online adaptation map to improve feed-forward estimation in subsequent time-steps. Short-term and long-term variations were accommodated through this algorithm and real-time experimental validation shows a large reduction in EGR prediction error using this approach.

3.2 Test Facility Development

A GM EcoTec 2.0L 4-Cylinder LTG was used for this research because it represents the current state-of-the-art in mass production high efficiency gasoline engines. The test engine (see table 5) is turbocharged, direct fuel injected, and is equipped with dual-independent camshaft phasing systems. The combustion chamber bowl on the head has four valves and a pent-roof shape with a cavity for the fuel injector. The piston crown is shaped to allow wall guided spray injection. Ignition is achieved using high-energy coil-on-plug coils triggered by TTL level ECU signals. A BorgWarner K03-2074 twin-scroll turbocharger with internal waste-gate and blow-off valve is installed on this engine. A Low Pressure cooled EGR (LP-cEGR) configuration is also applied, as shown in 34. Exhaust gases are extracted downstream of the turbine. EGR passes through a cooler and is delivered to the intake air-path system upstream of the compressor. The EGR cooler is a tube-core type chosen for low pressure differential. Twin liquid-to-air intercoolers have been used to allow high boost/load capability. Production-intent engine controllers have been modified to include software hooks on specific engine control parameters.

Engine Type	In-line 4-cylinder SI
Displacement	1998 cc
Bore x Stroke	86 x 86
Compression Ratio	9.5:1
Intake System	Twin-Scroll Turbocharger (waste-gate controlled) with Intercooler

Valve Train	DOHC, 4-valves/cylinder with Continuously Variable Valve Timing
Fuel Injection System	Direct injection
EGR System	Low Pressure cooled EGR

Table 5: Engine Specifications.

A 430 kW AC engine dynamometer is used for the experimental portion of this research, as shown in 34. Crank angle resolved data acquisition is performed using an AVL-671 32-channel system. Cylinder pressures are measured using AVL GH12D piezoelectric sensors. Piezo-resistive Kulite transducers are used for dynamic pressure measurements in both the intake and exhaust ports of the test engine. Dedicated liquid cooling circuits have been utilized for exhaust manifold pressure transducers. The data are sampled at 0.5 crank angle degree intervals to properly capture all relevant gas exchange characteristics. K-type thermocouples are utilized for measurement of temperatures at specific locations on the engine.

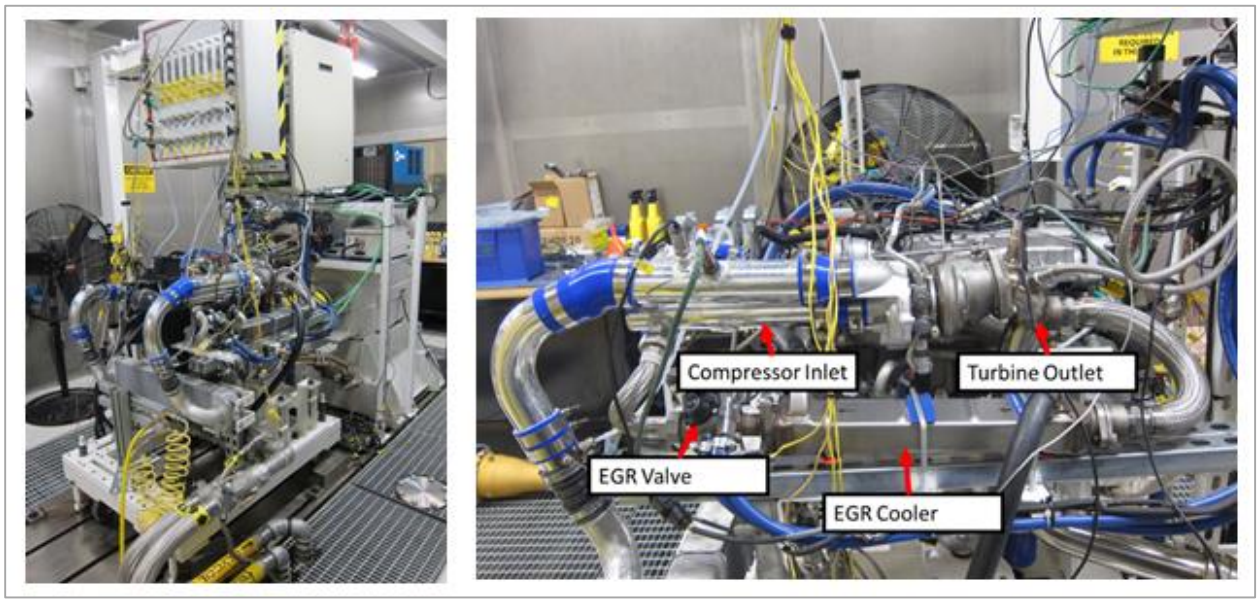

Figure 24: The engine dynamometer facility at CU-ICAR was used for control system development. A low-pressure cooled-EGR system was added to the engine to test intake oxygen sensor based feedback control algorithms under conditions with minimal pressure differential across the EGR valve.

A Bosch engine controller is modified to include software hooks on specific engine control parameters. An ETAS ES910 Rapid Prototype Controller (RPC) is used in conjunction with the base engine controller using CAN Communication Protocol (CCP) bypass communication. This is done to establish data interface between the base engine controller and the rapid prototype controller. EGR control systems developed in Simulink are compiled and deployed into the ETAS ES910, enabling real-time execution of control algorithms. The ES910 systems work with the calibration software INCA.

3.3 Control System Development

Architecture of control algorithms is influenced in part by the physical layout of the engine hardware. Initial control system development involved research to determine; (1) optimal intake oxygen sensor location, (2) EGR calculation using intake oxygen sensing, and (3) correction methods for cross-sensitivities that the intake oxygen sensor can exhibit with different intake gas compositions. Intake oxygen sensor location is a key factor in control system behavior since it will play a role in feedback signal delay as well as sensor cross sensitivity to ambient factors (e.g. pressure compensation, intake species, etc.). After intake oxygen sensor location was finalized, transport delay models were developed to ensure accurate EGR fraction measurement in the intake during transient conditions. The transport models require a feed-forward estimate of EGR mass flow through the EGR valve, which is difficult to determine when pressure differential across the valve is low. A new EGR valve flow model was developed to partially account for the influence of pulsating flow at the EGR valve, and improve mass flow estimation under low pressure differentials as compared to commonly used orifice flow equations. The EGR valve flow model also requires an accurate exhaust pressure estimate, so a control-oriented exhaust pressure estimation method was also developed. These models combined to provide an accurate estimate of EGR fraction in the intake under all operating conditions, allowing the signal to be used for feedback control and long term adaptation. A feedback control system, based on a Smith Predictor, was developed and tested in real-time over transient conditions. A long term and short term Extended Kalman Filter-based adaptation algorithm was also implemented and tested in real-time on the dynamometer cell. The algorithm proves capable of correcting large EGR valve mass flow modeling errors, and makes EGR control under low pressure differentials much more feasible than using open loop control alone.

3.4 EGR System Evaluation and Control Development

EGR and species transport is being investigated to identify system behavior with boundary changes of the EGR loop (engine speed, load) and during rapid/step changes in EGR request. Focus of the transport behavior is given to three crucial transport delays (shown in Figure 25); (1) between the exhaust oxygen sensor and EGR valve, (2) EGR valve to intake oxygen sensor, and (3) intake oxygen sensor to the individual cylinders.

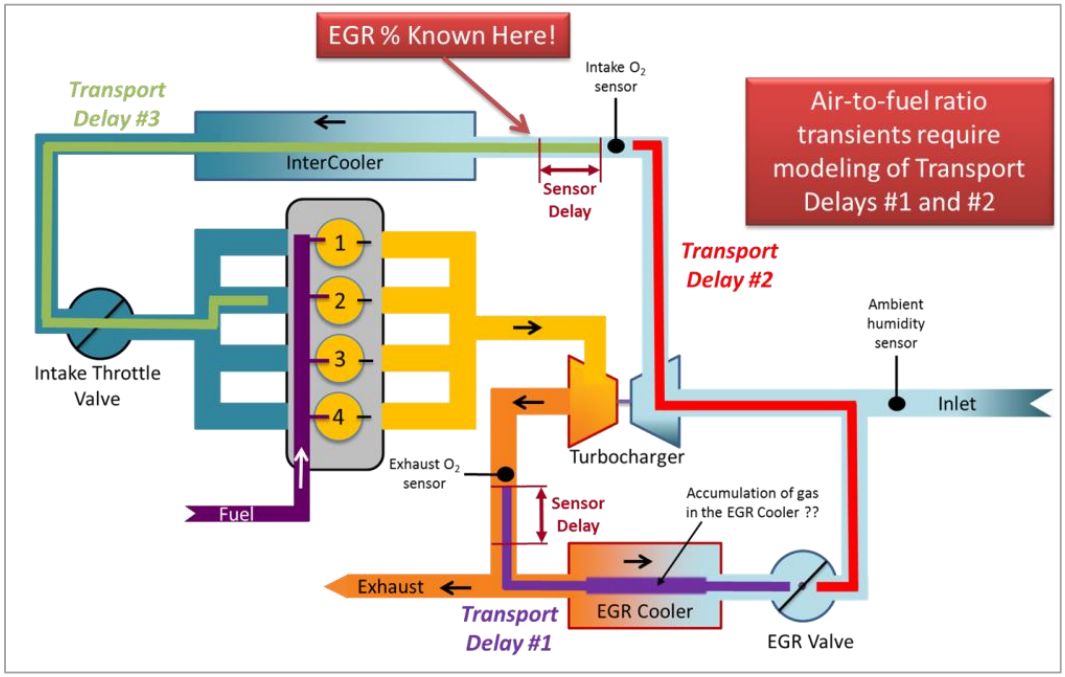

Figure 25: There are three important transport delays that must be considered in real-time to achieve accurate EGR calculation and valve control.

Several experiments were performed to quantify the transport characteristics of cooled exhaust gas across the air system on the test engine. The characterization was done by changing the EGR valve position in rapid steps. The delays were measured on an engine cycle scale wherein one cycle corresponds to two crankshaft revolutions beginning from the combustion TDC of a fixed reference cylinder. Oxygen sensors were located in three locations; in the exhaust after the turbine, in the intake path after the compressor and on the intake runner of cylinder 1. 25 shows that for a step change in the EGR valve position, the oxygen sensor post-compressor reports the EGR concentration change approximately 3 cycles after the change in valve position is

initiated. Similarly, the oxygen sensor on the intake runner reports the EGR concentration change approximately 10 cycles after the valve position change. Additionally, the effect of this EGR concentration change on combustion is detected as a change in the CA50 angle as the spark timing was held constant. Due to the close proximity of the Oxygen sensor on the intake, to the cylinder, the change in CA50 appears to occur at the same instant as the change in Oxygen concentration detected by the sensor intake runner. This can also be attributed to the dependence of the sensor response time on flow velocity. These transport delays would change significantly if air system components are modified or changed and hence the characterization process would have to be repeated for the modified air system (e.g. changes in pipe lengths and diameters, intercooler volume, etc).

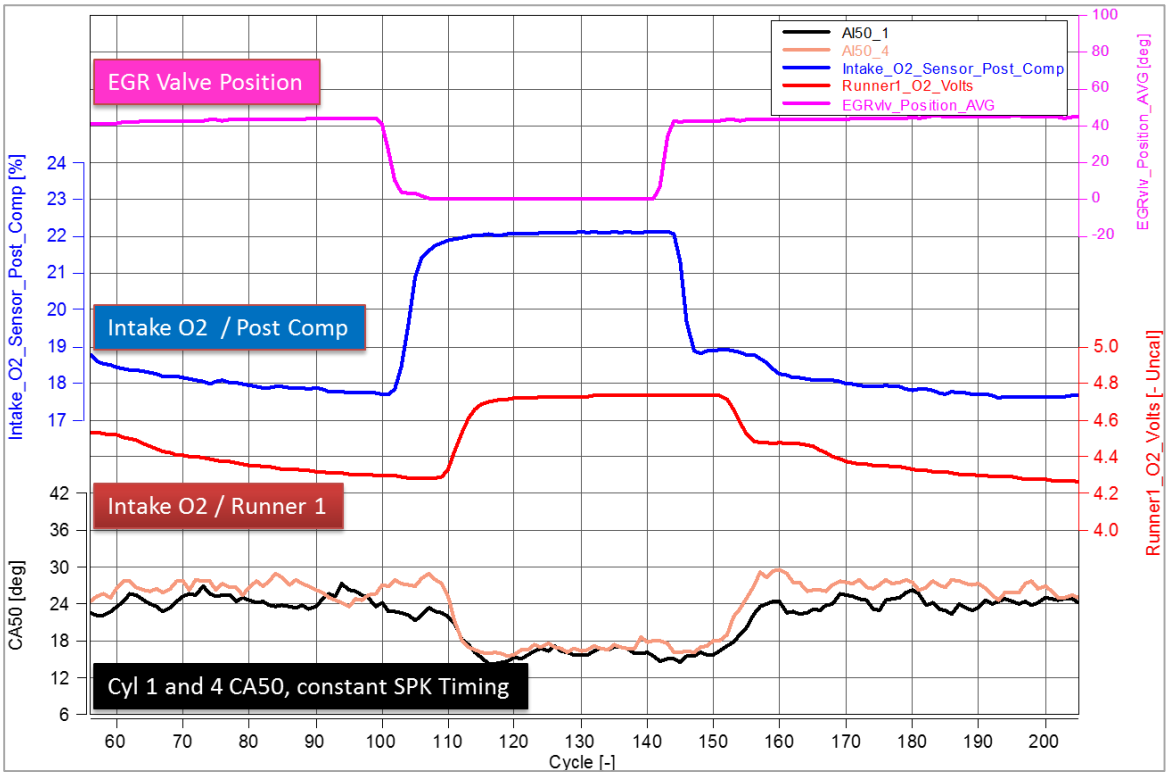

Figure 26: Transport delay characterization of recirculated exhaust gas using EGR valve position step changes.

Additional control complexity is created by the time response of the sensor, which depends upon its position in the system and operating conditions. Sensor delay depends on flow conditions, and mainly gas velocity, whereas sensor accuracy depends on gas composition. Figure 28 shows the sources of response time and output changes for the intake oxygen sensor, all of which was modeled for the purposes of real-time control and EGR estimation.

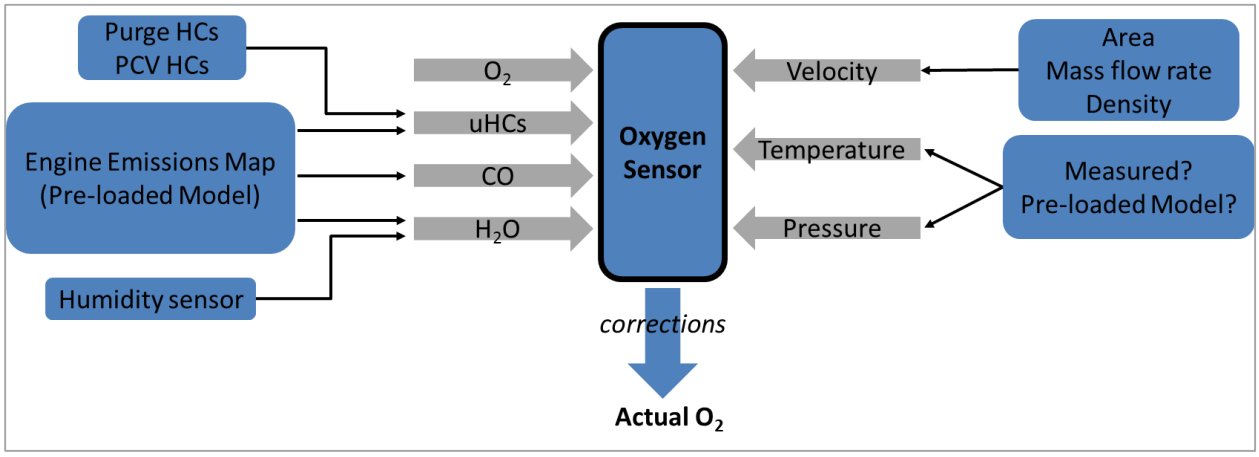

Figure 27: Intake oxygen sensor output is a function of local conditions and species concentrations. All of these factors are being modeled for the purpose of real-time control.

Using some initial measurements (provided to Clemson by Bosch) which correlate gas velocity with sensor delay, Figure 28 shows the sensor delay at different positions in the intake air path for a given engine speed and load.

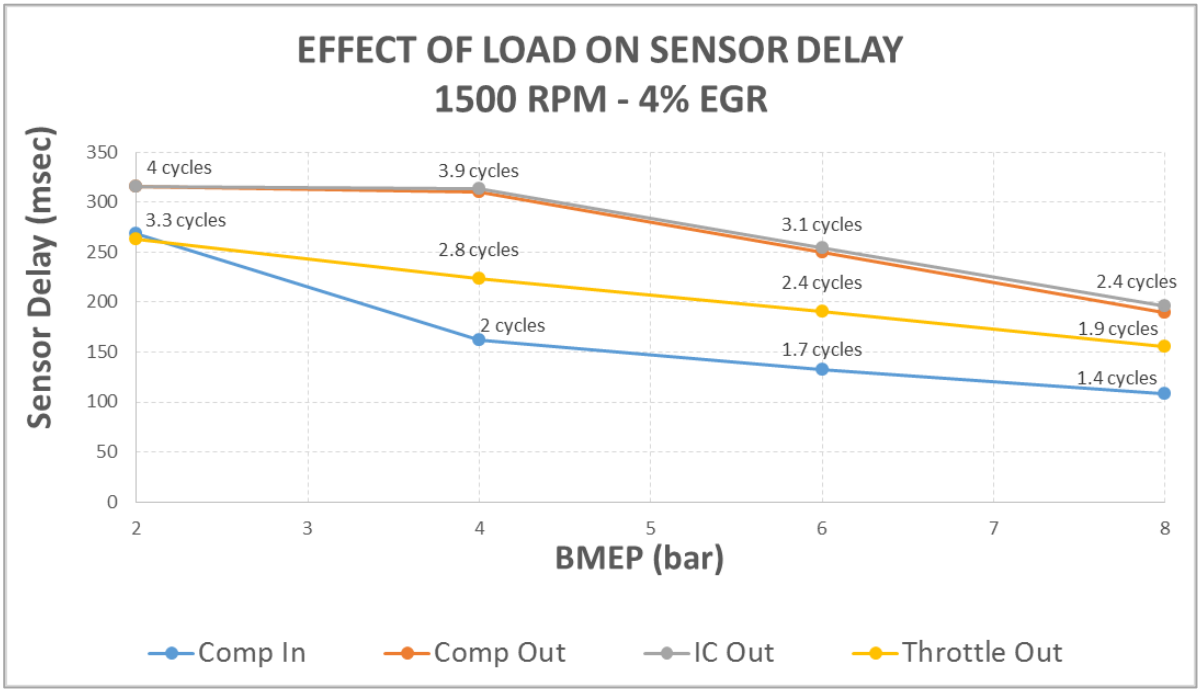

Figure 28: Modeled sensor response times for an intake oxygen sensor located at different positions. The compressor inlet location provides the lowest response time, which is desirable for control.

For real-time control applications, a simplified control algorithm is being developed. Control equations are being developed for the calculation of the EGR transport delay and control of the EGR valve. Valve control was based on the low pressure differential and the pressure pulsations coming through the exhaust of the engine. These equations was calibrated and validated according to the detailed physical GT-Power simulation model. However, they was extremely simplified in order to be able to run real-time.

A Uniform State, Uniform Flow Process, where the working fluids (air & exhaust gas) behave according to the Ideal Gas Law, is assumed for control purposes. The flow path is split into different sections based on the flow conditions. Each section was governed by constant temperature, pressure, mass flow rate and gas composition. As shown in Figure 29, an average cross sectional area and length is assigned to each section to further simplify the equations.

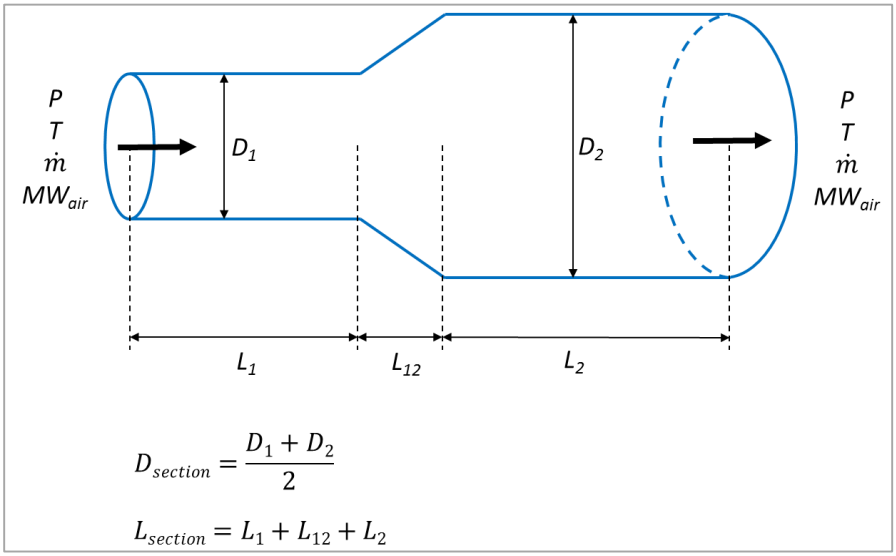

Figure 29: Intake duct modeling for the generation of real-time control equations.

A first rough estimation of the transport delay calculation is derived using this approach and gives reasonable results, as shown in Figure 30.

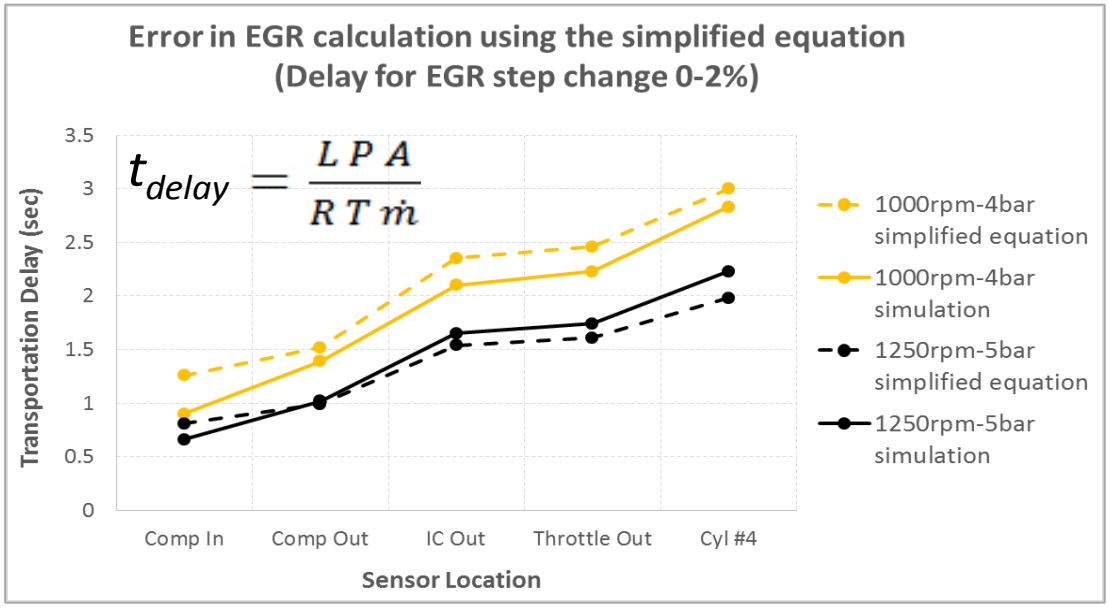

Figure 30: Error in transport delay calculation using a simplified flow calculation approach intended for real-time engine control.

The equations provide similar trends with the detailed simulation results. In this case, all the flow paths are considered to be straight lines. Through more detailed research and calibration of the results, certain correcting factors was applied to account for bend pipes, restrictions in the flow (valves), area changes, etc. Furthermore, the exhaust pressure pulsations need to be considered and included in the equation for better prediction at low average pressure ratios across the EGR valve. The simplified flow equation has been modeled in Simulink as a simple subsystem shown in Figure 3131. Several instances of this subsystem was implemented to model different control volumes in air system. The delays was applied to the constituent species of recirculated exhaust which influence the oxygen concentration measurement and the combustion.

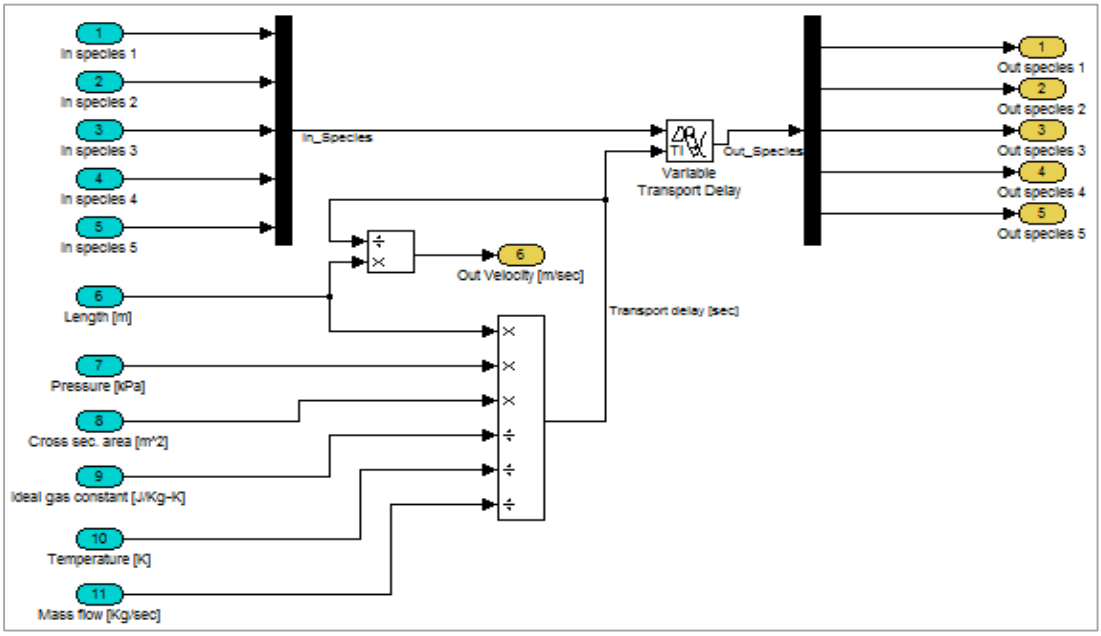

Figure 31: Simplified flow equation modeled in Simulink

Since the recirculated exhaust takes 3 cycles to reach the oxygen sensor after the compressor, first estimation of EGR mass flow to adjust the valve position will have to be derived from a feed forward model shown in Figure 3232 which will utilize the pressure difference across the valve as an input. Accordingly, the derived mass flow can either be simply obtained from a lookup table or from a orifice flow equation as per the choice of the user. This approach has been chosen because the pressure pulsations at the inlet of the EGR valve may cause reduction in accuracy of the mass flow estimation and a lookup table may be a more viable solution during real time operation.

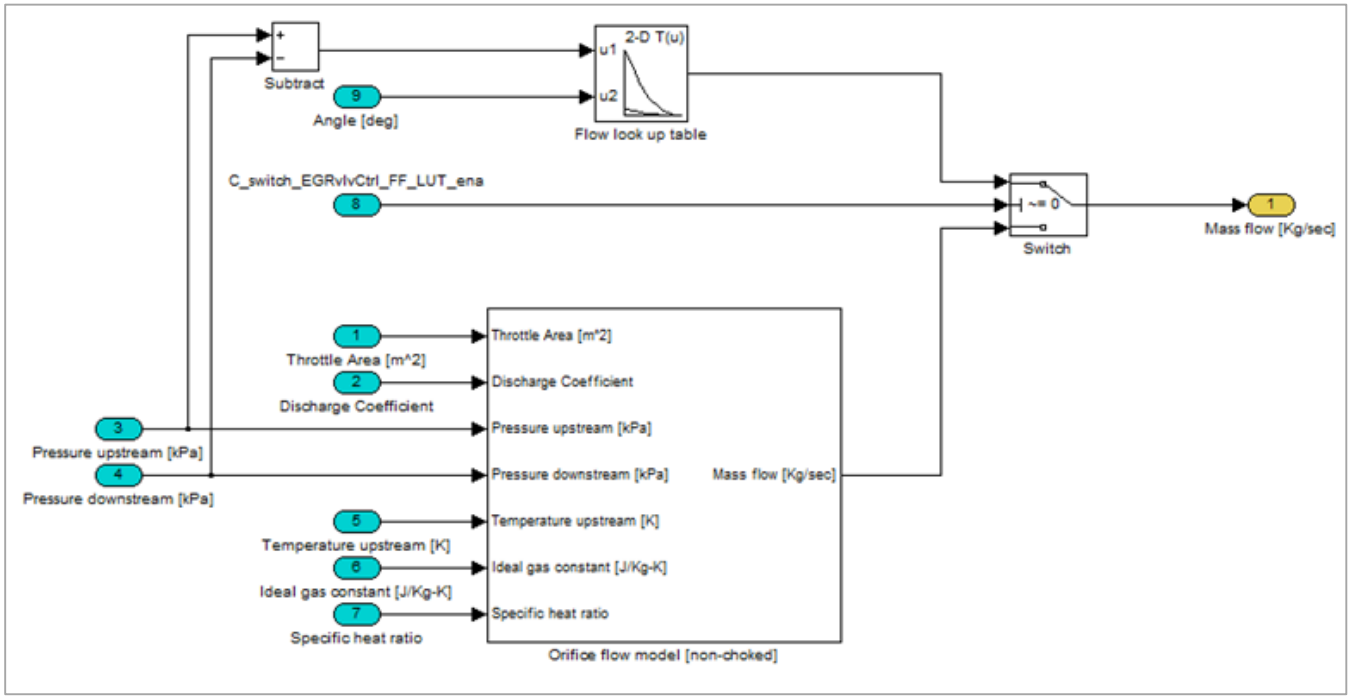

Figure 32: EGR Valve feed forward model.

The EGR control system model developed in Simulink was compiled and deployed into the ETAS ES910 which is a Rapid Control Prototyping platform enabling real time execution of the control system and it would also allow calibration and measurement of parameters defined in the model using the calibration tool INCA. The control system software and hardware architecture is shown in Figure 3333.

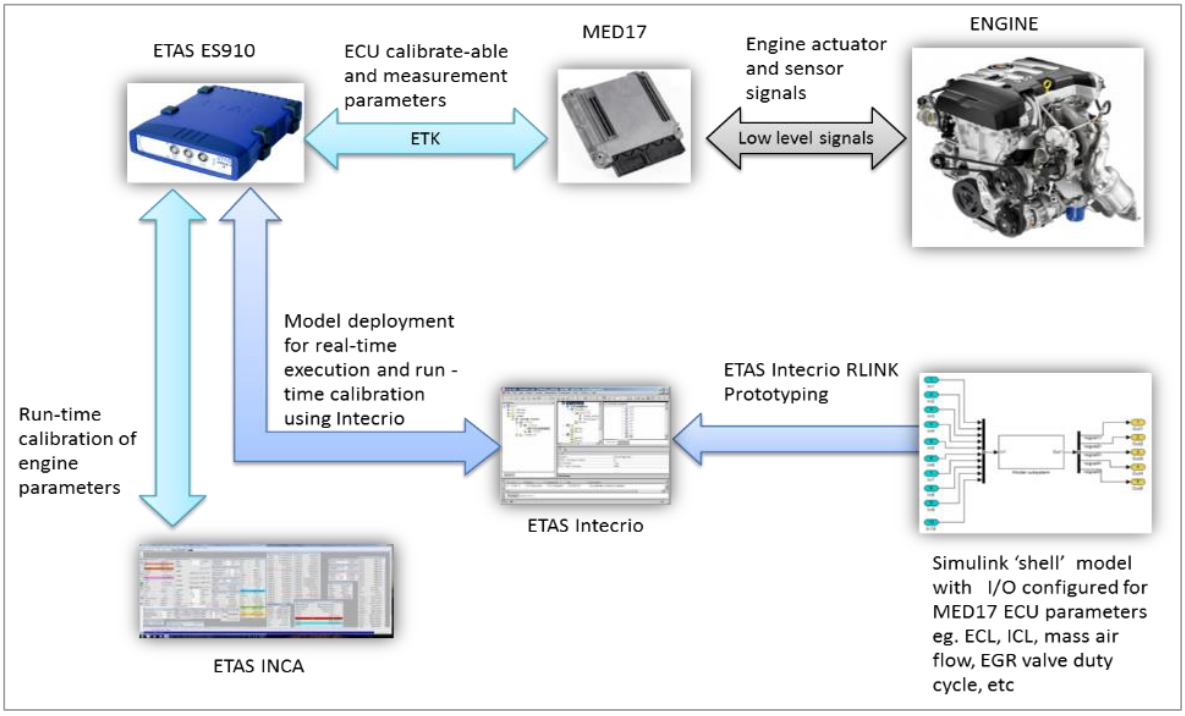

Figure 33: Control system software and hardware architecture

3.5 Simulation Development

A GT-Power model of the engine system was built to represent the setup created in the dynamometer cell at Clemson University. Geometric information related to the fuel injectors, combustion chamber shape, valve lift profiles, and geometric parameters of the entire gas flow path were used to build the model. Turbo maps (compressor and turbine) were supplied by BorgWarner, and their cooperation is greatly appreciated. The GT-Power model was assessed and validated using data from the engine operation in the dynamometer. Data from different engine speeds and loads were used in order to calibrate the model. Comparison of the P-V diagrams and pumping loops show very good approximation of the experimental results. In Figure 34 simulation results (blue lines) are compared with experimental data from cylinders 1 and 4 of the engine (red and green lines respectively). At some operating points large variations in the peak cylinder pressures can be detected between the two cylinders of the test engine, which likely results from cylinder-to-cylinder variations in EGR dilution. However, the simulations trace almost identically with at least one of the two experimental P-V traces, while the pumping loop trends are very closely followed by simulation results.

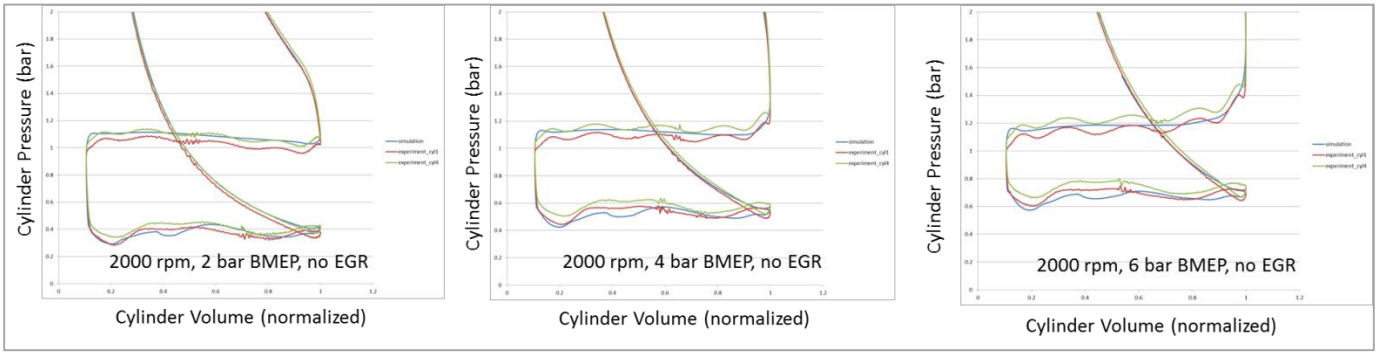

Figure 34: Sample GT-Power pumping loop comparison between simulation (blue lines) and experimental data of cyl.1, 4 of the engine (red, green lines) for a load sweep at 2000 rpm.

3.6 Intake Oxygen Sensor Location and In-Use Correction

Four different locations for the intake oxygen sensor were evaluated in order to find the one that delivers the most accurate results; (1) upstream of the compressor, (2) downstream of the compressor, (3) downstream of the charge air cooler and (4) downstream of the throttle. Main considerations that dictate the sensor location are sensor response time, possibility of water condensates reaching the sensor, mixing quality of the air-EGR mixture, and pressure pulsations.

These influences partially determine the EGR concentration feedback quality, which is mainly dictated by how immediate the sensor response is to any EGR valve actuation. Figure 44 shows the sources of response time and output changes for the intake oxygen sensor, all of which was modeled for the purposes of real-time control and EGR estimation.

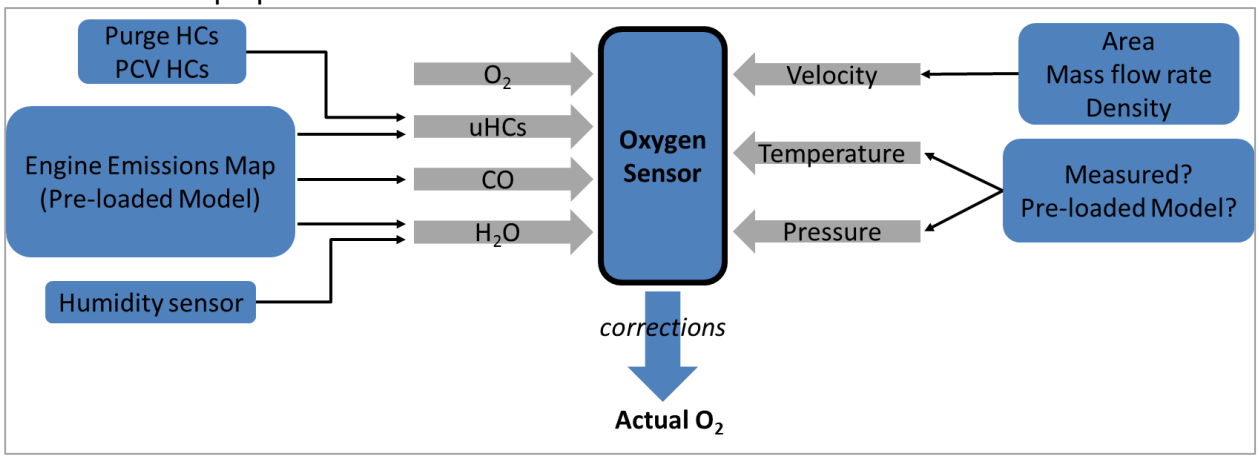

Figure 35: ANN outputs and (External EGR + Internal Residual) levels during a torque tip-out (2000 RPM with constant 10% external EGR) for an ANN-based VVT actuation control model compared to base model without VVT actuation.

Time response of the sensor depends upon its position in the system and operating conditions. Sensor delay depends on flow conditions, and mainly gas velocity, whereas sensor accuracy depends on gas composition. The outlet of the compressor and the intercooler-outlet sensor locations would provide similar response times. The response time for the throttle outlet location was strongly depended on throttle opening. Inlet of the compressor will provide the fastest response, however the mixture is not homogeneous right after the mixing location. Improper air-EGR mixing would generate errors in the sensor measurement. Besides, in such case, one of the main benefits of Low Pressure EGR configuration, which is good mixing, would not be capitalized in the feedback signal. Moreover, upstream of the compressor, exhaust pressure pulsations travelling through the EGR loop into the intake side, may cause instabilities in the sensor reading, since sensor output is dependent on (and being corrected for) pressure.
Water condensation limitations associated with adding an intake oxygen sensor in the LP EGR path were studied in detail. Besides damaging the compressor blades, possible water condensates of the recirculated gases could affect the measurement of the intake oxygen sensor. For that reason, DoE simulation studies (GT-Power) were used to quantify this effect, and results

are shown in 45 and 46. Three different locations in the LP EGR path are being shown. Downstream of the EGR cooler and before mixing with air, the most important parameter for water condensation is the EGR cooler outlet temperature (EGRcooler_Out). Below EGR cooler outlet temperatures of 60°C condensation is likely to occur for every EGR dilution level. After mixing with air upstream of the compressor, the main parameter that dictates condensation is the ambient temperature since air is the main component of the mixture. For EGR dilution above 10%, ambient air temperature less than 3°C will cause condensation (EGRcooler_Out temperature=85°C is assumed). In contrast, downstream of the compressor, the working fluid's elevated pressure drives the mixture above the saturation line and thus much colder ambient temperatures are required for the water to condensate. Finally, the post-intercooler location will also introduce challenges with water condensation due to the further decrease in mixture temperature. Thus, it is evident that several operating conditions can be found where the working fluid is below the saturation line and condensation occurs.

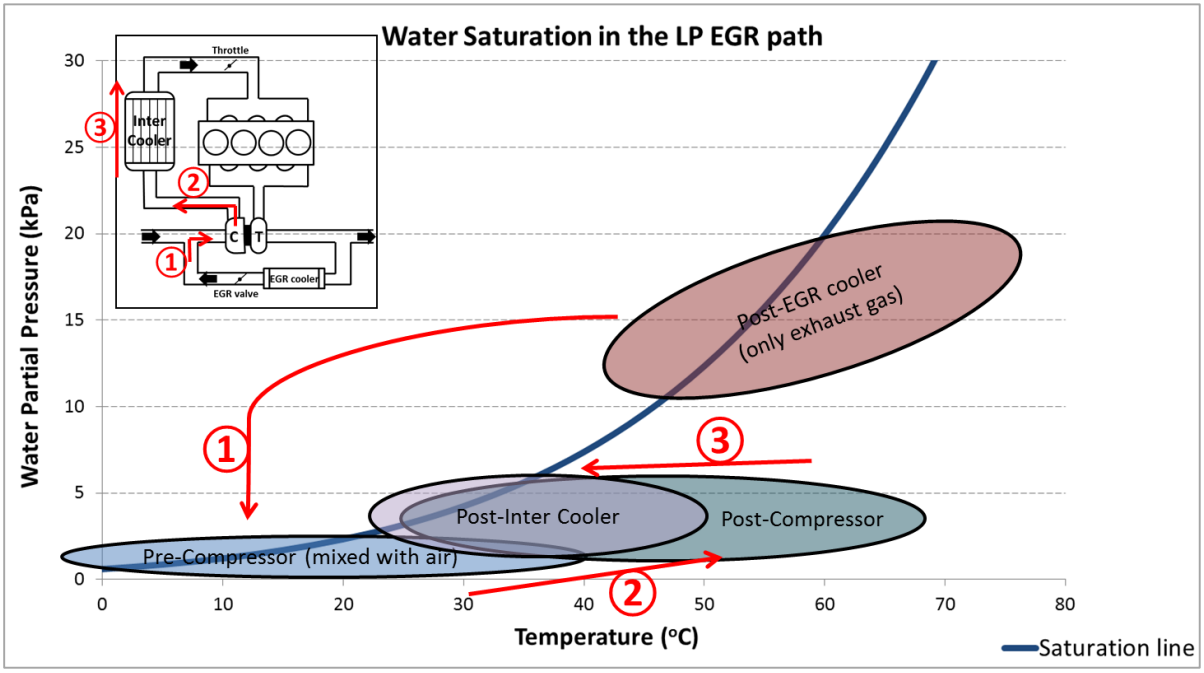

Figure 36: Water saturation potential in the LP-EGR path.

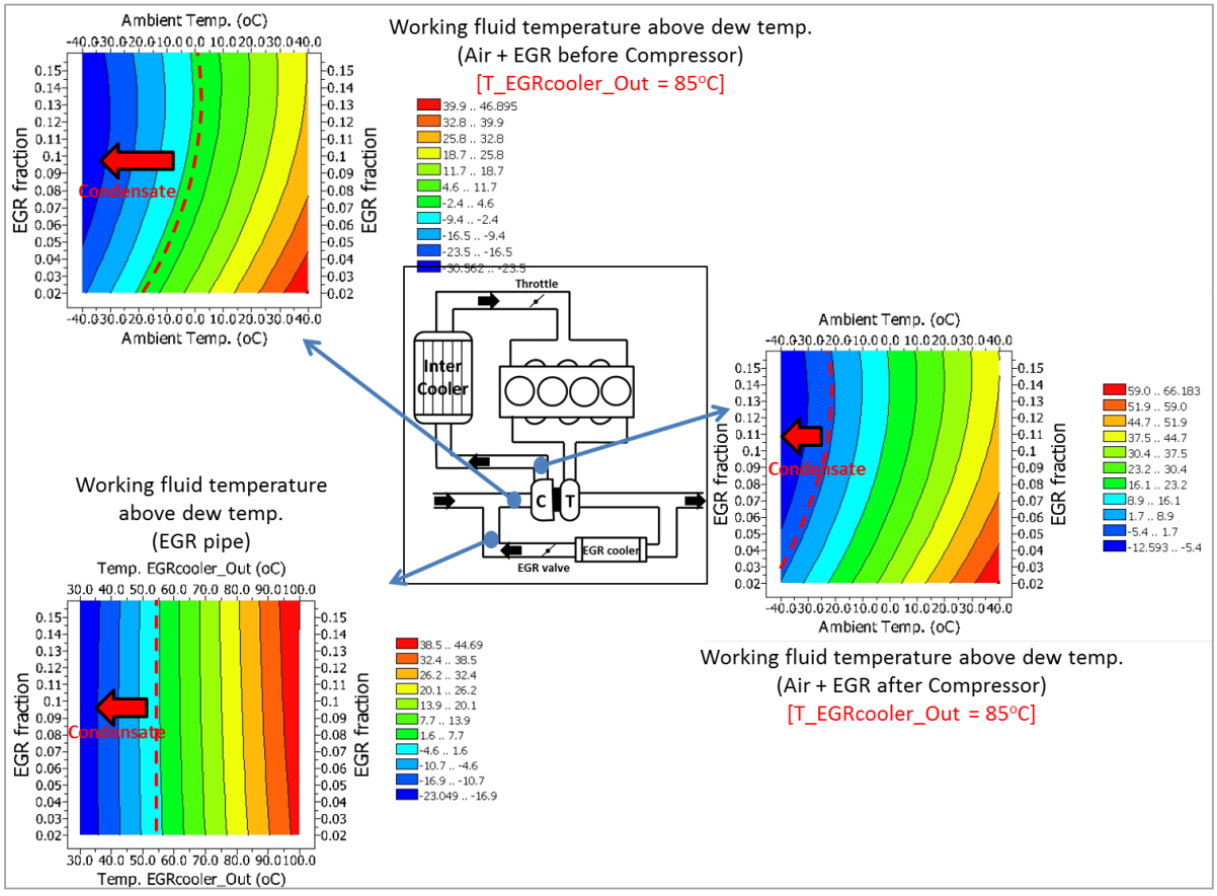

Figure 37: Working fluid temperature above dew temperature in three different locations of the LP EGR path. Negative values in the graphs depict water condensation is likely.

As far as the EGR feedback quality is concerned, the closest the sensor is located to the EGR valve, the more immediate the action of the controller may be to any EGR valve actuation. In addition to that, it is important to make sure that the sensor response time is always less than the transport delay from the sensor to the cylinders. This factor could set a limitation on sensor location, since post-throttle location could produce measurements that are very close to this constraint. Table 6 summarizes the aforementioned advantages and disadvantages of each oxygen sensor location.

SUMMARY	Compressor inlet	Compressor outlet	Intercooler outlet	Throttle outlet
EGR valve feedback	+++	++	+	--
Sensor Response Time	+++	-	-	++
Mixing quality	---	++	+++	+++
Pressure pulsations	---	-	+	+
Water condensation	---	+++	--	-

Table 6: Intake Oxygen Sensor Location Considerations

Analysis of experimental data provided by Bosch was conducted in order to characterize the sensitivity and accuracy of the LSU intake oxygen sensor. The data from Bosch are derived from emission test benches located in the intake and exhaust of the engine. In this way, the intake oxygen sensor signal can be compared to the actual EGR dilution as calculated from the intake O2 measurement. Without any correction, the sensor output deviates from the real EGR dilution, due to in-sensor reactions. The relative effect of different parameters on the sensor accuracy was quantified using JMP statistical software. Parameters that were studied include exhaust lambda, mass flow rate through the sensor, species concentrations in the exhaust and species in the intake. A multiple regression method was used through JMP software to identify correlations and provide 'best-case' linear equations of these parameters that correct the sensor output. Table 7 summarizes the accuracy statistics for different correction methods based on the inputs provided to the algorithm.

EGR Correction Inputs	R^2	RMSE (EGR %)	Max EGR Error (EGR %)

Linear regression of sensor output	0.885	1.93	4.44
λ	0.960	1.14	2.89
$\lambda, \dot{m}_{fl}$	0.967	1.04	3.02
$\lambda, \dot{m}_{fl}$, $exhaust\ species$	0.989	0.61	1.73
$\lambda, \dot{m}_{fl}$, $intake\ species$	0.999	0.16	0.43

Table 7: Statistics summary for different intake oxygen sensor correction methods based on the inputs provided to the algorithm.

3.7 Constraint Modeling: Knock, COV of IMEP, and Exhaust Temperature

A key objective of this project is to recognize the benefits from knowing the exact value of EGR with the help of intake oxygen sensor feedback, allowing more EGR to be utilized under certain conditions without violating constraints. Without feedback, EGR rates are limited due to the uncertainty in the exact amount entering the cylinders at each cycle. This intentional limiting of EGR increases the robustness of the calibration across mass-produced engines, but it also represents a fuel economy penalty. The intake oxygen sensor provides the possibility to minimize uncertainty in EGR quantity and thus increase the operational window of EGR without violation of constraints. The primary constraints considered for this research are knock, COV of IMEP, and exhaust gas temperature.

Cooled EGR is capable of suppressing knock onset and can therefore improve fuel economy by allowing engine operation at a more optimal combustion phasing. Knock-limited operation is defined by a required deviation from optimal spark timing (MBT) to reduce the change of end-gas auto-ignition (by reducing pressure and temperatures). An existing knock model provided in GT-Power that accounts for EGR dilution was utilized for this research.

Maximum exhaust gas temperature limitations for protection of engine system hardware reduce fuel economy. To limit exhaust gas temperature under high-load conditions, the engine is generally operated fuel-rich, which is inefficient and it reduces catalytic reduction of HC and CO. It is important to note that slightly rich operation can also produce higher torque levels than stoichiometric operation. The use of cooled EGR at high loads reduces exhaust gas temperature and in turn reduces the level of rich-fuel required to control exhaust gas temperature. The use of

cooled EGR will decrease volumetric efficiency at full load, and will likely also have a negative impact on peak torque output. Using high EGR dilution levels at high load is also difficult because an over dilution condition could occur during a rapid throttle tip-out. During a rapid tip-out internal residual gas fraction will increase quickly, while it may take much longer for external EGR to purge out of the intake system. This situation can cause over-dilution and has the potential to create misfires, so it also limits peak EGR dilution at high loads. For this research, exhaust gas temperature is constrained to be less than 900 degrees C, and limiting peak EGR to avoid over-dilution during tip-out was partially considered. A camshaft phasing control system to mitigate tip-out over-dilution was studied, and is discussed later in this document.

One potential fuel economy benefit of increased EGR quantity is reduced pumping work. However, excessively high levels of EGR increase COV of IMEP, causing emissions and drivability issues. COV of IMEP is commonly viewed as a stochastic process, so an empirical correlation for COV of IMEP is required to capture this constraint in a 1-D simulation environment. Empirically it is observed that COV of IMEP is a relatively strong correlation to combustion duration, and EGR generally extends burn duration. Engine dynamometer measurements were used to develop a correlation between the CA10-CA90 duration (burn duration), which is the crank angle duration between the instant where 10% of the air-fuel mixture is consumed and the instant where 90% of the mixture is consumed.

To establish a COV of IMEP correlation experimentally the engine was operated at three operating conditions. At each operating condition a fixed valve overlap duration and timing was maintained to minimize the effect of internal residual exhaust gas on the dilution of the mixture. External cooled EGR flow rate was increased gradually from levels corresponding to conditions resulting in COV of IMEP lesser than 3% to approximately 4-6%. The general empirical limit for COV of IMEP is 3%, but higher values can be tolerated under some circumstances. 37 shows the correlation between the COV of IMEP and CA10-90 duration at three operating conditions. Based on these results, it can be seen that the COV of IMEP limit is breached when burn duration exceeds 22-24 Crank Angle Degrees. This is used as the basis to establish a burn duration limit as a constraint in GT Power simulations to provide a more accurate representation of real world operational limits on the engine.

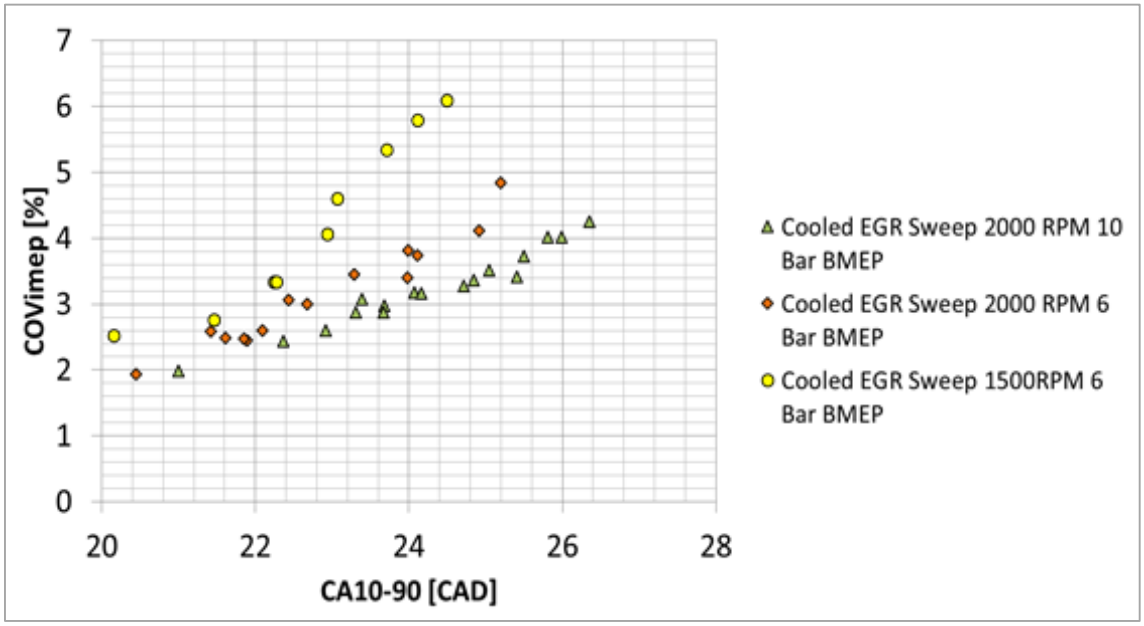

Figure 38: Correlation of COV of IMEP with CA10-CA90 duration for constraint modeling in GT-Power.

3.8 EGR Transport Delay Modeling

The recirculated exhaust gas path has been categorized into three fundamental sections, as shown in figure 39. The first section which begins at the UEGO (turbine outlet location) and ends at the EGR valve consists of the EGR cooler and some exhaust components. Transport across this section has been modeled to be an open-loop function of the position of the EGR valve and the pressure differential across the EGR valve. Most significant exhaust species concentrations except unburned-HCs are calculated real-time as a function of exhaust lambda. Estimation of these species fractions is critical due to their influence on the intake oxygen sensor signal. The second transport section begins at the EGR valve, flows through the compressor, and ends at the intake oxygen sensor. Transport in this section has a significant impact on closed-loop EGR valve control performance and stability due to 'dead-time' behavior. The final control algorithm utilizes a tunable Smith-Compensator with PID control to reduce EGR concentration oscillations on rapid EGR valve transients. The third and longest section begins at the intake oxygen sensor and ends at the cylinders. Prediction accuracy of this delay is crucial for control of spark timing and fuel mass, as EGR concentration affects combustion duration and displaces air mass in the cylinder.

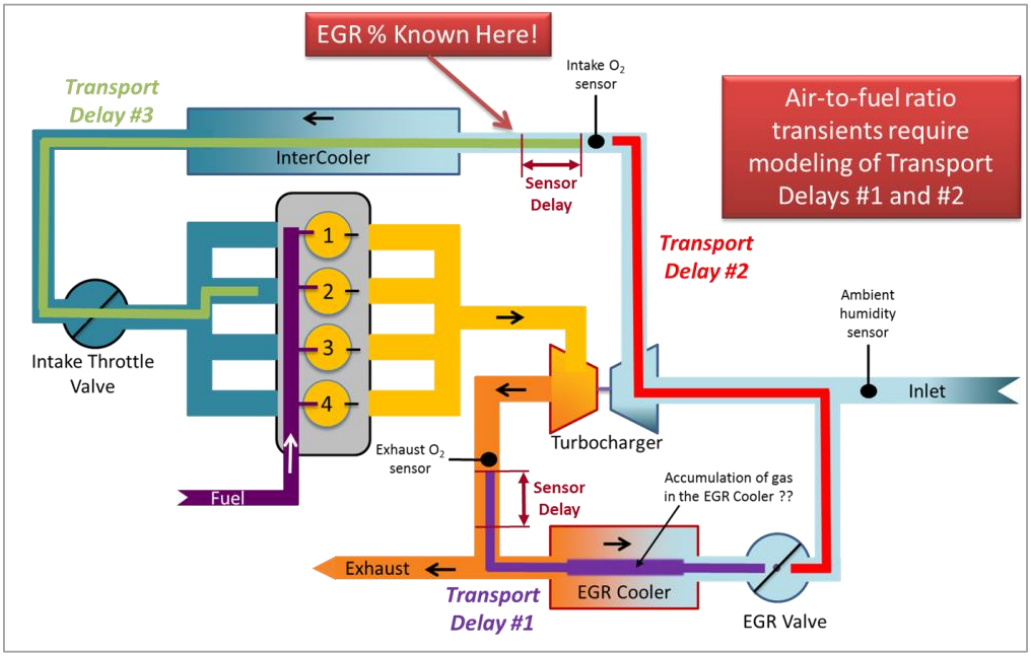

Figure 39: The EGR prediction and control models account for three transport delays in the engine air path to accurately determine EGR concentration and valve position using the intake oxygen sensor.

Several experiments were performed to quantify the transport characteristics of cooled exhaust gas across the air system on the test engine. The characterization was done by changing the EGR valve position in rapid steps. The delays were measured on an engine cycle scale wherein one cycle corresponds to two crankshaft revolutions beginning from the combustion TDC of a fixed reference cylinder. Oxygen sensors were located in three locations; in the exhaust after the turbine, in the intake path after the compressor and on the intake runner of cylinder 1. Figure 48 shows that for a step change in the EGR valve position, the oxygen sensor post-compressor reports the EGR concentration change approximately 3 cycles after the change in valve position is initiated. Similarly, the oxygen sensor on the intake runner reports the EGR concentration change approximately 10 cycles after the valve position change. Additionally, the effect of this EGR concentration change on combustion is detected as a change in the CA50 angle as the spark timing was held constant. Due to the close proximity of the Oxygen sensor on the intake, to the cylinder, the change in CA50 appears to occur at the same instant as the change in Oxygen concentration detected by the sensor intake runner. This can also be attributed to the dependence of the sensor response time on flow velocity.

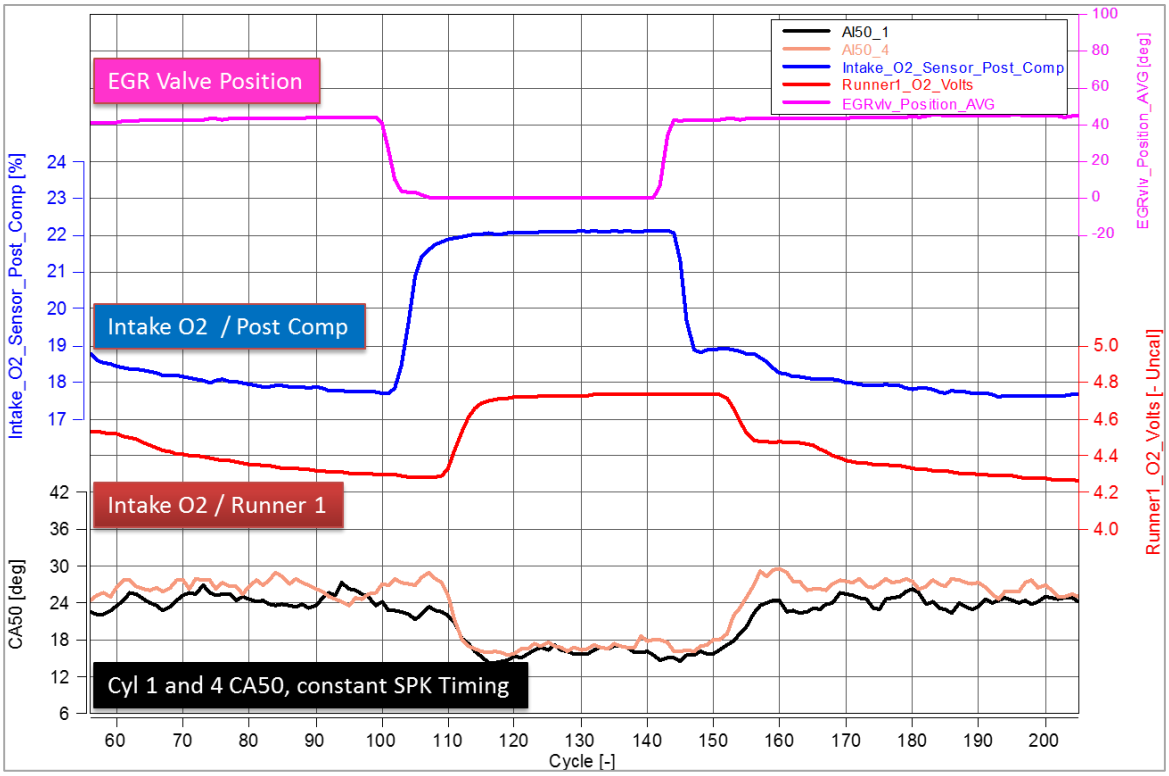

Figure 40: Transport delay characterization of recirculated exhaust gas using EGR valve position step changes.

A Uniform State, Uniform Flow Process, where the working fluids (air & exhaust gas) behave according to the Ideal Gas Law, is assumed for control purposes. The flow path is split into different sections based on the flow conditions. Each section is governed by constant temperature, pressure, mass flow rate and gas composition. As shown in figure 49, an average cross sectional area and length is assigned to each section to further simplify the equations.

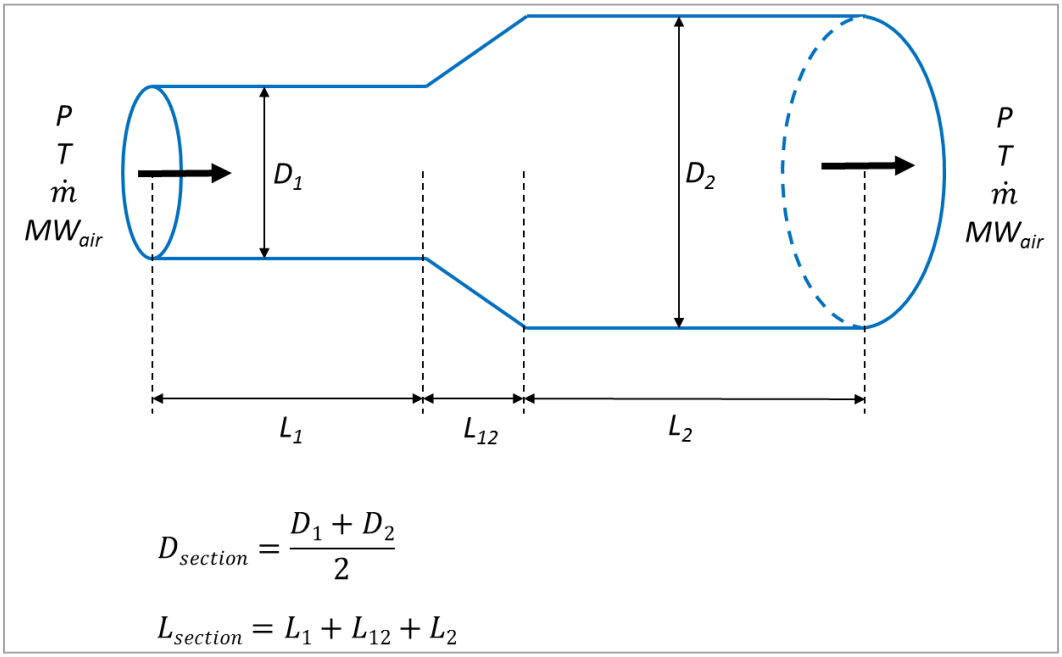

Figure 41: Comparison of actual and control model transport delays from engine experiments.

A first rough estimation of the transport delay calculation is derived using this approach and gives reasonable results, as shown in figure 42. The equations provide similar trends with the detailed simulation results. In this case, all the flow paths are considered to be straight lines. Through more detailed research and calibration of the results, certain correcting factors can be applied to account for bends, restrictions in the flow (valves), area changes, etc. The simplified flow equation was modeled in Simulink, and several instances of this subsystem was implemented to model different control volumes in the gas path. The delays are applied to the constituent species of recirculated exhaust which influence the oxygen concentration measurement and the combustion.

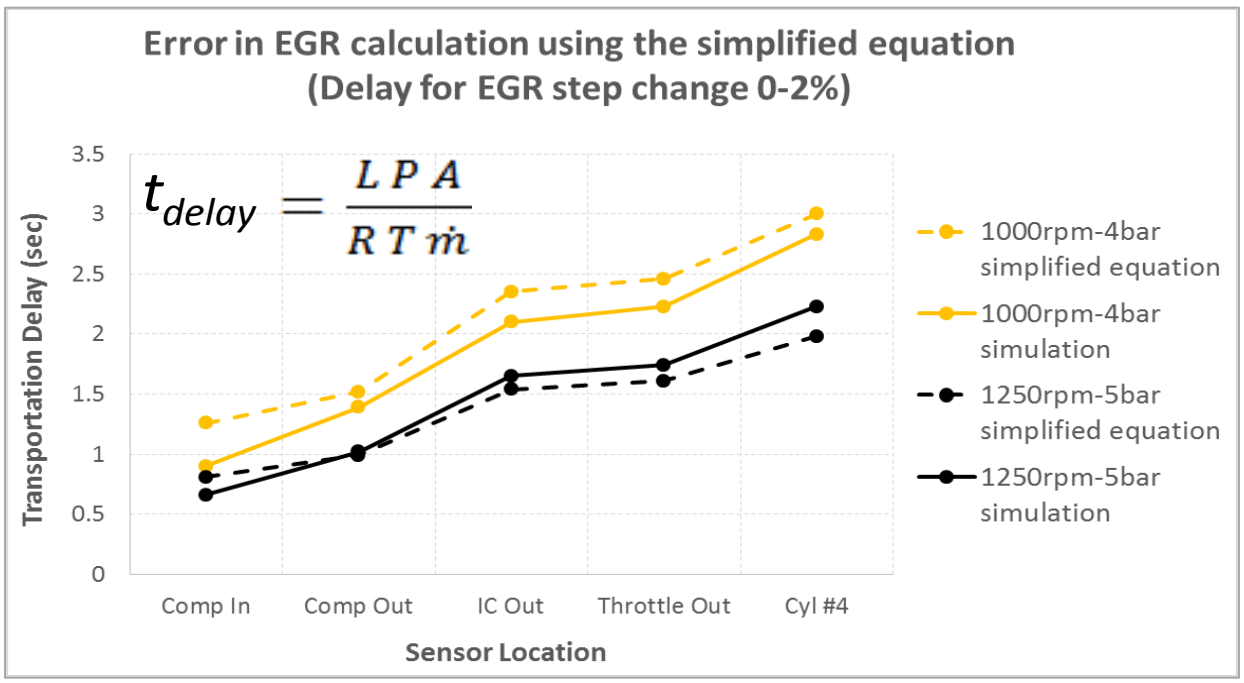

Figure 42: Error in transport delay calculation using a simplified flow calculation approach intended for real-time engine control.

The control model was dynamometer-tested in real-time using an ETAS-ES910 Rapid Prototyping controller. The EGR mass flow rate and engine speed were varied to obtain a wide range of conditions and transport delays in the EGR system. The exhaust lambda was changed in steps while maintaining a steady EGR flow rate. Validation results are shown in figure 43. The transport delays for each of the three section of the EGR flow path are shown individually. Results show that transport delays calculated by the control model through the entire flow path show good accordance with measured transport delays on the engine during both high and low mass flow operation. The vast majority of the points lie within the +-1 engine cycle band.

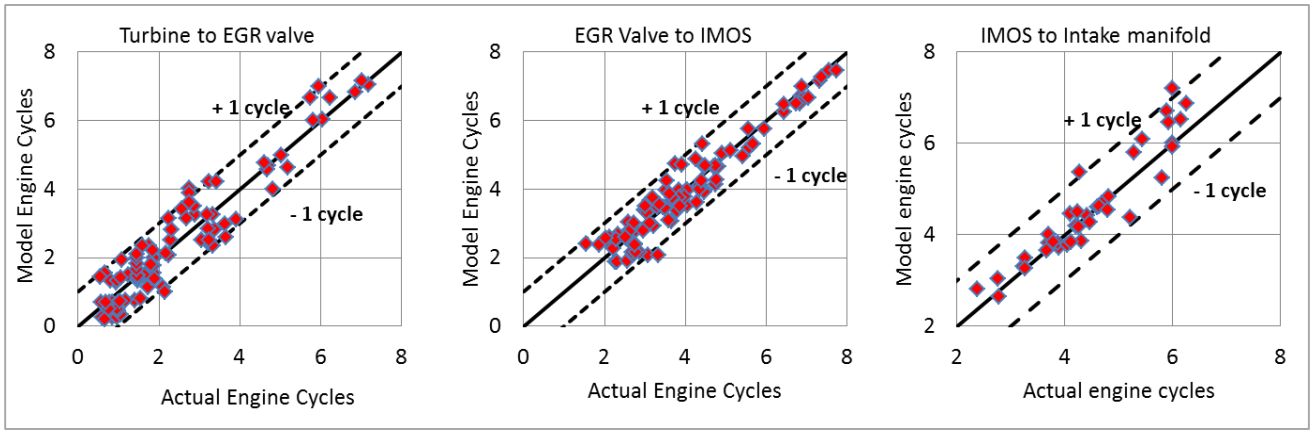

Figure 43: Comparison of actual and control model transport delays from engine experiments.

3.9 EGR Valve Flow Model

The primary actuator used to control flow through the EGR system is a butterfly valve, referred to here as the EGR valve. A common method to model EGR mass flow rate across the EGR valve is using the compressible orifice flow equation. The assumption for this model is that the pressure at the inlet and exit of the valve is steady. However, as seen in figure 44, the pressure at the inlet and exit of the EGR valve can fluctuate, causing unsteady flow.

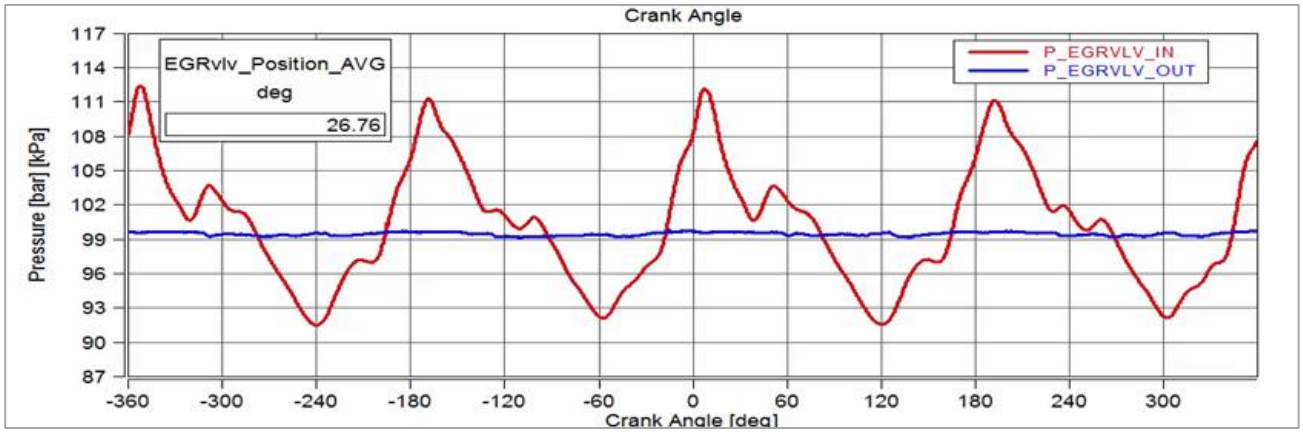

Figure 44: Instantaneous, crank angle resolved Pressure at EGR valve inlet and exit for 1300 RPM, 9 Bar BMEP (Top) and 1800 RPM 7 Bar BMEP (Bottom).

In addition to flow pulsations, the time averaged pressure ratio is very close to 1 which causes inaccuracies in the traditional orifice flow model. In order to have a more physically relevant model to predict EGR mass flow rate the effect of flow inertia also has to be considered in the EGR valve flow model. A dynamic orifice flow equation has been investigated in (4) for pulsating differential pressure and it is of the form:

$$\frac{d\dot{m}}{dt} = \frac{\pi * d^2 * C_c}{4L_e}\left[\Delta p - \frac{8(1-\beta^4)\dot{m}^2}{C_D^2 * \pi^2 * d^4 * \rho}\right] \quad [1]$$

C_D - Discharge Coefficient
β – Ratio of orifice and pipe diameter
C_c – Contraction coefficient
L_e – Effective lengthΔp – Pressure differential across valve
d – Orifice diameter

The dynamic orifice flow model shown in Equation [1] is a first order non-linear differential equation. The discharge and contraction coefficients are tuning parameter curves as functions of orifice diameter. In order to evaluate the accuracy of this model for the Low-Pressure EGR system, a model-fitting Matlab routine was developed. This routine minimized the error between measured and modeled EGR mass flow rate for 120 out of 240 available experimental data points using a global, constrained optimization subroutine (training data). The remaining 120 experimental data points were used to evaluate the accuracy of the model with interpolated coefficients (validation data). As shown in figure 53, accuracy of the dynamic orifice flow model is higher compared to the conventional orifice flow equation. The correlation coefficient between modeled and measured mass flow improved from 0.894 to 0.96 and the Root Mean Square Error decreased from 3.33 kg/hr to 2.5 kg/hr. As the accuracy of the dynamic orifice model is still not high enough to be reliable for control oriented applications (without adaptation using an intake oxygen sensor), a further characterization of tuning parameters is necessary. It is suggested that tuning parameter curves be characterized as 2D functions of pressure ratio and valve open area in future applications.

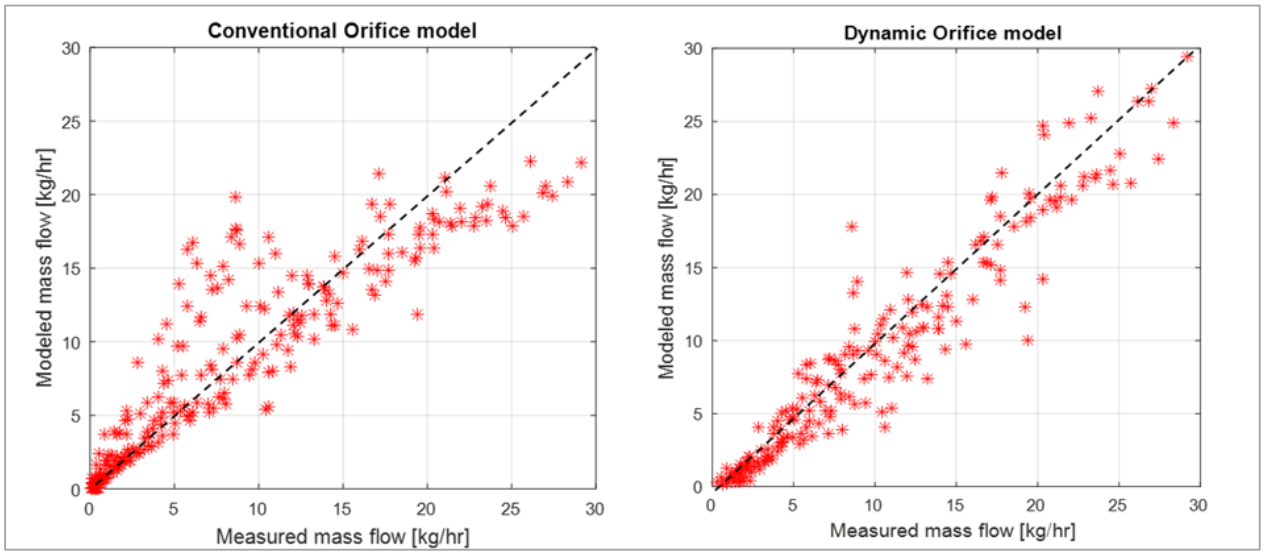

Figure 45: Comparison between modeled and measured EGR mass flow for conventional orifice flow model (left) and dynamic orifice flow model (right).

3.10 Exhaust Pressure and Temperature Modeling for Control

To best utilize the intake oxygen sensor information for EGR valve control open-loop models of the intake and exhaust system are required. These models compliment the information provided by the intake oxygen sensor, and are used as part of the larger control structure. To create an open-loop algorithm for EGR control both exhaust temperature and pressure models have been developed. These models are coupled together and provide the input to the orifice flow equation that determines EGR flow through the valve. Both models are physics-based and require minor calibrations. The sole input to the coupled system is turbine-outlet temperature, which is generally known through pre-existing ECU models. For the purpose of this control algorithm development, a sensor is used to determine that input.

The purpose of these models is to give estimation for turbine-outlet pressure that was used by the control algorithm to determine the pressure differential that drives EGR through the valve. Figure 46 shows a schematic of the exhaust system. The temperature model works in a forward direction (starting at the engine) while the pressure model works backwards (starting at atmosphere); however both are coupled and run real-time. Turbine-outlet temperature is used as input in order to determine catalyst-inlet temperature that was used in the pressure model. On the other end, the pressure model assumes catalyst-outlet pressure is known (ambient conditions) and uses the temperature estimations to calculate turbine-outlet pressure by modeling both sections of the exhaust pipe.

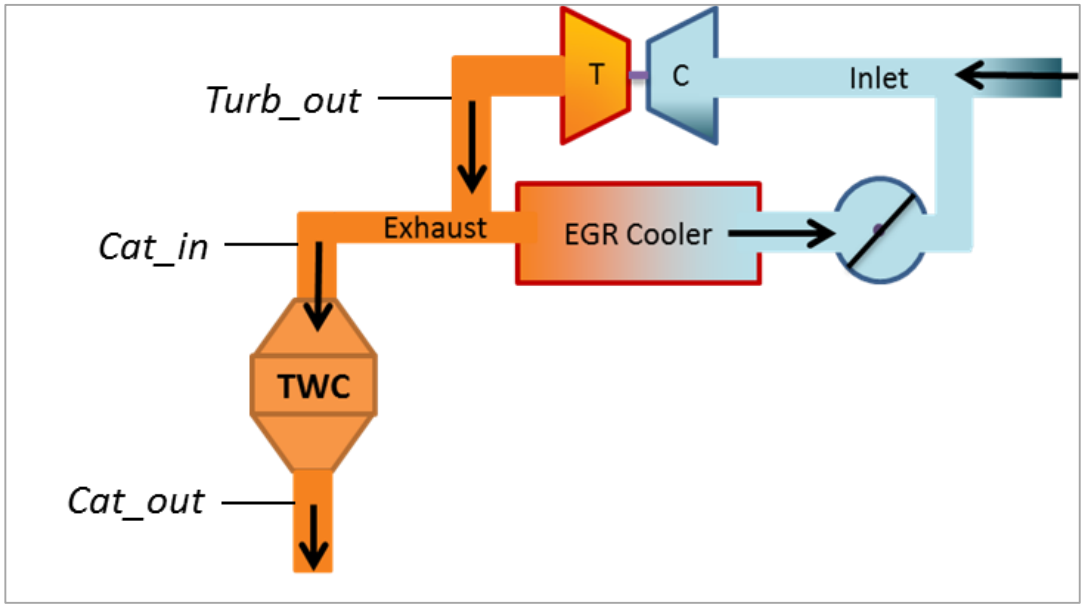

Figure 46: Schematic of the engine exhaust system split into different sections. Exhaust pressure and temperature models were created for integration into the larger EGR valve control structure that utilizes intake oxygen sensing.

3.11 Exhaust temperature model

For the temperature model, the system of equations consists of a steady-state heat transfer equation along with a low-pass (unity gain) filter. The filter captures the dynamic behavior of the system and also smoothens the noise of the input signal. It is preferred over solving a first-order ODE for wall temperature in order to minimize computational effort. The model uses the turbine-outlet temperature as an input and calculates the (steady-state) catalyst-in temperature by handling the first section of the exhaust pipe as a single lumped control volume:

$$T_{gas_{out_{ss}}} = T_{ext} + \left(T_{gas_{in}} - T_{ext}\right) e^{\frac{-h_{tot} * A}{\dot{m} * c_p}}, \qquad [2]$$

Exhaust gas heat capacity is calculated according to the Raznjevic correlation (1) for stoichiometric combustion and is $c_p = f\left(T_{gas_{in}}\right)$. For the heat transfer coefficient, a correlation with gas velocity is determined and fitted to experimental data:

$$h_{tot} = 82.13 + V_{gas}^{-0.4243} \text{ , where } V_{gas} = \frac{\dot{m}}{\rho_{exh} * A} \quad [3]$$

Density of the exhaust gas is calculated using the ideal gas law. However, experimental results from a wide range of operating conditions show that density remains relatively constant and equal to ≈0.4 kg/m^3. As far as exhaust mass flow is concerned, it is part of the control loop architecture and determined as:

$$\dot{m}_{exh}(\mathrm{t}) = \dot{m}_{engine}(\mathrm{t} - \tau_d) - \dot{m}_{EGR_{model}}(t-1) \quad [4]$$

Engine mass flow is derived from ECU signals for fuel quantity, air flow (from MAF sensor) and EGR (from intake oxygen sensor measurement). A one cycle time delay is applied to this signal to approximate manifold dynamics. EGR mass flow in Equation [4] is determined as the previous output of the feed-forward model. The same exhaust mass flow approach is used for the pressure model as well.
Concerning the 'external' (sink) temperature required in Equation [2], a correlation with inlet gas temperature is found and fitted to experimental data:

$$T_{ext} = 485.4 + T_{gas_{in}} * 0.0863 \quad [5]$$

The steady-state temperature prediction (Equation [2]) is supported with a unity gain filter that captures the transient response of the system:

$$\begin{aligned} T_{gas_{out}}(i) &= w * T_{gas_{out_{ss}}}(i) + (1-w) * T_{gas_{out}}(i-1) \\ T_{gas_{out}}(1) &= T_{gas_{out_{ss}}}(1) \end{aligned} \quad [6]$$

The weighting factor of the filter, w, plays a crucial role in the dynamic response of the temperature model. A correlation between gas velocity and the weight factor was found and experimental results are used to determine the coefficients:

$$w = 0.0269 * V_{gas}^{0.0627} \quad [7]$$

Experimental validation of the derived equations was conducted with test data sets (acquired at Clemson University) that are not used for training purposes (validation data). Figure 47provides an example model output for a short transient test. The blue line (model) generally matches experimental measurements (red) within ~15K, a level that is within the uncertainty of the measurement.

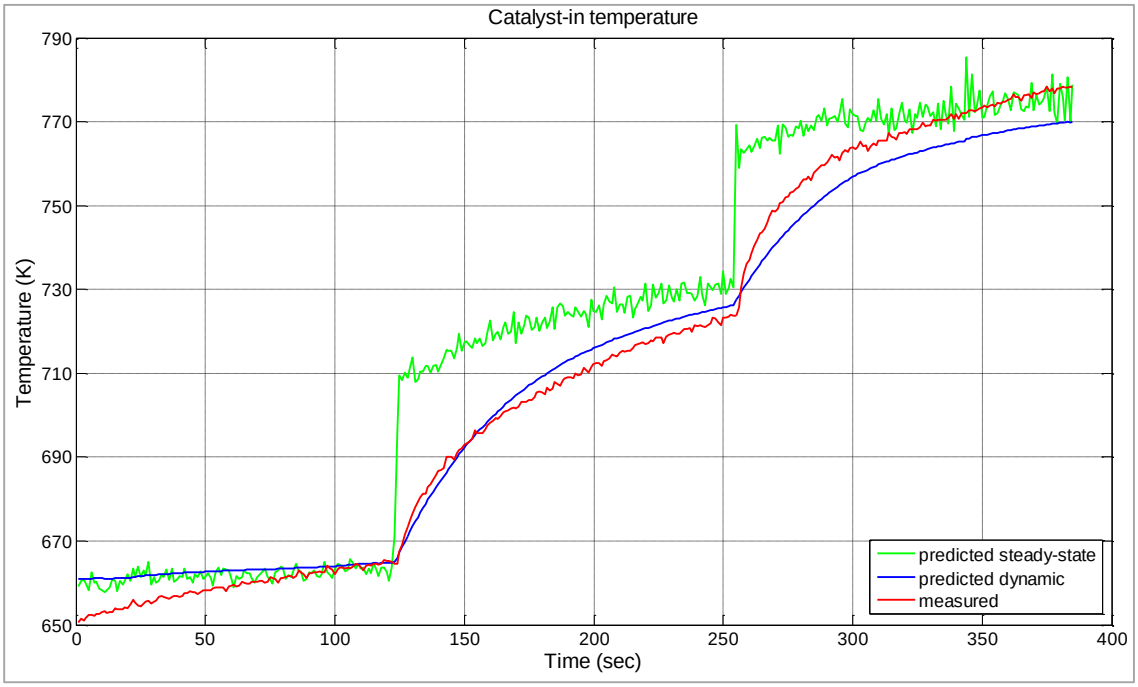

Figure 47: Experimental validation of the temperature model (RPM step changes). The 'predicted dynamic' results are from the final model.

3.12 Turbine Outlet Pressure Model

The pressure model is derived by splitting the exhaust pipe into two sections. The model uses the known catalyst-outlet pressure (ambient) to back-calculate the EGR inlet (turbine-outlet) pressure. The pressure drop in that system is calculated using the assumptions that flow through the exhaust pipes is turbulent, while flow through the catalyst is laminar. As a result, the Darcy-Weisbach (2) equation is used for the lumped first section of the exhaust pipe where flow is turbulent and the Hagen-Poiseuille (3) equation is used for the laminar catalyst flow.

In more detail, the pressure drop for the laminar flow through the catalyst is found by:

$$\Delta P_{cat} = \frac{28.5}{D^2} L * \mu * V \qquad [8]$$

Gas velocity is determined by $V = \frac{\dot{m}}{\rho A}$, with density being approximated by Equation [9].

$$\rho = \frac{P_{cat_{out}}}{287 * T_{cat_{in\ prediction}}} \quad [9]$$

The dimensions, D and L, of a single catalyst channel are used (assumed D=1mm). The area found in the gas velocity equation represents the total catalyst flow area. The number of catalyst channels (N) is used as the fitting parameter of the equation. N = 6,939 is found through non-linear regression with experimental data.

Constant dynamic viscosity of $3.48 \cdot 10^{-5}$ Pa-s is used for the exhaust gases, determined as a weighted average between the dynamic viscosity of nitrogen and carbon dioxide at 500°C. Different dynamic viscosity correlations with temperature were also studied to determine the effect on pressure model. The Sutherland (4) equation and the Heywood correlation (5) were used and the results compared with the single-value approach. The results suggested that the effect of a detailed model for dynamic viscosity is negligible and thus a constant value is used for this pressure model.

For the pre-catalyst turbulent flow pressure drop, the Darcy-Weisbach equation is used:

$$\Delta P_{\mathrm{turb-to-cat}} = f_D * \frac{L}{D} * \frac{\rho V^2}{2} \quad [10]$$

Density is calculated by the ideal gas law using Equation [11].

$$\rho = \frac{(P_{cat_{out}} + \Delta P_{cat})}{287 * T_{cat_{in\ prediction}}} \quad [11]$$

The lumped exhaust pipe dimensions, L and D, are used and gas velocity is calculated as previously discussed. The friction factor (f_D) is used as the fitting parameter, f_D = 0.355 is determined through non-linear regression with experimental data.
These coupled pressure and temperature models were tested in real-time on the engine to evaluate the accuracy of the EGR-inlet (turbine-outlet) pressure prediction that was used as input to the feed-forward EGR valve control. **Error! Reference source not found.**8 shows the error statistics between experiment and model for the sample transient tests shown in 56 and 57.

	Test 1	**Test 2**
Average Absolute Error (kPa)	0.160	0.153

Maximum Absolute Error (kPa)	0.792	0.831
Standard Deviation (kPa)	0.128	0.133

Table 8: Exhaust Pressure Model Error from Experimental Testing

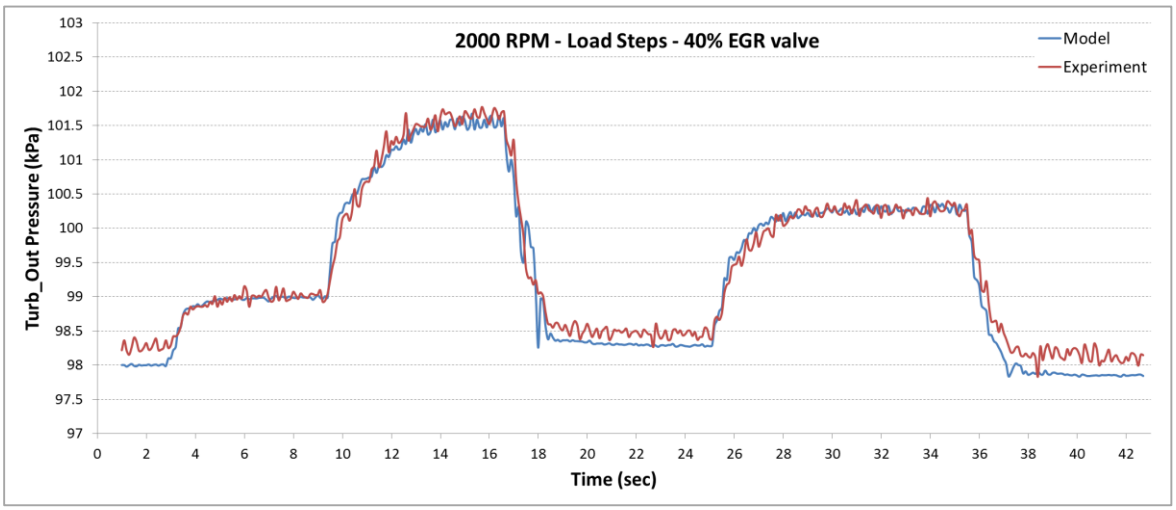

Figure 48: Real-time experimental validation of the coupled pressure-temperature model (2000 RPM, load step changes).

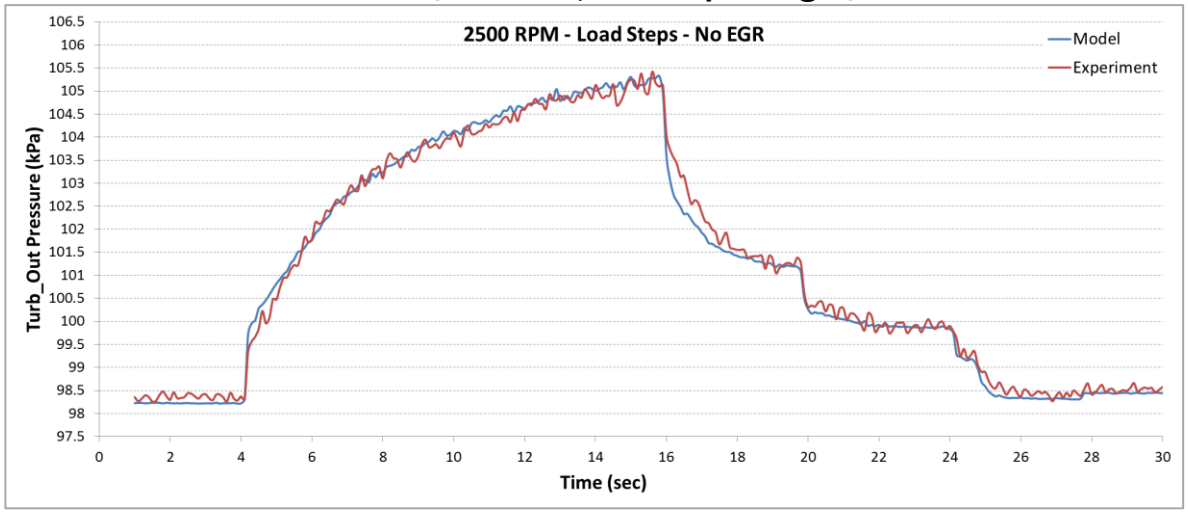

Figure 49: Real-time experimental validation of the coupled pressure-temperature model (2500 RPM, load step changes).

3.13 EGR Valve Mass Flow Model Development

The open-loop EGR control system requires a model for EGR valve mass flow estimation. The EGR mass flow model is based on the isothermal orifice flow using Equation [12]. This is a slightly simplified version of the standard orifice flow equation (6) that can be used to model mass flow of exhaust gas at lower temperatures with minimal loss in accuracy.

$$\dot{m} = \frac{C_d \cdot A_{th} \cdot P_{in}}{\sqrt{R.T}} \cdot \left\{ \frac{2P_{out}}{P_{in}} \left[1 - \frac{P_{out}}{P_{in}} \right] \right\}^{1/2} \qquad [12]$$

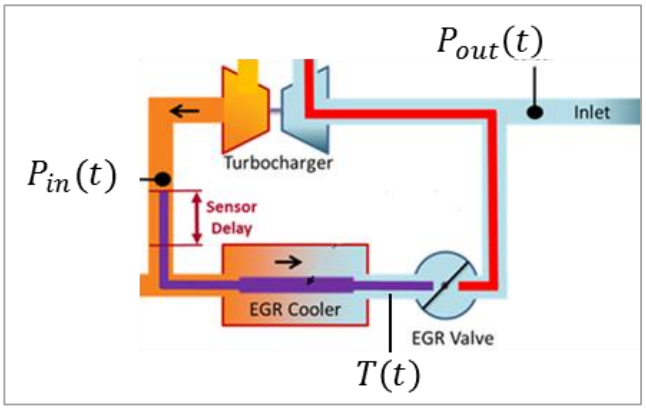

Figure 50: Locations of inputs used for EGR mass flow model.

The pressure, P_{out}, at the outlet of the EGR system is measured using a pre-existing production sensor. The temperature input, T, is a direct measurement. The discharge coefficient, C_d, is the only calibration parameter in this model and it varies as a function of EGR valve position. In reality the exhaust pressure is not steady due to blow-down pressure waves from the cylinders propagating through the turbine. The amplitude, frequency and shape of these pressure pulsations varies with engine operating conditions. The primary frequency of these pulsations is directly proportional to the engine speed and hence engine speed is used as an additional parameter in determination of C_d. To determine C_d, 180 steady state measurements at different engine speeds, loads and EGR valve positions were recorded. An optimization routine was executed to minimize the difference between the modeled and measured EGR mass flow rates by modifying C_d. The final C_d 'map' used is shown in figure 51.

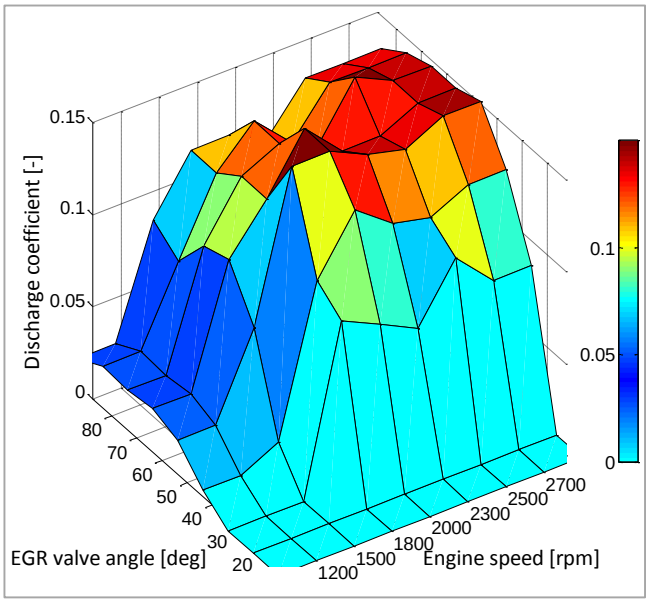

Figure 51: Discharge coefficient map used for Open loop EGR mass flow model.

Comparison between the modeled and measured EGR mass flow rate is provided in figure 52. The majority of the points from the open-loop model lie within the 10% tolerance region. The corelation coefficient between the modeled and measured EGR mass flow rate is 98.7%. There are a significant number of points which lie outside the 10% tolerance band. This can be attributed to the high sensitivity of the model to pressure ratio closer to unity. As shown in figure 53, there is clearly a steep gradient as pressure ratio approaches unity. This necessitates a consideration of more physical phenomenon affecting the mass flow at near unity pressure ratios. The exhaust pressure pulsations would be the most likely candidate for influencing EGR mass flow at these conditions. For low pressure differential conditions an unsteady model is used, which is described in detail when discussing the Extended Kalman Filter for model adaptation.

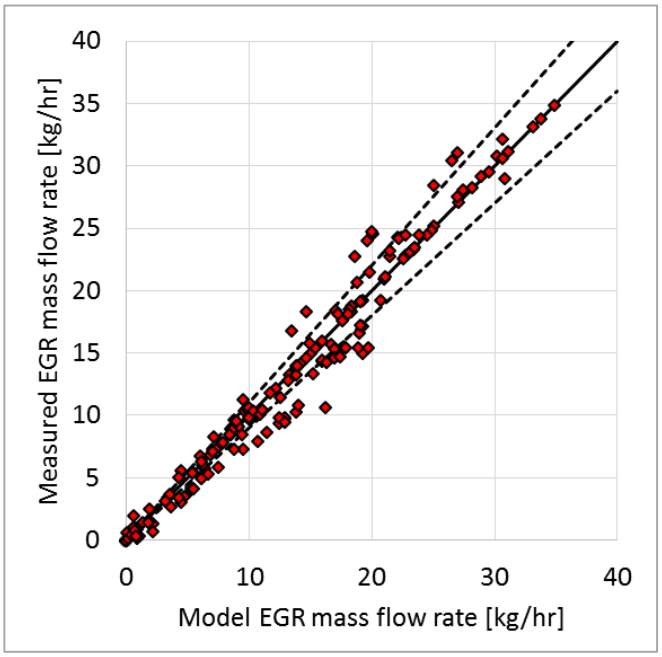

Figure 52: Comparison between modeled and measured EGR mass flow rate.

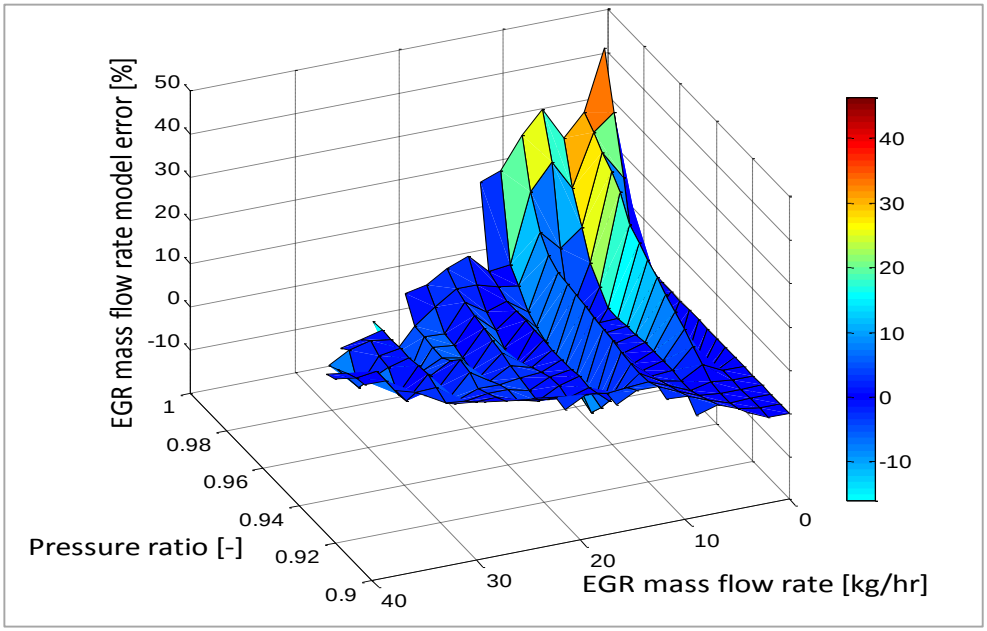

Figure 53: Relationship between EGR mass flow model error, Pressure ratio and measured EGR mass flow.

3.14 EGR Valve Control System with Transport Delay

The intake oxygen sensor offers the opportunity to perform closed-loop EGR dilution control. However, the intake sensor is downstream of the EGR valve which is the actuator to control EGR mass flow rate. Due to gas transport phenomenon and sensor response time, there is a time-varying dead-time delay between the EGR valve actuation and measurement feedback from intake oxygen sensor. Because of this delay, the performance of the closed loop controller is restricted due to stability concerns. A Classical Smith Predictor based PID controller is implemented as the closed loop control architecture to allow higher controller gains without inducing instabilities associated with the transport delay. The overall architecture of the closed loop EGR fraction controller is shown in figure 54. A Sliding Mode Controller is also used to control the EGR valve itself. The multiplier K is used to adjust the output of the Smith predictor portion of the feedback loop. Setting K to 0 effectively makes the controller purely feedback based. Setting K to 1 enables the Smith Predictor portion of the feedback controller.

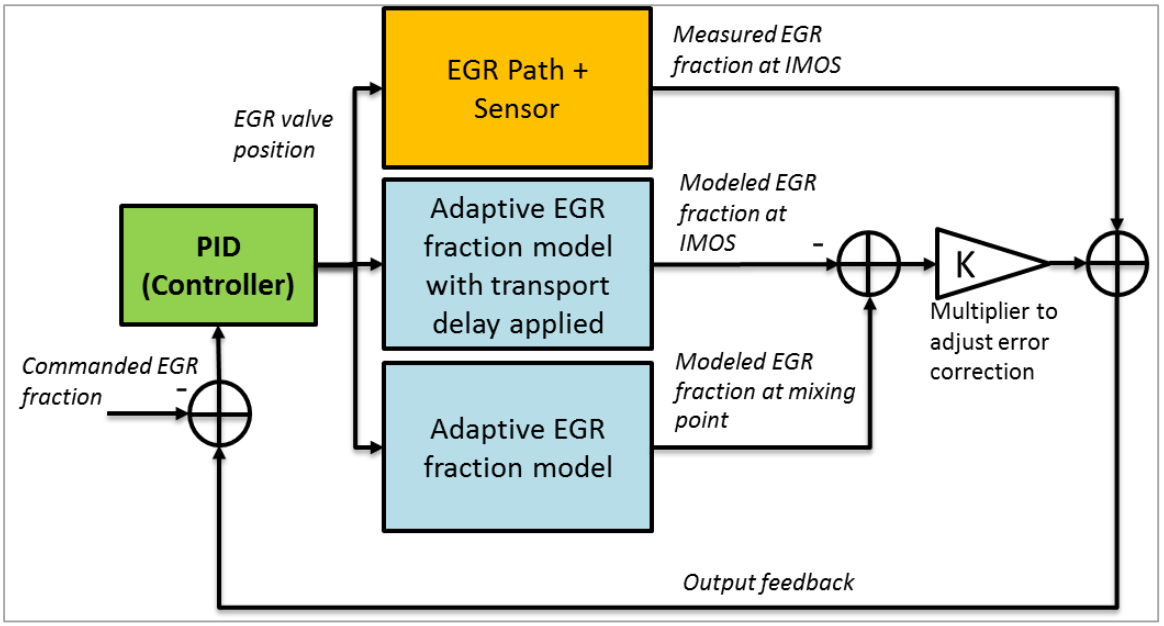

Figure 54: Closed loop EGR fraction control architecture using Smith predictor and Adaptive EGR fraction model.

The Classical Smith Predictor architecture requires a total plant model and a delay-free plant model for adjustments in the error between the commanded and measured parameters. In reference to figure 54, the total plant model and the delay-free plant model are defined as follows. The

delay-free plant model output is the EGR fraction at the location A. This is modeled using Equation [13].

$$EGRf_A(t) = \frac{\dot{m}_{EGR}(t)}{\dot{m}_{Air}(t) + \dot{m}_{EGR}(t)} \quad [13]$$

where, $\dot{m}_{EGR}$ is the modeled EGR mass flow rate and $\dot{m}_{Air}$ is a direct measurement from the production MAF sensor.

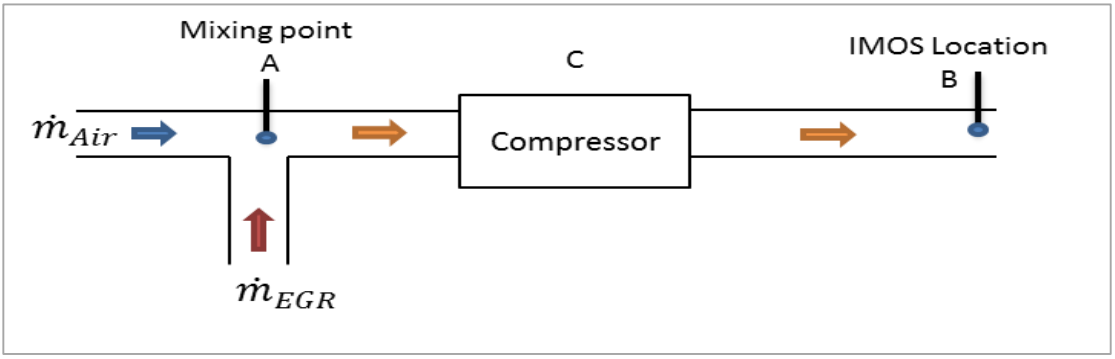

Figure 55: Simplified schematic of air-path from the EGR mixing location to the intake oxygen sensor.

The total plant model is the EGR fraction at the intake oxygen sensor (location B) and is given by:

$$EGRf_B(t) = EGRf_A(t - \tau(t)) \quad [14]$$

Where, $\tau(t)$ is the sum of delays across the various sections between the mixing point A and intake oxygen sensor location B given by:

$$\tau(t) = \tau_{AtoC}(t) + \tau_C(t) + \tau_{CtoB} \quad [15]$$

The transport delay $\tau_i(t)$ for the i-th section between mixing location A and the sensor (location B) can be calculated by the following equation:

$$\tau_i(t) = \frac{L_i . P_i(t) . A_i}{\dot{m}_i(t) . R . T_i(t)} \quad [16]$$

Where, L_i and $A_i$are the length and cross sectional area of the individual sections; $P_i(t)$, $T_i(t)$ and $\dot{m}_i(t)$ are the Pressure, Temperature and mass flow respectively.

Figure 56 shows a sample comparison between conventional PID and Smith Predictor based PID control for EGR fraction control. It is evident that the oscillations caused by the phase lag between intake oxygen sensor feedback and EGR valve actuation are strongly mitigated by the Smith Predictor based controller. The overshoot is also greatly reduced due to instantaneous virtual feedback from the EGR mass flow model.

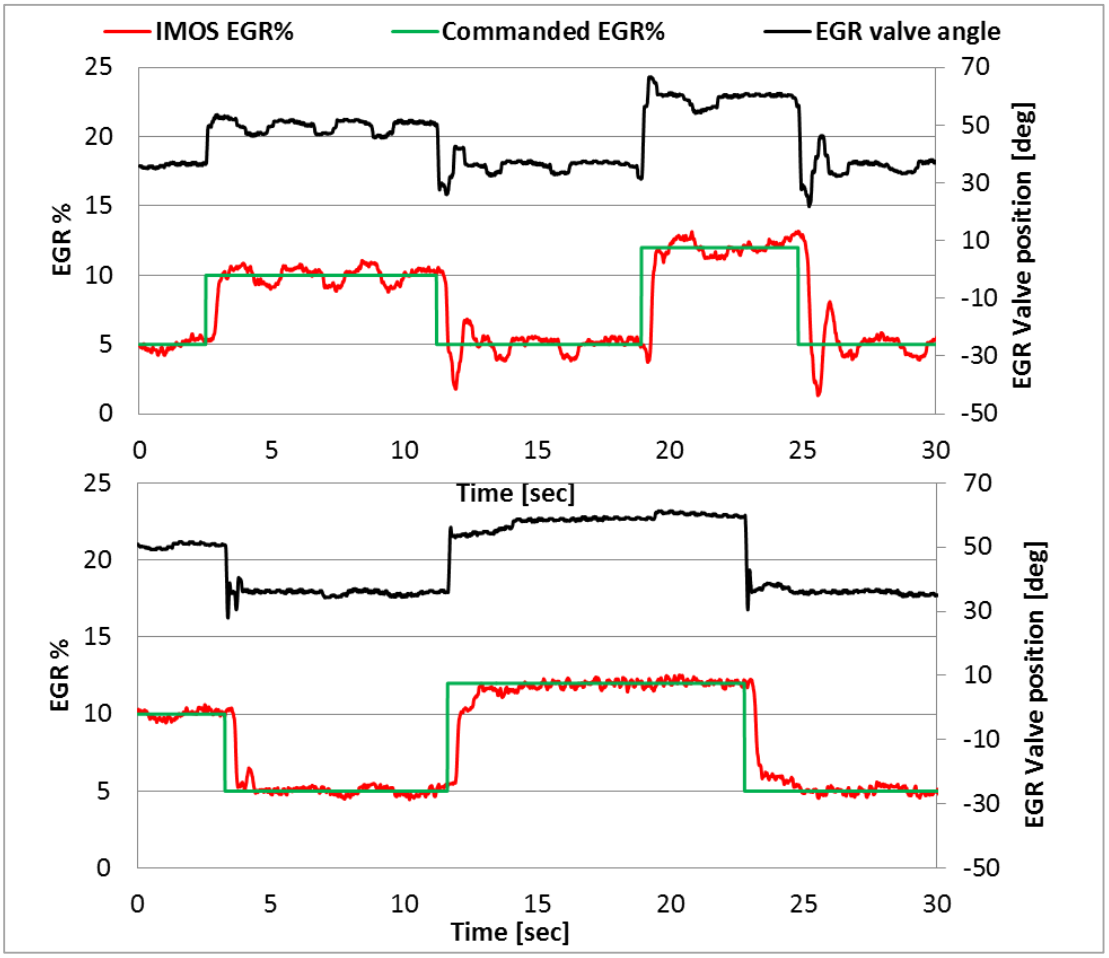

Figure 56: Conventional PID (top) and Smith Predictor based (bottom) EGR fraction control at 2000 RPM and 9 Bar BMEP.

The position command issued by the EGR fraction controller is interpreted as a set-point input by the EGR valve position controller. A first order sliding mode controller was developed with the assumption that the EGR valve is a rotational spring mass damper system with a linear spring and fixed damping. The sliding line is defined by Equation [17]:

$$S = \tilde{\theta} + C\dot{\tilde{\theta}} = 0 \quad [17]$$

Where, $\tilde{\theta}$ is the difference between desired and measured valve angle, and C is the slope of the sliding line.
The motor torque is a discontinuous input $M.Sgn(S)$ which appears in the derivative of S, as shown in Equation [18]:

$$\dot{S} = \left[K - \frac{B}{C} - \frac{J}{C^2}\right]\tilde{\theta} - M.Sgn(S) = 0 \quad [18]$$

Where, K, B and J are valve parameters stiffness, damping and inertia respectively and M is the controller gain. The convergence of $\tilde{\theta}$ to the sliding line, S, occurs in finite time and asymptotic convergence of $\tilde{\theta}$ to zero occurs only if:

$$S.\dot{S} < 0 \quad [19]$$

The above condition is satisfied only if the value of M is such that:

$$M > \left[K - \frac{B}{C} - \frac{J}{C^2}\right]|\tilde{\theta}| \quad [20]$$

With this method M and C are chosen experimentally without requiring knowledge of K, B and J explicitly. However, since the execution rate of the valve position controller is 1 kHz, which low enough to excite un-modeled valve dynamics (e.g. equivalent to gear backlash), chattering occurs once the valve reaches the sliding line. This is partially mitigated by switching from discontinuous input $M.Sgn(S)$ to continuous input $\int M.Sgn(S).dt$ within a calibrated proximity of the sliding line, S. In figure 57 the PI control clearly overshoots the set-point for the fast sine wave command signal, and the sliding mode controller shows superior performance. For a slow sine wave command, the PI control is very similar to Sliding Mode control in tracking the set-point.

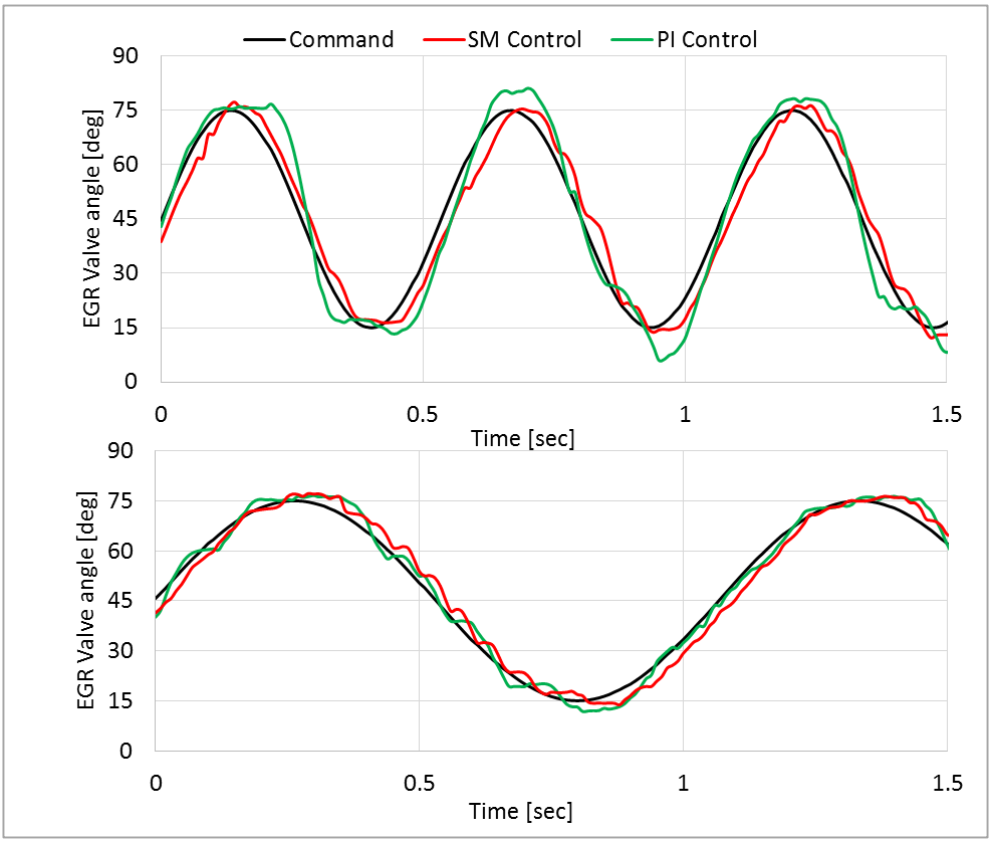

Figure 57: Comparison between PI control [Green] and Sliding Mode control [red] for fast [top] and slow [bottom] EGR valve position command signals [black].

The entire closed-loop control architecture was evaluated during transient engine operation, where engine speed and load were varied using dynamometer speed control and throttle position. The minimum load achieved during this test was 5 Bar BMEP and maximum load was 9 bar BMEP. Figure 58 shows the profile of the transient test along with the commanded and measured EGR fractions and the EGR valve position. The region highlighted from 265 seconds to 310 seconds shows oscillatory EGR fraction. This occurs mainly due to EGR fraction PID controller tuning not being optimized for low EGR and air mass flow conditions in the air path at low engine speeds and throttle opening. The highlighted excursions in measured EGR fraction at 355 and 388 seconds occur due to the rapid change in pressure differential caused by fast engine speed and throttle valve transients. In order to eliminate these excursions, future prediction (or measurement) of pressure differential across the EGR system is required to exercise timely control of EGR valve position.

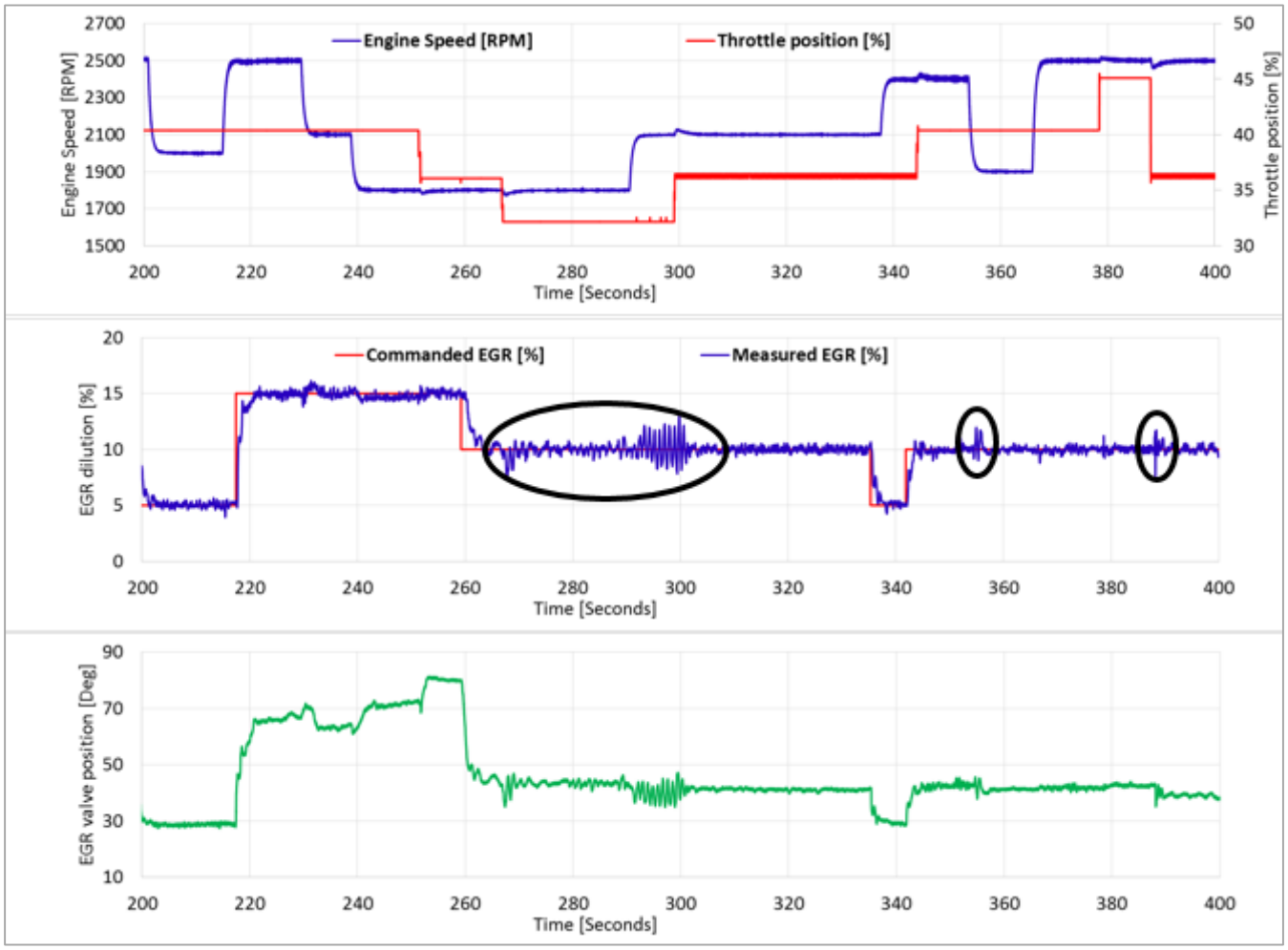

Figure 58: EGR fraction control during transient engine operation.

3.15 Expanded Cross Sensitivity Study of IAO2

ORNL collected data in the previous quarter regarding the sensor response to propylene, nitrous oxide, ammonia and carbon monoxide. Analysis of that data showed the ammonia and nitrous oxide components do not likely pose a significant risk to sensor error and would be too difficult to account for individually in the sensor signal due to the complex exhaust modeling required to properly characterize their quantity. The effects of carbon monoxide and propylene were seen as

a possible contributor to sensor error, and therefore additional testing was done with other hydro-carbon and exhaust gas species to identify what measures might be taken to reduce the errors generated.

A second measurement study was performed, but this time analysis was done using the following species in a fixed concentration of air with the additional test gases displacing the nitrogen in the flow reactor bench:

- Hydrogen (H_2)
- Methane (CH_4)
- Propane (C_3H_8)
- Gasoline (Indolene)
- Ethanol (CH_3CH_2OH)
- Propylene (C_3H_6, checked again for reference to earlier testing)

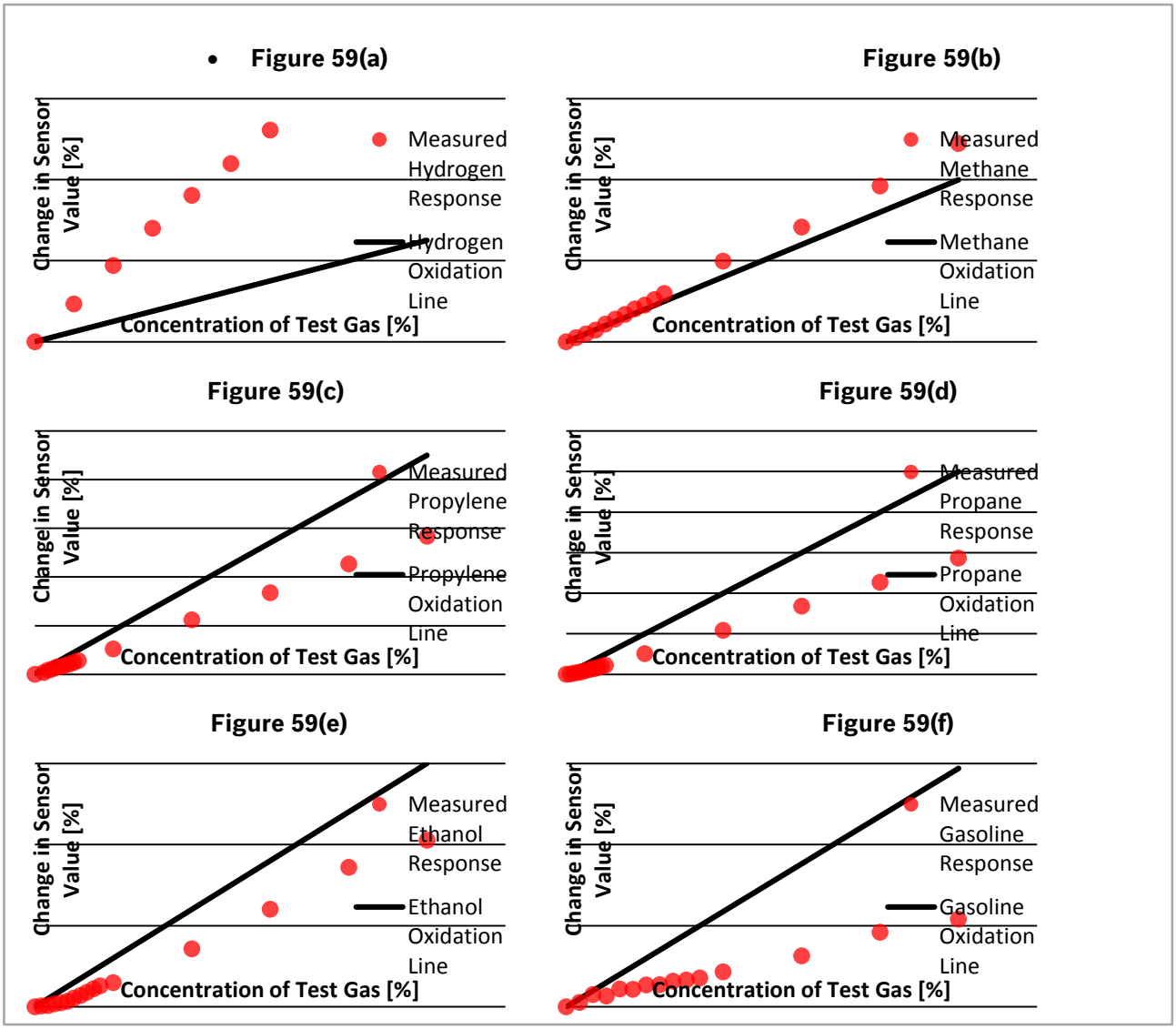

Figure 59: Comparison of the reactant response against the oxidation reaction that will happen at the sensor element. Some species have disproportionate response to the input gas levels due to changing diffusion barrier coefficients when they are present.

As can be seen in Figure 5959 c-f, the longer chain hydrocarbons have similar effects relative to their respective oxidation reactions. In all cases, the effect on the diffusion barrier is less than the expected oxidation reaction would indicate. This does not mean that the gasses aren't oxidized, but rather that the presence of these gasses at the element causes a change in the diffusion barrier coefficients affecting the transport of oxygen across the barrier. This means that for

most species re-circulated through the exhaust stream, as well as possible purge vapors, that correcting for these mixtures can likely be accomplished using a bulk offset rather than specific characterizations. Additional work is ongoing to identify the potential error this approach may have, but it seems as though this was sufficient to correct for these constituents.

Figure 5959b shows that similar to carbon monoxide in the previous quarterly report, methane has a near perfect oxidation effect on the sensing element. Since this is a departure from the other longer chain species, this may require a model for the production of carbon monoxide and methane in the exhaust gasses of the engine. Doing so would make correction easier and simple models could be used to generate a conservative value for exhaust concentration of CO and CH_4.

Figure 5959a is perhaps the most interesting, In the presence of Hydrogen, the sensor has a disproportionate reaction. While still linear, this means that the presence of even a small amount of hydrogen in the exhaust gasses produced by a rich combustion can cause large sensor errors. This is particularly the case under full load enrichment in turbocharged engines where additional fuel is injected in order to keep the exhaust manifold temperatures low enough to protect the turbocharger turbine. Since this is a large motivation to the use of EGR, it is likely that a situation will occur where EGR is being used to reduce exhaust temperatures, while still requiring some reduced level of enrichment. As with methane and carbon monoxide, it was necessary to have a simplified model of hydrogen generation for a given engine and apply some correction offset to the sensor output once enrichment begins to occur.

3.16 Control System Adaptation using an Extended Kalman Filter

An EGR control system adaptation algorithm has been developed and tested in real-time on the engine dynamometer at Clemson University. This adaptation algorithm enables accurate control system performance during highly transient operation and over the lifetime of the system and sensors. This algorithm adjusts the feed-forward controller prediction in real-time based on the output of the intake oxygen sensor. The developed open-loop (feed-forward) EGR control model captures the dynamic behavior of the system but suffers from stationary errors (bias). A method for reducing the estimation bias and at the same time account for system/sensor aging was developed.

The adaptation algorithm calculates, in real-time, control model correction parameters which correspond to different EGR mass flow rates and engine speeds. Instead of using a one-dimensional correction based on EGR mass flow, this two-dimensional correction aims to differentiate

the adaptation based on the exhaust conditions that are encountered in different engine speeds (i.e. amplitude and frequency of exhaust pressure pulsations, etc.). The orifice flow model is augmented with the correction parameters, and a non-linear observer of this augmented model is designed using the output of the oxygen sensor. An Extended Kalman Filter (EKF) is implemented, since it is a widely used and frequently applied methodology for systems that contain sensor noise. The joint state and parameter estimating EKF provides simultaneous online adaptation and bias compensation. In this way, both short-term variations (operating-point dependencies) and long-term drift (component aging) are handled by the EKF-based adaptation.

$$\frac{d\dot{m}}{dt} = \frac{\pi * {d_{eff}}^2 * C_c}{4L_e}\left[\Delta p - \frac{8(1-\beta^4)\dot{m}^2}{C_{D-corr}^2 * \pi^2 * {d_{eff}}^4 * \rho}\right] \quad [21]$$

A dynamic orifice flow model is used as the state equation, shown in Equation [21] in continuous form. Pressure differential is regarded as a single input parameter. This signal is derived as the difference between exhaust pressure model prediction and the intake pressure measurement. Discharge coefficient (C_D), contraction coefficient (C_C) and effective length (L_e) are tuning parameter curves that are functions of EGR valve angle. These tuning parameters are calibrated offline for different operating conditions using experimental data. In order to better capture the effects of pulsating exhaust flow for different engine conditions, the discharge coefficient map is also corrected based on the engine speed using Equation [22]. K_N is the speed correction factor which is experimentally calibrated as a function of EGR valve angle.

$$C_{D-corr} = 0.1 * C_D * K_N * RPM \quad [22]$$

With this method the input vector becomes: $u = [va, \Delta p, RPM]$, where va is the EGR valve angle. The output of the system is corrected EGR mass flow ($\dot{m}_{corr}$). The parameter vector 'theta' (θ) is used to augment the state vector and represents the corrections to EGR flow prediction. This parameter tracks the slow variations of the system (i.e. aging) and thus, in the model, it is described by Equation [23]. Theta parameters change slowly with time, based on the difference between model prediction and sensor feedback that acts on the calculation of Kalman gain.

$$\dot{\theta} = 0 \quad [23]$$
$$\text{where, } \theta = [\theta_1^{RPM_1} \dots \theta_n^{RPM_1}, \theta_1^{RPM_2} \dots \theta_n^{RPM_2}, \dots, \theta_1^{RPM_m} \dots \theta_n^{RPM_m}]$$

As a result, the augmented state vector becomes: $x_{aug} = [\dot{m}, \theta]$. The theta vector in Equation [23] consists of several different parameters with total dimension of $[n * m]$. The size of this matrix is based on the chosen discretization for engine speed $[m]$and EGR mass flow $[n]$. Each

theta parameter corresponds to a different set of EGR mass flow and engine speed. In the validation results shown in this report, a 5x3 discretization is chosen, thus 15 theta parameters are used.

To capture engine operating point specific model bias (fast dynamics) a parameterized function is introduced. This function applies the EGR mass flow correction directly in the measurement equation of the system:

$$\dot{m}_{corr} = \left[1 + q_{fcn}\left(\dot{m}_{pred}, RPM, \theta\right)\right] * \dot{m}_{pred} \quad [24]$$

This parameterized function is presented in Equation [25] and is a two-dimensional interpolation as a function of EGR mass flow and engine speed. The model uses the appropriate theta parameters corresponding to the current engine speed and interpolates between these parameters based on EGR mass flow prediction.

$$q_{fcn}\left(\dot{m}_{pred}, RPM, \theta\right) = \theta_i^{RPM} + \frac{\theta_{i+1}^{RPM} - \theta_i^{RPM}}{\dot{m}_{i+1} - \dot{m}_i}(\dot{m} - \dot{m}_i) \quad [25]$$

The intake oxygen sensor signal that feeds the EKF is associated with transport delays from the EGR valve to the sensor. Aiming to reduce system complexity, transport delay is not introduced in the model equations, since this would require one more state variable and one more state equation. Instead, data from several consecutive time-steps are saved in buffer/memory and EKF correction is applied to the appropriate data-set based on the current transport delay (which is already calculated and included in the control model).

Extended Kalman Filters (EKF) are designed for non-linear systems. EKF linearizes the system model at every time-step in order to calculate the optimal Kalman gain. In an effort to reduce real-time computational effort, linearization of the discretized augmented dynamic orifice flow model (implemented in Simulink) is conducted offline for different operating points. Each operating condition is determined by grid-points for the inputs (pressure differential, valve angle, engine speed) and the state (EGR mass flow). The linearized tables that characterize the system for each point are saved in memory. Thus, in real-time operation, based on the current operating conditions, the linearized matrices for the model are determined through interpolation between the corresponding grid-points of the model inputs and the state.

The final EKF model was incorporated with the EGR valve control model and real-time validation is conducted on the engine dynamometer. Several theta parameter discretization sizes for EGR

mass flow and engine speed were tested in order to evaluate the effect of theta-vector length on the adaptation performance. In the results shown below, a 5x3 discretization is chosen with EGR mass flow grid-points being [0.0010, 0.0025, 0.0040, 0.0055, 0.0070] (kg/sec), while engine speed grid-points are [1500, 2000, 2500] (RPM).

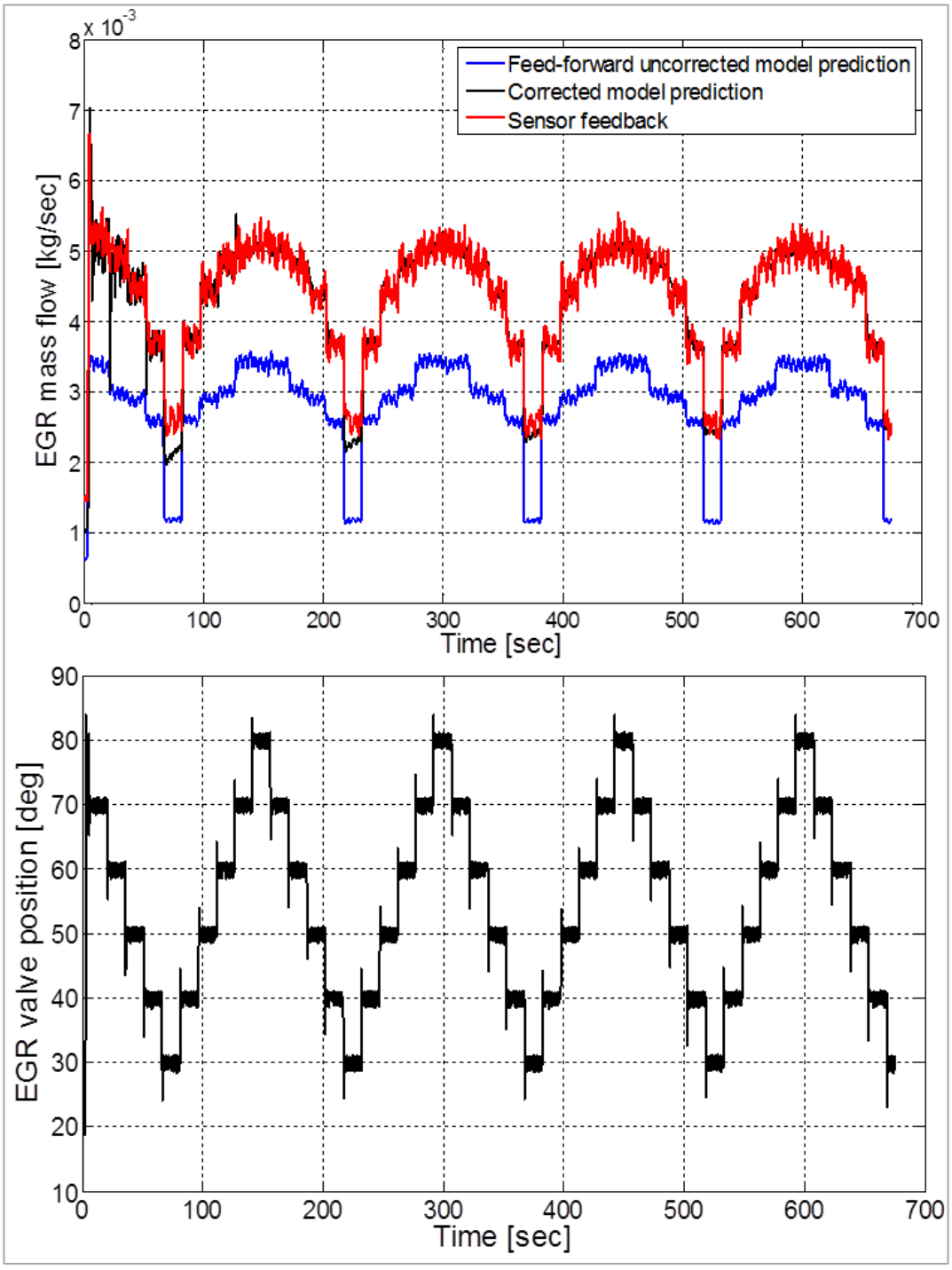
x 10^-3
Feed-forward uncorrected model prediction
Corrected model prediction
Sensor feedback
EGR mass flow [kg/sec]
Time [sec]
EGR valve position [deg]
Time [sec]

Figure 60: Comparison of feed-forward uncorrected model prediction (blue), corrected model prediction (black) and sensor measurement (red) for EGR valve steps at 1750 RPM and constant throttle position (engine load ≈7 bar BMEP) during real-time testing of the adaptation algorithm.

Figure 60 presents the results of an EGR valve pattern repeated several times at 1750 RPM and constant throttle position, in order to assess the performance of the adaptation algorithm. The upper graph shows the comparison between predicted, corrected and measured EGR mass flow. The lower graph displays the EGR valve pattern. It can be seen that after the completion of the first full EGR valve profile, theta parameters have been adapted. When the engine operates again at the exact same engine conditions, the corrected prediction follows the measurement very close. In further repetitions of the same pattern the prediction error has been minimized. Figure 61 presents a transient experiment used to assess the adaptation behavior of the EKF when several engine parameters are being changed simultaneously. The engine is run in transient mode for several minutes before the start of the recording so that theta parameters are already adjusted to different engine conditions. Figure 61 shows the results for the first 300 seconds of the experiment. The upper graph compares the feed-forward uncorrected prediction, the corrected prediction and the sensor measurement. The lower graph captures the simultaneous changes on engine speed, throttle position and EGR valve position. The engine load in these experiments was kept between 5-9 bar BMEP.

These real-time validations prove the effectiveness of the adaptation algorithm to correct the calibrated feed-forward estimation and provide a very accurate EGR mass flow prediction to the EGR controller. Besides the error minimization, this algorithm provides an online adaptation map (through the theta parameters) that improves feed-forward estimation in subsequent time-steps while it is also able to capture any long-term variations due to aging of the system.

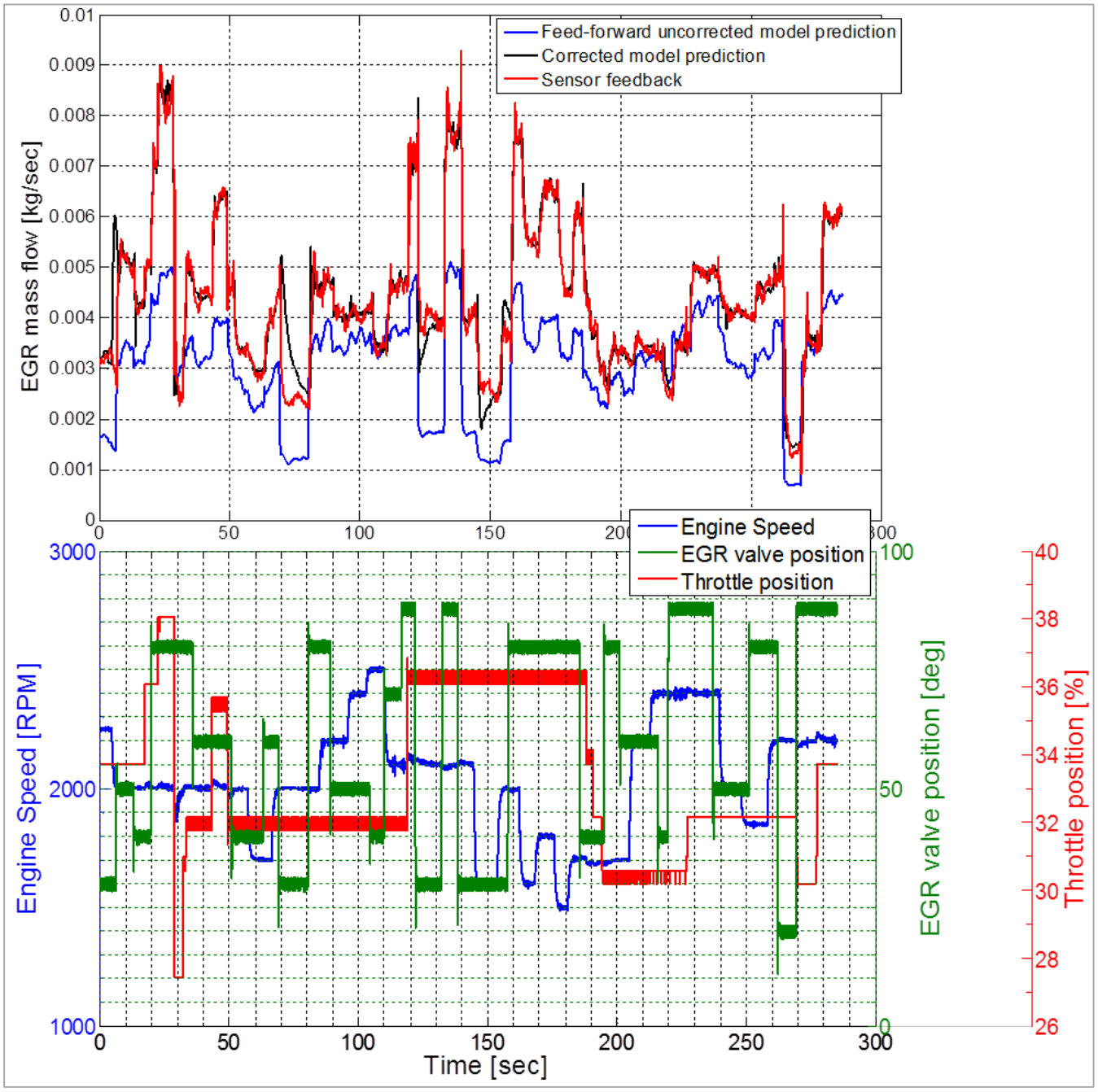

Figure 61: Comparison of feed-forward uncorrected model prediction, corrected model prediction and sensor measurement for engine transient conditions during real-time testing of the adaptation algorithm.

3.17 Assessment of LP-cEGR Fuel Economy Benefits

The goal of this fuel economy study is to evaluate potential benefits associated with the accuracy of EGR measurement (utilizing intake oxygen sensors) and control, using GT-Power simulation. A low-pressure cooled-EGR (LP-cEGR) system is evaluated on a downsized turbocharged spark-ignition engine for this study. Three case studies are considered including optimum EGR dilution (associated with near-perfect EGR control), reduced EGR dilution (associated with current state-of-the-art for EGR control) and operation without EGR (associated with the base engine without external EGR). Fuel efficiency losses compared with the optimum EGR dilution case are correlated with current state-of-the-art techniques for EGR control that include uncertainties in EGR estimation. Additionally, these losses are correlated with the accuracy level of the intake oxygen sensor in measuring EGR. Due to these uncertainties, optimum EGR level is reduced by a certain amount to ensure that over-dilution and misfires are avoided under all operating conditions. On the other hand, the fuel efficiency study comparing engine operation with and without EGR is conducted to quantify the benefits of using LP-cEGR over different drive cycles.
Optimized EGR dilution for part-load operation is derived from simulation using a Design of Experiments (DoE) approach with GT-Power. Control actuator calibration at each operating point (engine speed and load) was determined using a Design of Experiments (DOE) method that considered 200 individual experiments to determine settings that provided the lowest brake specific fuel consumption (BSFC) (i.e. best fuel economy). The results were then optimized to obtain actuator values that give minimum BSFC under knocking and combustion duration limitations.
Based on manifold absolute pressure (MAP), as shown in 38, EGR uncertainty corrections are applied in order to evaluate their impact on fuel efficiency (“reduced EGR” case).

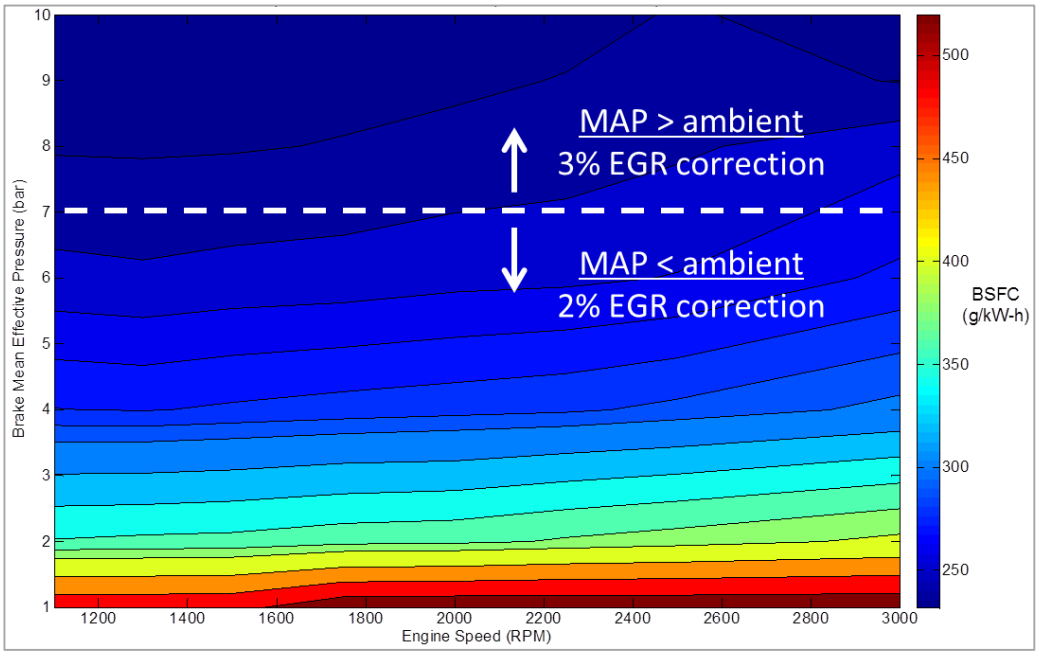

Figure 62: Optimized part-load BSFC map (Brake Specific Fuel Consumption) indicating the uncertainty corrections in EGR estimation that characterize the "reduced EGR" case.

DoE simulation results of the "optimum EGR", "reduced EGR" and "no EGR" (base engine) cases are imported in a Simulink vehicle model. The vehicle is a 2013 Cadillac ATS with 2.0L Turbo engine (LTG specification engine). Figure 63 compares the "optimum" and "reduced" cases and represents fuel efficiency gains over current state-of-the-art for EGR control. Similarly, Figure 64 compares the "optimum" and "no EGR" cases and presents fuel efficiency gains over the base engine that operates without EGR configuration. Engine operating points for FUDS (red) and FHDS (black) cycles are also shown on the figures. The fuel efficiency results for each drive cycle are summarized in table 9.

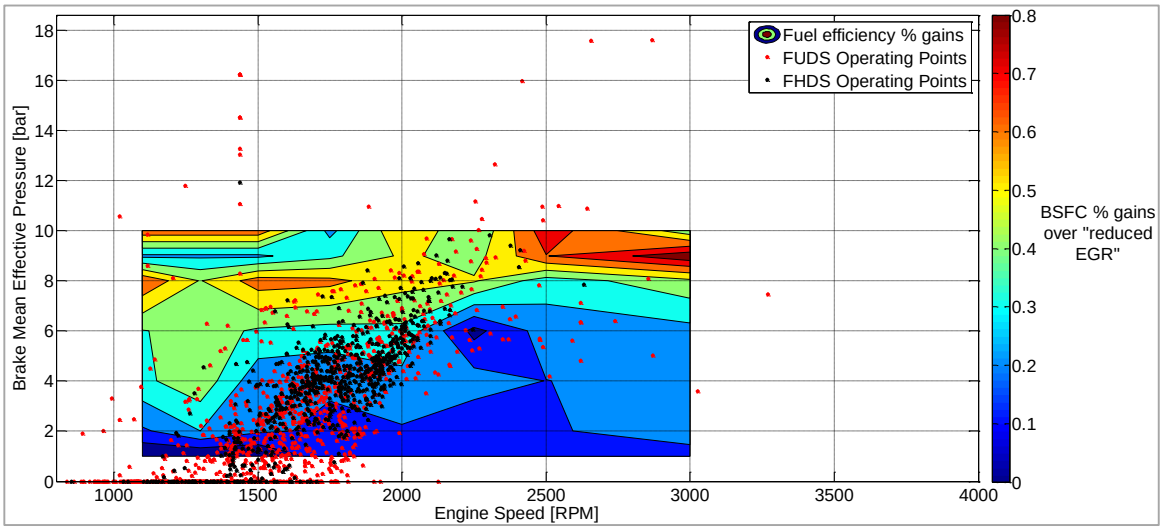

Figure 63: Fuel efficiency benefits over current state-of-the-art for EGR control, along with the operating points for FUDS (red) and FHDS (black) cycles.

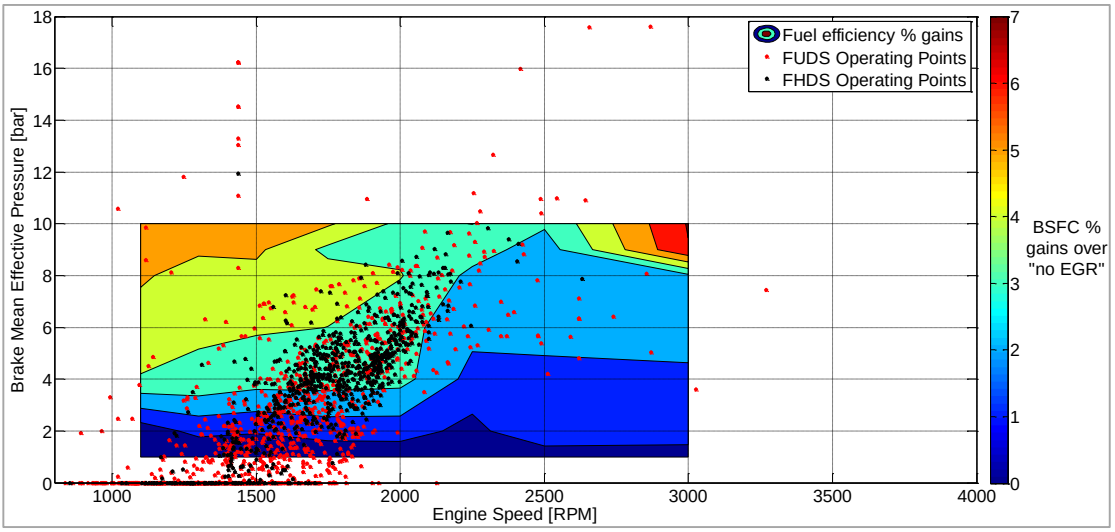

Figure 64: Fuel efficiency benefits of optimum EGR dilution over base engine without EGR configuration, along with the operating points for FUDS (red) and FHDS (black) cycles.

	Optimum EGR (associated with ideal dilution)	Reduced EGR (associated with operation 2-3% away from ideal dilution)	Efficiency benefits (Optimum vs Reduced EGR)	No EGR (base engine)	Efficiency benefits (Optimum vs No EGR)
FUDS	26.2 MPG	26.1 MPG	0.4 %	25.6 MPG	2.3 %
FHDS	41.4 MPG	41.2 MPG	0.5 %	40.1 MPG	3.2 %

Table 9: Summary of fuel efficiency results for FUDS and FHDS cycles.

Finally, the sensitivity of fuel efficiency to EGR error is evaluated in different operating points to estimate intake oxygen sensor accuracy requirements. Sensor accuracy requirements are qualitatively summarized in figure 65. Three different areas can be identified in the engine operating regime:

- Exhaust temperature control oriented EGR introduces high accuracy requirements at high loads
- Knock control introduces high EGR accuracy requirements
- Low load operation, where internal EGR is more crucial to fuel efficiency, can be characterized as a low accuracy requirement region

Figure 65 presents these three areas on top of the engine operating regime, limited by the max torque curve of Cadillac ATS, and also includes the part-load fuel efficiency gains of using an intake oxygen sensor for EGR control as compared to the current state-of-the-art (for EGR control).

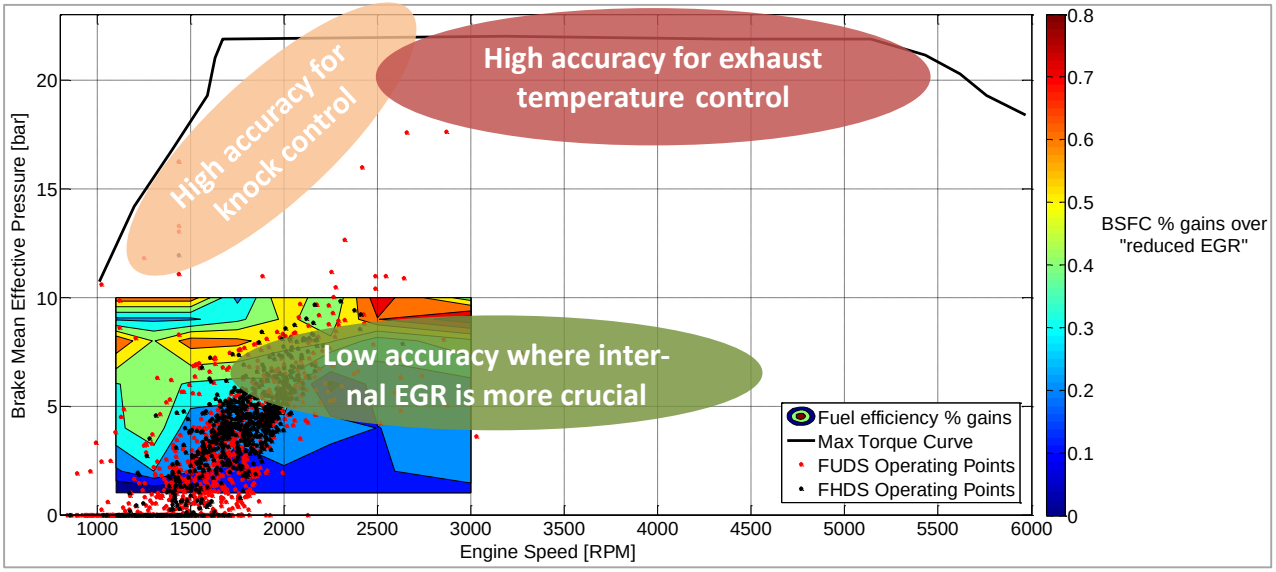

Figure 65: Qualitative sensor accuracy requirements over the entire engine operating regime, along with part-load fuel efficiency benefits over the current state-of-the-art for EGR control.

To quantify the effect of EGR error on fuel efficiency, a sweep of EGR dilution is performed in GT-Power for different operating conditions under combustion duration (characterizing COV_{IMEP}), knocking and exhaust temperature constraints. For each point in the EGR sweep analysis the remaining engine actuators (intake cam location, exhaust cam location, combustion phasing – CA50) are optimized to provide a fair comparison for EGR sensitivity. Figure 66 summarizes this analysis for three points at different parts of the operating regime and quantifies the fuel efficiency sensitivity per 1% EGR increments.

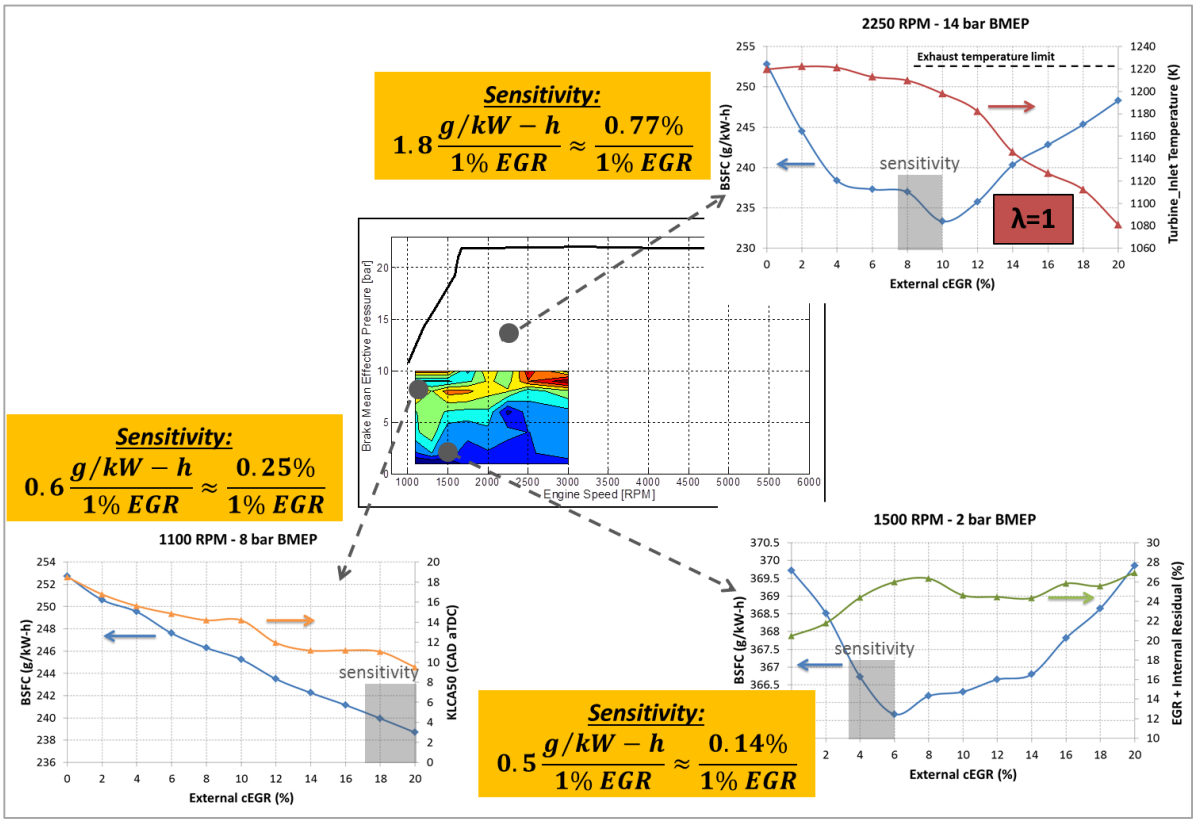

Figure 66: Fuel efficiency sensitivity per 1% EGR dilution for different operating conditions; EGR sweep performed under combustion stability, knocking and exhaust temperature limitations; the rest of engine actuators are optimized in each point of the graphs.

3.18 Actuator Control Strategies for Further Improvement of Fuel Economy with EGR

The intake oxygen sensor improves EGR path control, and allows for higher EGR levels than traditional model-based control approaches. The use of higher EGR levels improves fuel economy, but has the potential to further complicate transient engine control, particularly in aggressive throttle tip-outs. An engine control strategy to mitigate this issue was briefly investigated during this project. The strategy is used to control both external and internal EGR levels during transient operation. It uses Variable Valve Timing (VVT) actuation to limit the burned gas dilution to an acceptable level to avoid misfires, since any EGR valve actuation is associated with long transport delays to the cylinders. The rate of the throttle valve tip-out along with the rate of VVT actuation are also studied since they both affect the burned gas dilution during these conditions.

The base control algorithm to address aggressive transients was developed during this project, and the concept appears promising.

Using the Design of Experiments (DoE) results from GT-Power simulations, Artificial Neural Networks (ANN) were trained to predict the valve timings required to maintain a threshold on Residual Gas Fraction (RGF). In this way, the control algorithm mitigates the effect of high external EGR levels which, due to the long EGR path, could over-dilute the engine causing misfire during the tip-out. The RGF input to the ANN is predictive based on the operating conditions of the final state of the tip-out. The ANN outputs are constrained based on VVT actuation rate limits (~100 CAD / second) and are filtered to provide smooth intake and exhaust valve commands. Figure 67 shows the outputs and the effect of the ANN-based VVT actuation during a torque tip-out at 2000 RPM as compared to a model without the VVT control algorithm. The total burned mass fraction (external EGR+RGF) is maintained at the same levels during the tip-out, due to the reduced valve overlap, while EGR rate remains constant at 10%. The increased levels of burned mass fraction for the base model without VVT actuation are likely associated with misfires during the tip-out.

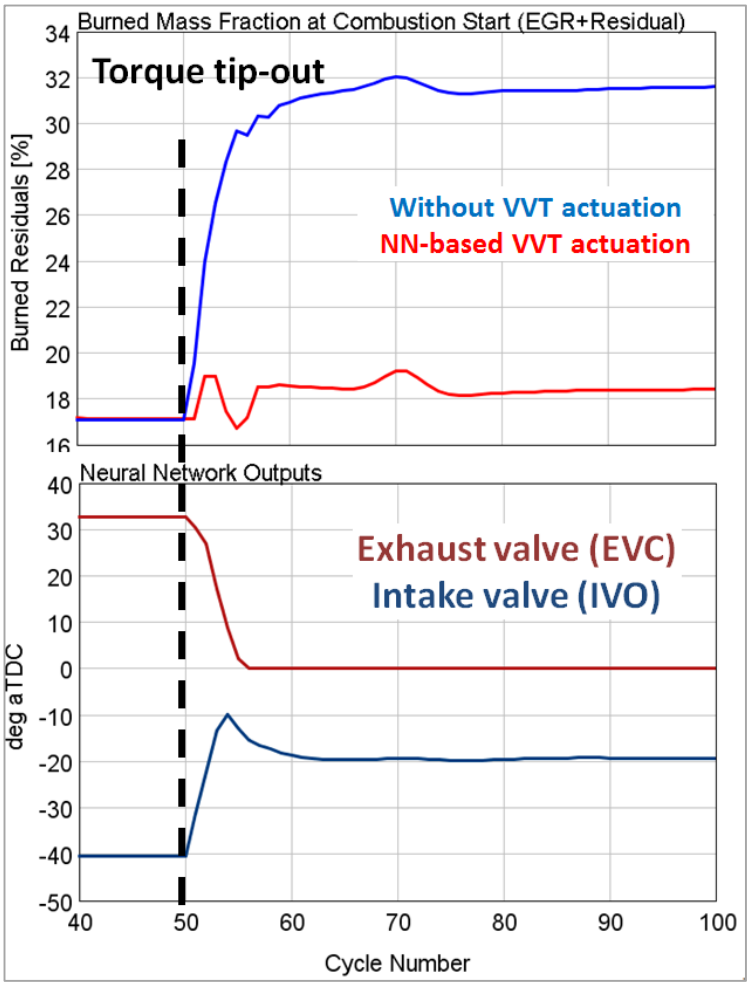

Figure 67: ANN outputs and (External EGR + Internal Residual) levels during a torque tip-out (2000 RPM with constant 10% external EGR) for an ANN-based VVT actuation control model compared to base model without VVT actuation

4 Patents and Publications

4.1 Patents

The following patents were file by Bosch during the course of this project:

Title	Inventor	Affiliation	Date Reported	DoE "S" No

Mounting Flange Heat Shield	David Boyd, Craig Magera	Bosch	3-18-2013	S-135, 897
Gas Sensor with Shielding	David Boyd, Craig Magera	Bosch	3-27-2013	S-135, 896

Table 10: Patent Filings.

4.2 Publications

The following publications were submitted to the SAE World Congress for publication in the April 2016 distribution:

Title	Author	Affiliation	Date
Control Algorithm for Low Pressure – EGR Systems using a Smith Predictor with Intake Oxygen Sensor Feedback	R. Koli	Clemson	2015
Physics-Based Exhaust Pressure and Temperature Estimation for Low Pressure EGR Control in Turbocharged Gasoline Engines	K. Siokos	Clemson	2015

Table 11: Publications.

5 Conclusions

5.1 Project Challenges & Future Directions for Research

The most challenging aspect of Low-Pressure EGR control is open-loop prediction of EGR mass flow driven by pressure differential very close to 0. As this pressure differential increases beyond 2 kPa the mass flow can be predicted more accurately with the classical orifice flow equations. However, at lower pressure differential, the noise of the system along with small errors (~0.5kPa) in predicting the pressure differential have a severe impact on accuracy of EGR mass flow prediction. Hence a more comprehensive approach to engine mass flow modeling along with existing sensor feedback may provide higher accuracy in predicting open-loop EGR mass flow. Additionally, intake throttle valve and fast engine speed transients have an impact on the pressure differential itself and cooperative control of EGR valve and Intake throttle valve may be required to minimize excursions in EGR fraction during transients.

5.2 2nd Generation Sensor Concept (IM2)

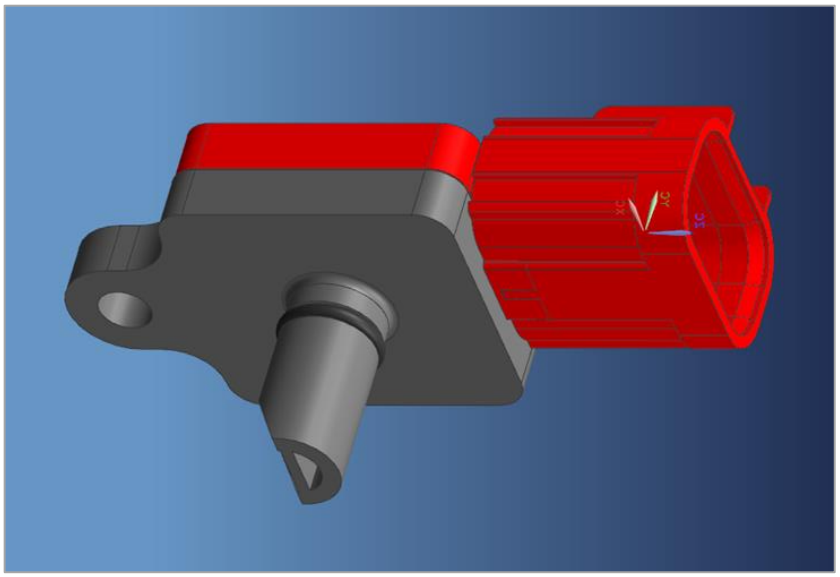

Figure 68: CAD rendering of 2nd generation sensor concept.

The 2nd generation of the IM1 sensor (IM2) was reduced in the size compared to the size of 1st generation (IM1) sensor. A rendering of the 2nd generation sensor (IM2) is shown in figure 69 above. The housing will consist of an over-molded two-piece design with a single bolt attachment. Protection from Soot, water and oil was provided via the snorkel inlet hole which will also be utilized as the ignition suppression mechanism. The design for the new sensor element will require the development of new materials so that the IM2 sensor was able to more accurately measure oxygen content compared to the IM1 sensor. Currently there is a materials investigation in process to identify the right materials for the IM2 sensor to achieve the accuracy improvements necessary, but there is not yet a definitive selection of materials for the IM2 sensor.

6 References

(1) Ngy Srun, “Exhaust Heat Exchange in a Pipe of an Internal Combustion Engine. EGR Cooler and Passenger Compartment Heating Applications”, Seoul 2000 FISITA World Automotive Congress, June 12-15, 2000, Seoul, Korea

(2) Jukka Kiijarvi, “Darcy Friction Factor Formulae in Turbulent Pipe Flow”, Lunowa Fluid Mechanics Paper 110727, July 2011

(3) D.N. Tsinoglou, G.C. Koltsakis, D.K. Missirlis, K.J. Yakinthos, “Transient modelling of flow distribution in automotive catalytic converters”, Applied Mathematical Modelling 28 (2004) 775-794

(4) Crane Company. 1988. Flow of fluids through valves, fittings, and pipe. Technical Paper No. 410 (TP 410)

(5) J. Heywood, “Internal Combustion Engines Fundamentals”, McGraw-Hill Education, 1988

(6) L. Guzzella, “Introduction to Modeling and Control of Internal Combustion Engine Systems”, Springer, 2nd Edition, 2010